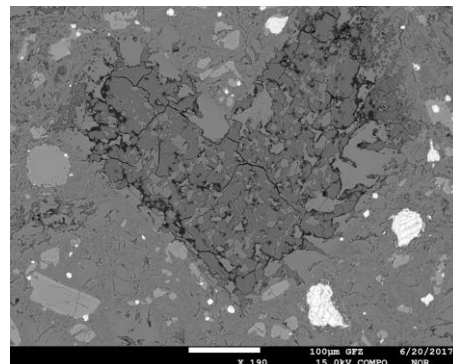MSc Applied Earth Sciences

Petroleum Engineering and Geosciences

Effects of Thermal Shock on the Creation of Microfractures and Mechanical Properties of Various Volcanic Rock Types, including Samples from the Indonesian Geothermal Field (Tangkuban Perahu)

Tulus Imaro – 4489276

August, 2017

TUDelft

[This page is intentionally left blank]

Effects of Thermal Shock on the Creation of Microfractures and Mechanical Properties of Various Volcanic Rock Types, including Samples from the Indonesian Geothermal Field (Tangkuban Perahu)

By

Tulus Imaro

in partial fulfilment of the requirements for the degree of

Master of Science
in Applied Earth Sciences

at the Delft University of Technology,
to be defended publicly on Tuesday August 29, 2017 at 01:15 PM

Supervisor:	Dr. Auke Barnhoorn	Applied Geophysics & Petrophysics, TU Delft
Thesis Committee:	Prof. Dr. David Bruhn	Petroleum Engineering, TU Delft
	Dr. Richard Bakker	Petroleum Engineering, TU Delft
	Dr. Fiorenza Deon	Petroleum Engineering, TU Delft

TUDelft

[This page is intentionally left blank]

Preface

This thesis is a collaboration project between TU Delft and GEOCAP (Geothermal Capacity Building Program Indonesia-Netherlands). Four laboratories are involved in the experiment activities. They are:

- Geoscience and Engineering Lab at CITG building TU Delft
- GFZ German Research Centre for Geosciences in Potsdam
- Material Sciences and Engineering Lab at 3ME building TU Delft and
- GeoScience Lab at Faculty of Geo-Information Science and Earth Observation (ITC) at University of Twente

Some activities also supported the realization of this thesis such as the presentation at European Geosciences Union (EGU) General Assembly 2017 in Vienna (Austria) and a field visit to West Java – Indonesia in March 2017. Unless it is written in the text body, all people involved / technicians in-charged for the laboratory results are acknowledged in the reference.

T. Imaro
Delft, August 2017

Contents

List of Figures

List of Tables

List of Graphics

Abstract

This thesis aims at investigating the effect of a thermal shock of a couple of hundred degrees on the creation of the thermal microfractures and in what way the mechanical properties of volcanic rocks change. In the geothermal field, thermal microfractures can contribute to increase the permeability and produce more steam to the surface. We exposed basaltic andesite and andesite rocks from Tangkuban Perahu (Indonesia), a granite from Benin (West Africa), a basalt from the Eifel (Germany) and a basalt rock from Reynifsjara (Iceland) to temperatures of 200, 300, 400 and 500°C before cooling them rapidly by placing them in cold 20°C water. Initially, most of the sample rocks show less than 1% of porosity, excluding andesite Tangkuban Perahu (~6%) and basalt Reynisfjara (~14%), and permeability for all rocks is below detectable value (2.6 mD by Ruska gas permeameter for specified core geometry). In the geothermal field scenario, it indicates the pores were not connected and the steam may not easily flow through the rock. After the heating stage and thermal cooling, significantly increased values of porosity are observed in most of the rocks. However, only the two high porosity rocks gained permeability; the andesite Tangkuban Perahu (7-11 mD) and basalt Reynisfjara (4.45 mD). The changes in Young's modulus, Poisson's ratio and ultimate compressive strength of the various samples were also determined by using an unconfined Uniaxial Compressive Strength (UCS) apparatus in which both heat treated and non-heat treated samples were placed. The results show the rock strength decreases with increasing thermal shock. Similarly, we see a decrease in both Young's modulus and Poisson's ratio with increasing thermal shock. To recognize the thermal shock effect visually, the samples were imaged using a micro-CT scan before and after heating treatment. The resolution of the CT scanner was 30 µm at best when the whole sample is scanned. It is noticed that the porosity increases after the heating experiment. Additional mini-cores (~10 mm x 8 mm) from the whole core are also scanned at 14 µm resolution. The scans showed the porosity on the outside part of the cores is up to 10 times higher than the inner part. In Indonesia, the geothermal reservoir temperature varies from 200-300ºC. By injecting cold water from the surface at a high rate, the water temperature remains low and can thus create the thermal shock that opens up existing fractures and forms new ones. In that way, it can increase fluid path ways around the well bore and along existing natural fractures.

Keywords: thermal shock, microfractures, ultimate compressive strength, Young's modulus, Poisson's ratio, Brittleness Index (BI), micro-CT scan.

1. Introduction

1.1 Thesis Background

The geothermal fields are mostly located in the volcanic areas that possess different rock characteristic in each location. The geothermal energy is considered as clean energy as it uses the heat from the Earth. It supports the green technology development and reduce the climate change's effect by massively lower the CO_2 emission. Besides its usage as an energy source, it also can be used to dry agricultural products, crops sterilization, and cultivation of certain crops. Some geothermal fields are suspected to have a low permeability reservoir. Fracturing is one of the methods to increase the heat production of those fields. This method is common and has been applied for many oil and gas wells and also likely to be successful to be implemented in the geothermal field.

In Indonesia, specifically, the demand of the electricity undoubtedly will increase over the coming years due to increase population and economic growth (World Bank Group, 2017). Together with the commitment to the international agreement on greenhouse emissions, the Indonesian government puts an effort to limit the impact of climate change (United Nations, 2015). Currently, geothermal energy is being used as one of the energy sources for power generation, it contributes 26% of nation-wide electricity (IEA, 2014). The total potential of geothermal energy in Indonesia, including the reserve, is 29,543.5 Mw scattered around the country. However, only 1,438.5 MW capacity is installed and the electricity produced from 11 existed operated fields is 9,963,655 MWh in 2015 (Ministry of Energy and Mineral Resources of Indonesia, 2016). The development of this energy source is quite promising, but its realization is still under development and below the government target to achieve 7200 MW capacity in 2025 (Saefulhak, 2017). In order to achieve the target, several technical solutions should be assessed and implemented to create fractures in the reservoir. In the oil and gas fields, hydraulic fracturing is a common method to increase the production as this method create the fracture by injecting fluid. In this thesis, we limit the fracturing method to the thermal induced fracture and analyze the various thermal shock effect on the creation of the microfractures in the sample rock.

1.2 Theoretical Background

The Enhanced Geothermal System (EGS) designs the flow path between the injection and production well to produce the heat to the surface by fracturing the rock formation sufficiently (US Department of Energy, 2017). Geothermal reservoir is located at the igneous rock (Omdal, 2015) and the observed igenous rock in this thesis (from Indonesia geothermal fields) is basaltic andesite and andesite. By comparing the laboratory result and the rock characteristic (Coates & Parsons, 1966), this rock is considered as a very strong rock (uniaxial compressive strength is greater than 25,000 psi) . Therefore, high pressure is required in the hydraulic

fracturing process to create better communication between injection and production wells. However, another fracturing method that can decrease the toughness of the rocks is the thermal induced fracturing (Enayatpour & Patzek, 2013). Thermal induced fracture has proven numerically to increase the productivity of the tight formation by 20% (Enayatpour & Patzek, 2013). Therefore, it can be part of the EGS. The thermal induced fracture are created by applying the thermal shock to the rock formation. Within a short time, the rock material is exposed to the very high temperature difference (around 80 to 480ºC) and deform the rock as a result. This deformation condition can be quantified further by evaluating the elastic moduli from the compressive stress and strain of the rock.

Other than elastic moduli, many factors also affected the fracturing method such as the in situ stress, mineralogical composition, the presence of pre-existing fractures and the manner of the well completion (Yang, Sone, Hows, & Zoback, 2013). Elastic moduli will be assessed to observe the rock characteristic under various heating treatments. As the initial premise, when the rock is getting more brittle, the Young's modulus increases and the Poisson's ratio decreases (Rick Rickman, 2008). The material is brittle when it breaks without significant deformation (Cho, 2014). The two static elastic moduli will be assessed together with the ultimate compressive strength to confirm the rock behavior and its thermal microfractures implication.

The microcracks, induced by the heating experiment, are the result of the differential thermal expansion between grains thermoelastic moduli and thermal conductivities (Kranz, 1983). This theory will also be examined by inspecting the porosity and permeability cores after the heating treatment. In addition, the porosity will be correlated to the minerology composition as the microcracks are significantly affected by the amount of the quartz in the rock because of its large thermal expansivity (Kranz, 1983).

1.3 Thesis Objective

This thesis investigates the various rock mechanic properties of the geothermal rocks that were exposed in the various thermal shock. Basaltic andesite, andesite and granite rocks from different location are evaluated in this thesis such as basaltic andesite and andesite rocks from Tangkuban Perahu (Indonesia), basalt rocks from Reynisfjara beach (Iceland), basalt rock from Eifel (Germany) and the granite rock from the Adeoti mining site (Benin). In the beginning, the thermal shock experiment is conducted in order to see the generation process of microcracking. The geomechanical behavior is also tested by applying uniaxial compressive pressure and create the fractures. Moreover, the direction of the fractures is visualized from the photograph or the CT Scan result. The process is followed by the minerological investigation to observe a deeper understanding of these specific sample rocks. Minerology allows to classify the rock and assign them to a specific geothermal environment.

The core research question in this thesis is: "How do the various thermal shocks affect the rock mechanic properties in the geothermal fields?" which is followed by the process in determining whether the certain field is good to conduct the hydraulic fracturing based on the Brittleness Index anlysis. This main research question is investigated in some factors such as elastic properties, in situ stress, internal existed fractures, and mineralogy.

1.4 Scope of Thesis

Set of experiments are mainly performed in the Geoscience and Engineering Lab of TU Delft at CITG building together with the other third-party labs (GFZ German Research Centre for Geosciences in Potsdam and Material Sciences and Engineering Lab at 3ME building TU Delft). These experiments included:

1. Large series of rock mechanical experiments at different temperature and pressure conditions to a set of samples from Indonesian volcanic rocks, and other geothermal areas around the world, to understand the mechanical behavior and be able to predict the type of fracturing behavior of these rocks. The physical and mechanical properties are determined by the experiments such as density, porosity, permeability, velocity, Young's modulus and Poisson's ratio.

2. Placing the fractured rock sample into the micro-CT scanner to get high-resolution 3D images (60 to 30 μm) of fracture planes and fracture network connectivity.

3. Conducting XRF (X-ray Fluorescence) and XRD (X-ray Diffraction) analysis of the Indonesian volcanic rocks and other areas.

4. Doing flow/permeability tests before and after the fracturing experiments to see the relation of geomechanics properties, and fracture characteristic, to the fracture performance

1.5 Location of the Rock Sample

a. Tangkuban Perahu, West Java – Indonesia

Tangkuban Perahu is one of the active volcanoes in Indonesia and located in the northern part of Bandung. It erupted in 1910 and currently has 9 active craters (Badan Geologi Kementerian Energi dan Sumber Daya Mineral, 2014). The rocks were taken from Domas crater from the elevation 2084 meters above sea level (coordinate: 6°45'30.4"S 107°36'49.3"E). The status of the Tangkuban Perahu area for the geothermal development is currently still under exploration with the obstacles of power purchase agreement and forestry permit (Directorate General of New Renewable Energy and Energy Conservation Indonesia, 2015). During the visit to this site, several rocks have been collected based on the macroscopic appearance and the visible minerals such as basaltic andesite, andesite and pumic rocks. The figures below show the visited location during the fieldwork and the sampling site (Domas crater).
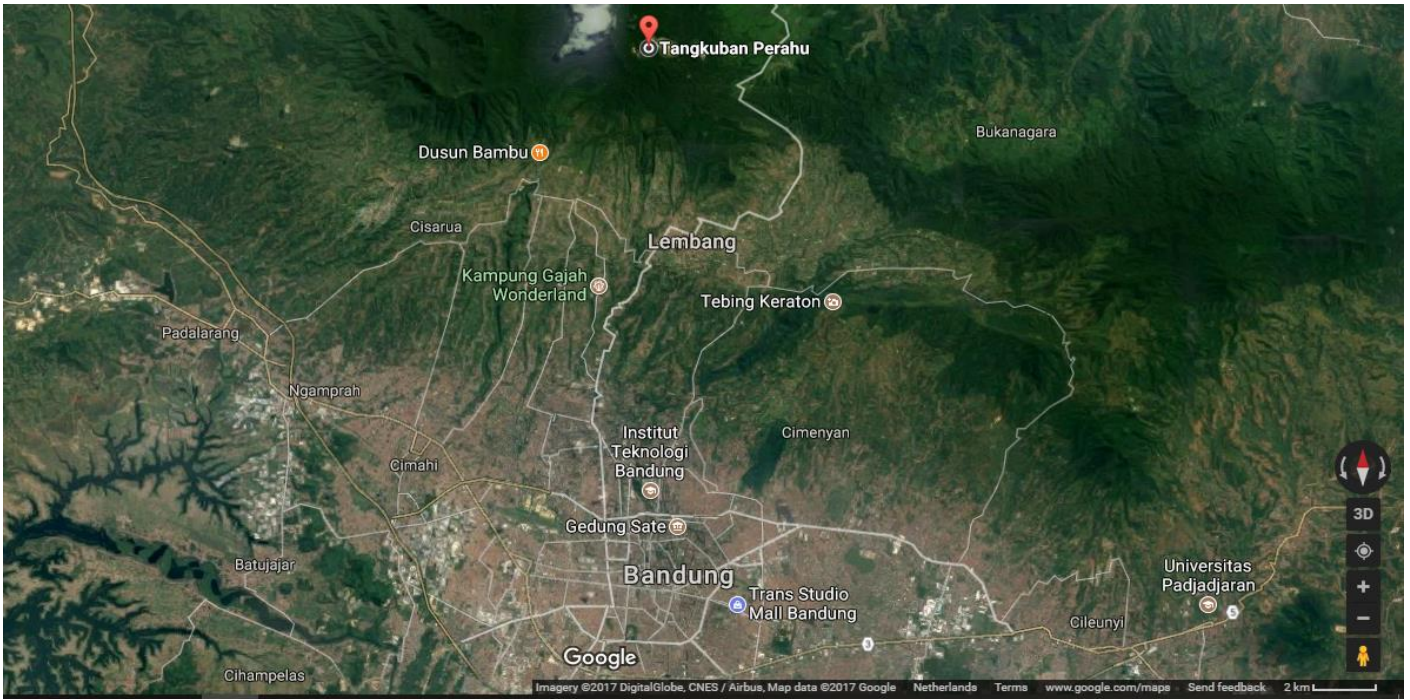
Figure 1 Tangkuban Perahu location from Bandung city

Figure 2 Location of the collected samples (Domas crater)

Figure 3 Domas crater on-site picture

b. Reynisfjara Beach – Iceland

The columnar basalt in this beach extend eastward along the shoreline and form the large vaulted cavern called Halsanefshellir Cave (as showed on the Figure 5 below). The sample rock was taken from the cave. The author took the loose block which have come loose by natural process, hammering the cave wall could induce fractures. Yellow star in the second image below represents the location where the sample rock was taken.
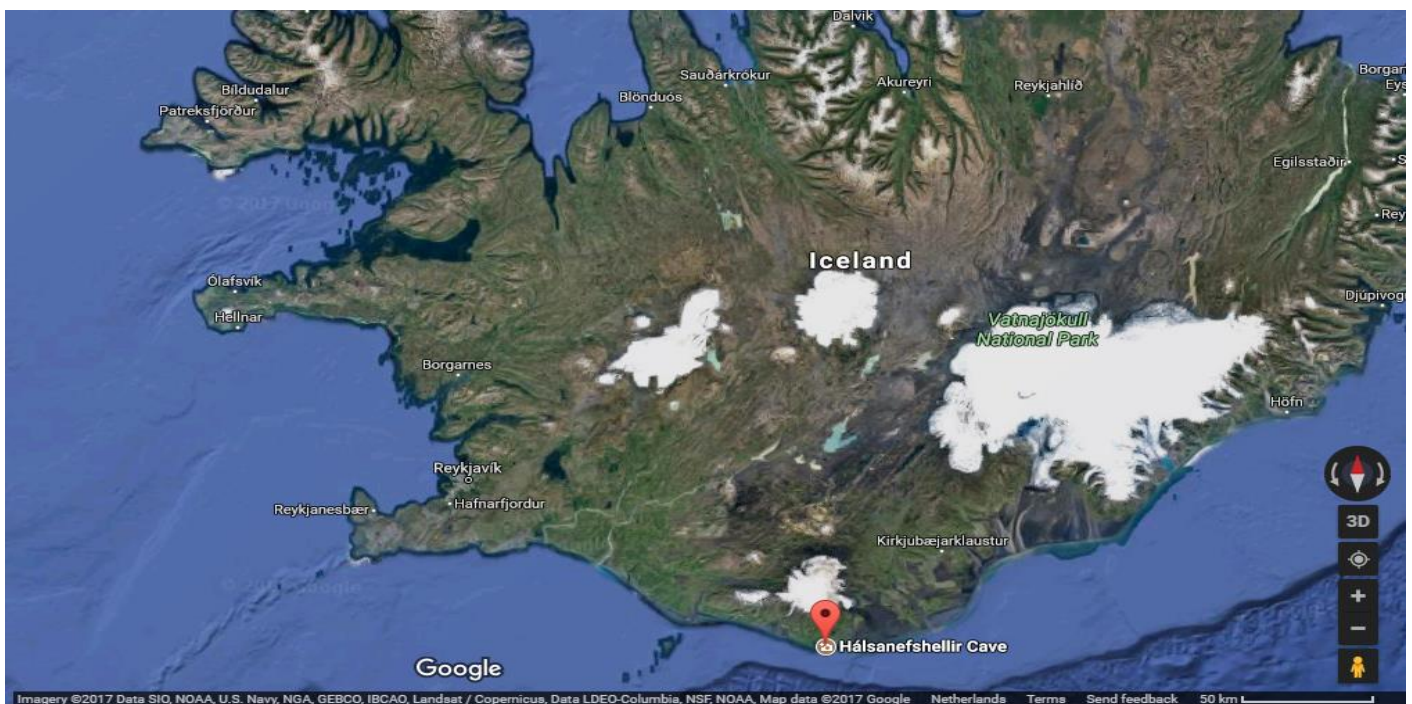
Figure 4 Halsanefshellir cave location (Reynisfjara beach)

Figure 5 On site picture of Halsanefshellir cave

3. Eifel (Germany) and Benin (West Africa)

Basalt rock from Eifel and granite from Benin were both available in the CITG basement for the research project. There was no site visit to collect the sample. Eifel is located in the western part of Germany and to the south from the Netherlands. The sample rock in Eifel was taken around the mining area. The granite rocks were taken in the Adeoti and Colas mining area and were distributed to the Dutch offshore dredging company. These rocks were merely used to do laboratory test before using the limited rock samples from Indonesia fields.

Figure 6 Eifel location from other big cities in Germany

2. Methodological Approach

2.1 Sample Preparation

There are 5 rocks used in this thesis: basaltic andesite Tangkuban Perahu (Indonesia), andesite Tangkuban Perahu (Indonesia), basalt Eifel (Germany), basalt Reynisfjara (Iceland) and granite Benin (West Africa). These rocks are taken from different locations and posses different characteristic. All samples have been collected on the surface outcrops. No drilled cores have been used for the experiment. Granite Benin was collected from the offshore dredging location, basalt Eifel was from the adjacent location of the mining area and the basalt Reynisfjara was collected on the spot on the basalt cave. For both rocks from Indonesia, they were collected from the original geothermal field where the fumaroles existed. The rocks from Tangkuban Perahu are quite diverse. It contains some different types of rocks such as basaltic andesite, andesite and pumice. In this case, pumice cannot be drilled due to its fragility. The pictures of the original rocks can be seen at the appendix (Appendix 2: Original rocks).

The core size for this experiment is ideally 60 millimeters (mm) length with 30 mm diameter. The diameter should be at least 10 times of the average of the grain size in the rock and the length to diameter ratio is 0.5:1 (Ulusay, 2015). In terms of the flatness, the end of the core should be within an error of 0.02 mm and not beyond 0.001 rad or 0.025 mm in 25 mm perpendicular to the axis of the core (Ulusay, 2015) . However, practically the limitation value of the angle on the Soiltest engineering test equipment is within 10 degrees. It limits the length difference between the cylinder surface (as the diameter surface remains constant based on the cylinder block used during the core drilling) in order to give a uniform force during compaction. All cores are measured below 10 degrees before proceeding to the next experiment activity. The criteria of the straightness, parallelism, and flatness should be within the tolerance.

An additional treatment was done to the andesite rock from Tangkuban Perahu because the pycnometer did not work for this rock. It was estimated that the rock has much alteration that restrains the ultra-pycnometer chamber to reach a stable pressure. Pycnometer works by employing the Archimedes' principle of fluid (gas) displacement and the technique of gas expansion (Micromeritics Instrument Corporation, 2001). The measurement stops when the pressure change of helium in a calibrated volume is stable, but it was not the case. The reason of the not-functioning pycnometer remains unknown. One of troubleshooting was to immerse the sample cores into a volume of water for a period of time (3-4 hours) and put it in the oven (40ºC) for a day to remove the water. However, the treatment did not overcome this issue and the porosity measurement was conducted by compiling the single runs.

In terms of the orientation, basalt rock from Eifel (Germany) is quite unique than the other basalts (Iceland and Tangkuban Perahu) because it has a columnar shape. Due to its creating process that was associated with the pressurized and depressurized cycle (P.Y., 1994), the author would like to see whether the characteristic of the basalt columnar rock is different between different orientation. Therefore, the X, Y, Z planes are introduced in this experiment to see the isotropy characteristic of the rock.
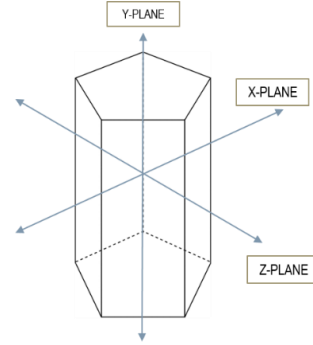
Figure 7 Columnar basalt rock from Eifel (left) and illustration of the basalt three different planes (right)

This orientation application is only applied to the basalt rock from Eifel because other basalt rocks do not have a columnar shape and those rocks are considered as isotropic in the whole rocks. The cores from all types of rock can be seen below.

Figure 8 Tangkuban Perahu basaltic andesite cores (left) and andesite cores (right)

Figure 9 Eifel basalt cores (left) and Benin granite cores (right)

Figure 10 Reynisfjara basalt cores (left) and Tangkuban Perahu pumice rock (right)

Other 2 core sets from Tangkuban Perahu (basaltic andesite and andesite) and two (only) sample cores from Reynisfjara were drilled and cut for the Brazilian test. Each core's diameter size remained the same with the previous core (30 mm). However, the length is cut around 15 mm (length) to set the strip loads covers the

core's periphery. The ratio of the diameter over the length is now 1:0.5 (reversed to the cores for the UCS test).

2.2 Disqualification of the Sample

In the making process, some rocks resulted in a non-straight shape (bent). Some cores do not have flat end surfaces. Grinding machine in the geomechanics basement lab is capable in flattening certain type of rock with certain strength. However, due to its excessive strength, some basalt and granite rocks took longer time in grinding the surfaces or even could not give a parallel result. Those cores, with excessive unparalleled surfaces, are kept as the backup or used for the XRD/XRF and Electron Microprobe Analyzer (EMPA) measurements.

2.3 Matrix Density, Porosity and Permeability Measurement

2.3.1 Matrix Density and Porosity Measurement

The pycnometer determines the density and porosity measurement based on the pressure change of the helium in the calibrated volume. The matrix density can be automatically derived after the mass value has been entered prior the run. In using the pycnometer, gas is ideally used as the displacing fluid due to its ability to penetrate the finest pores. Research grade helium is the recommended gas because of its small atomic covalent radius of 28 pm (or 2.8^{10-8} mm) and its characteristic as an ideal gas (small intermolecular forces) (Oliveira, 2012).

In order to have a sufficient density measurement, the volume used is not the bulk volume as it has pores inside. It uses the true volume of the solid particle (matrix or grain volume) that is measured by the pycnometer. Grain volume can be precisely determined if the water absorption is negligible as it can cause error 1-2% of the grain density (Manger, 1966). All the cores are considered dry because the density measurement was conducted after the core was storaged in the oven ($40^{o}C$) for at least 24-hours.

To calculate the porosity, the bulk volume (that was measured by the caliper, assuming ideal cylinder shape), minus the true volume of solid particle (measured by pycnometer) and devided to the bulk volume will give a percentage value of the porosity. Another porosity measurement methodology is quantifying the CT-Scan result. This method is quite tricky because the tiny pores can be considered as noises. The two methods can be compared to have a porosity range.

The density and porosity are measured before and after heating treatment to see the difference between those times. The procedure started with only one-cycle method (meaning it consists of one-time heating-cooling procedure) and followed by three-cycles method. The three-cycles method is only applied to the basalt Eifel as a trial to check whether three cycles gives a different result to the one-cycle method. After the heating, the

cores were left for a night inside the oven (with temperature 40ºC) in the laboratory to assure the fluid (water) inside the core is totally evaporated. The density result after the heating treatment is coming from the new mass and the new volume matrix. The density result should be compared to the volume bulk later (not the volume matrix) to observe its relation with the change of the porosity.

2.3.2 Permeability Measurement

The core permeability is measured by using the Ruska Gas Permeameter. The measurement works by flowing the Helium gas through the core and observe the pressure drop and the temperature of the gas entering the core. Each core is fitted to the rubber sleeve in order to prevent any gas flowing outside the core. There are three pressure-drops used in this experiment: 0.25, 0.5 and 1 atmosphere. By measuring each core's length and diameter, the permeability value can be obtained by using the Darcy's Law:

$$k = \frac{\mu Q L}{A \Delta P}$$

Where the k is the permeability of the sample in Darcy (or $0.9869x10^{-12}\ m^2$, μ is the air viscosity (0.018 cp at ambient conditions), L is the length of the core in m, A is the cross-sectional area of the core in m^2, ΔP is the pressure gradient from the pressure indicator in Pa and Q is the air flow in cc/sec that can be read from the flow meter graphs below (only the air flow at 0.5 and 1 atm are used for the correlation).
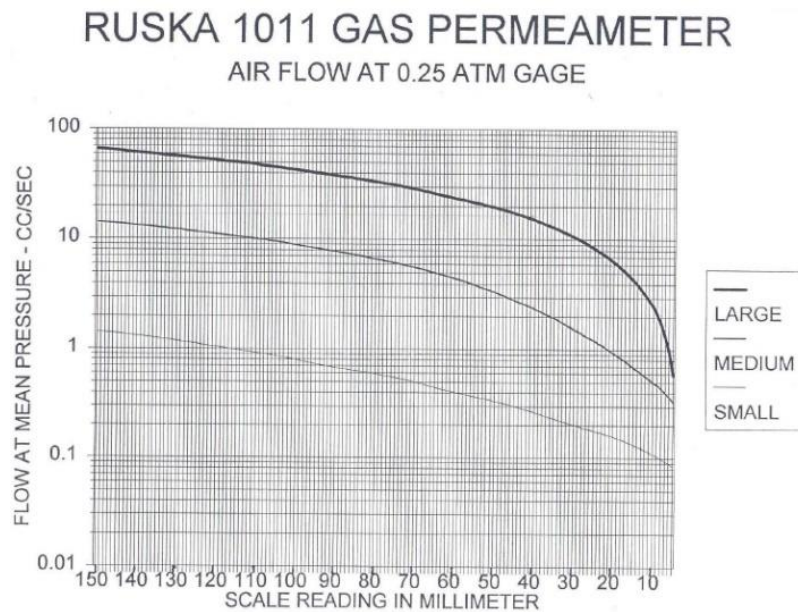
Figure 11 Flow meter reading at 0.25 atm

RUSKA 1011 GAS PERMEAMETER
AIR FLOW AT 0.5 ATM GAGE
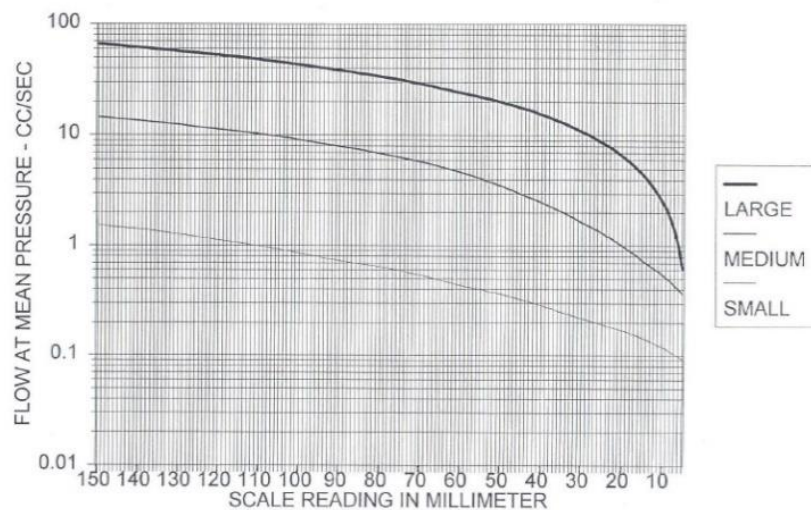
Figure 12 Flow meter reading at 0.5 atm

RUSKA 1011 GAS PERMEAMETER
AIR FLOW AT 1.0 ATM GAGE
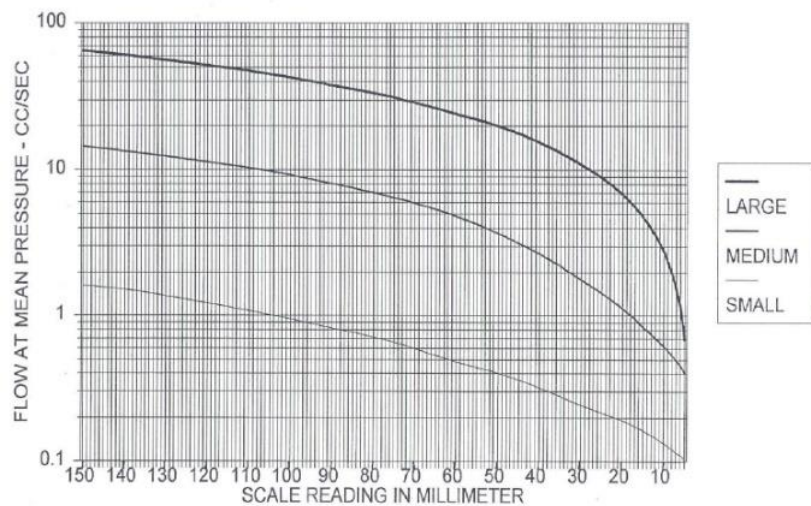
Figure 13 Flow meter reading at 1 atm

Darcy's Law used liquid in determining the permeability through the porous media. In this experiment, gas is used due to very small porosity values. Thereafter, the reading from the flow meter before the heating treatment is also very small (most of the cores have below detection value in all three pressure-drop graphs). Due to gas is used in this experiment, with pressure flow at below and equal to 1 atm, the overestimated permeability may existed in this practical. It is because the gas slippage effect in the small pores called Klinkenberg effect. Klinkenberg considered the mean free path that is inversely propotional to the pressure (Klinkenberg, 1941). At the small pressure, the mean free path of gas particle is longer thus it lets the permeability is showed higher.

2.4 Micro-CT Scan Sample Core

Some sample cores are scanned before and after the heating treatment by using the micro-Computed Tomography (CT) scanner. The output from the micro-CT scanner is the 3D voxels that can be used to visualize the core inner part. The voxel data was optimized by using the VGStudio Max software to provide half resolution data to ease the visualization process afterwards.

The main objective of using the micro-CT scanner is to observe the thermal induced fractures or cracks after the core is exposed to the certain thermal shock. Qualitatively, the observation will be focused on the fracture orientation. Quantitatively, some parameters can be obtained by using Avizo software, such as pore size, porosity distribution and macro fracture angle. The micro fracture direction is not possible to be detected with the micro-CT scanner as the scan resolution (30 µm) is still higher than the microfractures size (1-5 µm).

Tangkuban Perahu basaltic andesite and andesite rock are represented by 1 core with the highest possible exposed temperature, which have two time scanning before and after treatment. Granite Benin and basalt Eifel have 4 cores that represents each different thermal shock (from 200°C to 500°C) with increase every 100°C respectively. Basalt Reynisfjara cores are not scanned in order to focus on the other rocks. In addition, there are 2 small cores (5mm diameter and 30mm length) represent Basaltic andesite and Andesite Tangkuban Perahu were scanned to see the difference between outside and inner cores.

Figure 14 Small size core illustration (left) and small size cores from Tangkuban Perahu heated at 500°C (right)

In advance application, Avizo software gives the porosity value by analyzing and characterizing the pore space. The Volume Fraction module can be connected to the output of the axis connectivity module to get the amount of the connected porosity. In addition, the same module can be connected to the output of Auto Thresholding module to obtain the total porosity. The visualization of the connected and non-connected pore spaces also can be seen further. Followed by the porosity, once the grain diameter is known from the software, the absolute permeability can be derived by applying the Carman-Kozeny formula. However, these measurement methods required another license thus the porosity values are obtained by applying the thresholding and adjusting the intensity range only.

2.5 Thermal Microcracking Experiment

The thermal shock, occurred when the sample cores were exposed to high temperature difference suddenly, gives a result in creating or extending the cracks and increase the fluid pathway that connect to the network of the natural fractures (Enayatpour & Patzek, 2013).

Prior experiment, the water temperature is recorded by the temperature sensor and it showed a stable value between 16 to 19°C. Practically, to create the thermal shock, the cores that have been heated in the oven (at certain temperature) were plunged into a bowl of water within a second. Afterwards, the heat conduction at the water (2L volume of water) and the temperature of the cores were recorded.

Figure 15 Oven to heat the cores (left), thermal shock creation process (middle), temperature sensor (right)

Initially, the experiment used two thermos sticks to measure the core and the water temperature. However, after several runs, the record of core and water temperature do not show a valid value by some reasons.
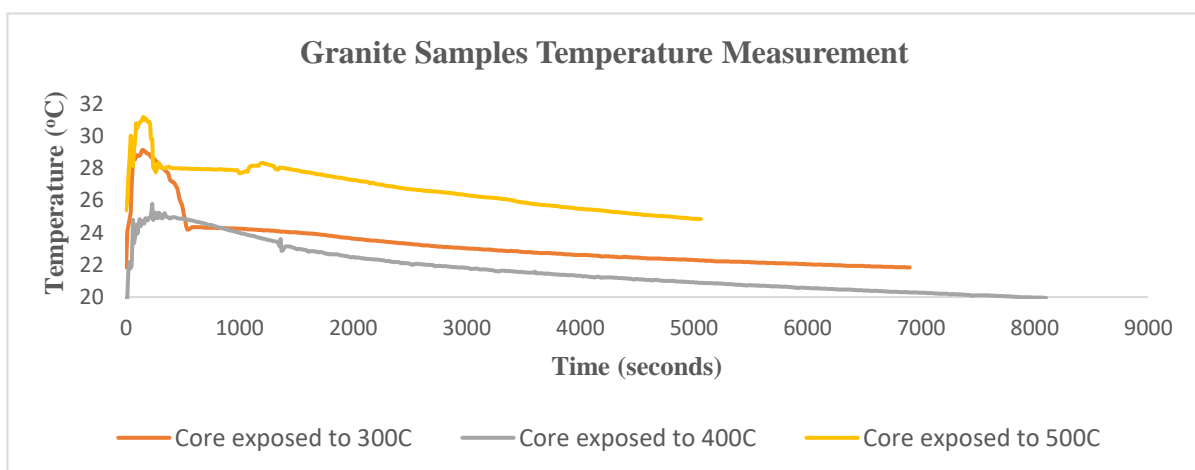
Graphic 1 Record of the core temperature change inside the water

First, the core temperature only shows the value after the cores were saturated inside the water (there is no proper device to measure the direct change from high to low core temperature). Second, the water temperature decrease is affected by ambient temperature. It is also affected by time shifting during the experiment. The temperature in the evening is lower than at noon. Third, the stick to measure the water temperature is located constantly around 2 centimeters from the core but it does not represent the whole water temperature in the bowl. Hence, based on these three reasons, the core and water temperature measurement after the heating treatment were terminated.
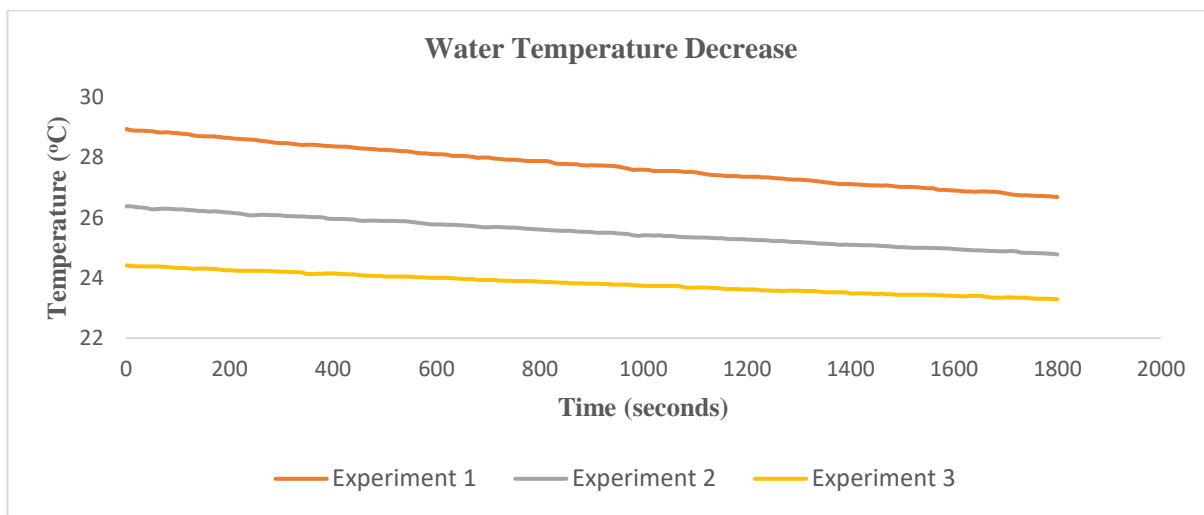
Graphic 2 Water temperature decrease rate

After the first heating treatment, followed by the porosity measurement, it was considered to see whether the cyclic procedure will affect the rock characteristic or not. Hence, three-cycle method was introduced to basalt Eifel as the preliminary test. The three-cycles means there are three repetitions before the core is tested in the UCS machine. The porosity and permeability are measured in every cycle to see the differences between before and after heating treatment. In addition, the cycles will determine the trend of the characteristic change over the number of treatment.
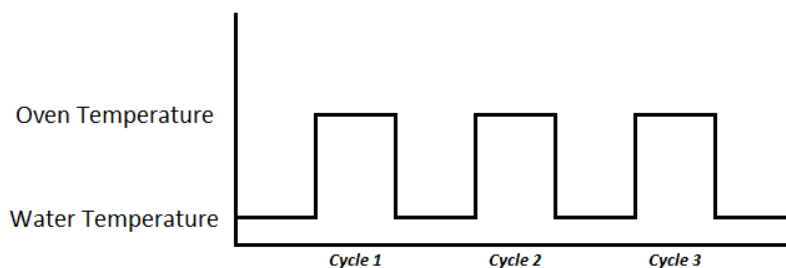
Figure 16 Illustration of three-cycle method

Core Temp (°C)	Water Temp (°C)	Difference(°C)
200	18.75	181.25
300	15.97	284.03
400	19.5	380.5
500	18.75	481.25

Table 1 Thermal shock temperatures for all cores

2.6 Unconfined Pressure Experiment and Static Elastic Moduli

Unconfined pressure practically means the core is under room pressure (or zero confined pressure) during the compression test. All deformation tests were done at room temperature (stable around 20°C). Some cores were set with the sonic acoustic cup to measure the wave propagation properties during compression. A small amount of shear coupling gel was smeared in the contact between the core surface and the cup surface. However, after the granite Benin and basalt Eifel have been tested, the acoustic cup deformed due to high load required to break the basalt. The new cup with the extra strength material has been made and used for the rocks from Indonesia and Iceland. It should not generate much differences during the acoustic measurement between difference cup.

In terms of the compression test, there are three values needed to review its strength or characteristic. The first one is the ultimate compressive strength (UCS) which describe the maximum load the core can withstand before it deformed permanently. The second one is the Young's modulus. It calculates the ratio of the stress applied to the axial strain produced. Third, the Poisson's ratio that is a ratio of lateral strain over the axial strain. The last two rations present the core elasticity behavior after different heating temperatures.

The Uniaxial Compressive Strength (UCS) machine is equipped with the hydraulic power supply, load frame, load cell, extensometer (strain measurement), controller (strain, load) and a computer. The axial strain is measured by the axial extensometer by using a pair of Linear Variable Differential Transducer (LVDT) which provide the actuator displacement. The radial strain is measured by using the circumferential extensometer that is put in the middle of the core during the experiment. To check whether the circumferential extensometer is in the proper place, the reading of the voltage that is created by its chain should be around -1.3 to -1.4V. This value represents the position of the chain is correctly perpendicular to the core's length direction and to show that the core diameter is in uniform size (some non-usable cores have a bent shape).

After the sample core is set with the sonic acquisition cup, the core is put in the center of the load chamber. The hydraulic pressure is applied step by step (by using the small movement button) to stand the core properly. The load protector in this step is set to maximum 2 kN to avoid any creation of premature crack. Once the core stands properly, the LVDT is set into a minimum contact as a zero basis. The reading of the axial stress and the three strains (axial, radial and volumetric) should be reset in one of the software window (to simulate the

initial condition). The step is followed by starting the program and drive the core to force contact. The axial load is keep increasing and the first crack is observed. In order to obtain the ultimate compressive strength, the axial load is keep increasing until the stress shows significant decrease value (a jump).

In some cases, the radial extensometer that was attached to a core was thrown away and the sample is broken. This phenomenon happened because the elastic zone of the core has been reached at high force load (>200 MPa). Therefore, the load frame must be completed with an impact resistant transparent door to keep the extensometer and core debris inside the load chamber. Another safety procedure is also applied to the axial load by setting the maximum value of the LVDT movement to 2 mm of axial displacement. This value represents the maximum position of the LVDT from the zero basis as it moves vertically down-top direction. Once it reaches the safety value, the UCS machine will stop automatically.

There are two ways to stop the axial loading force, either directly stop the load force or gradually decrease the axial load so that the remaining force is removed from the program. After the axial load is removed, the movement plate will be positioned back to the zero basis. By shutting down the hydraulic pressure, the tested core can be removed. The produced data did not include the steel strain in the axial strain data and the extensometer correction in the radial strain data. Therefore, the corrected axial and radial strain should be used in the analysis.

a. Steel Strain Calibration for the Axial Strain Correction

The iron hard steel metal was used during the compressive strength test. It has its own strain value over the compressive stress applied and was obtained from the calibration process in 2015 (Primarini, 2015). The calibration gives the equation of the iron hard steel which the measured axial strain subtracted this value in order to have the corrected axial strain values.
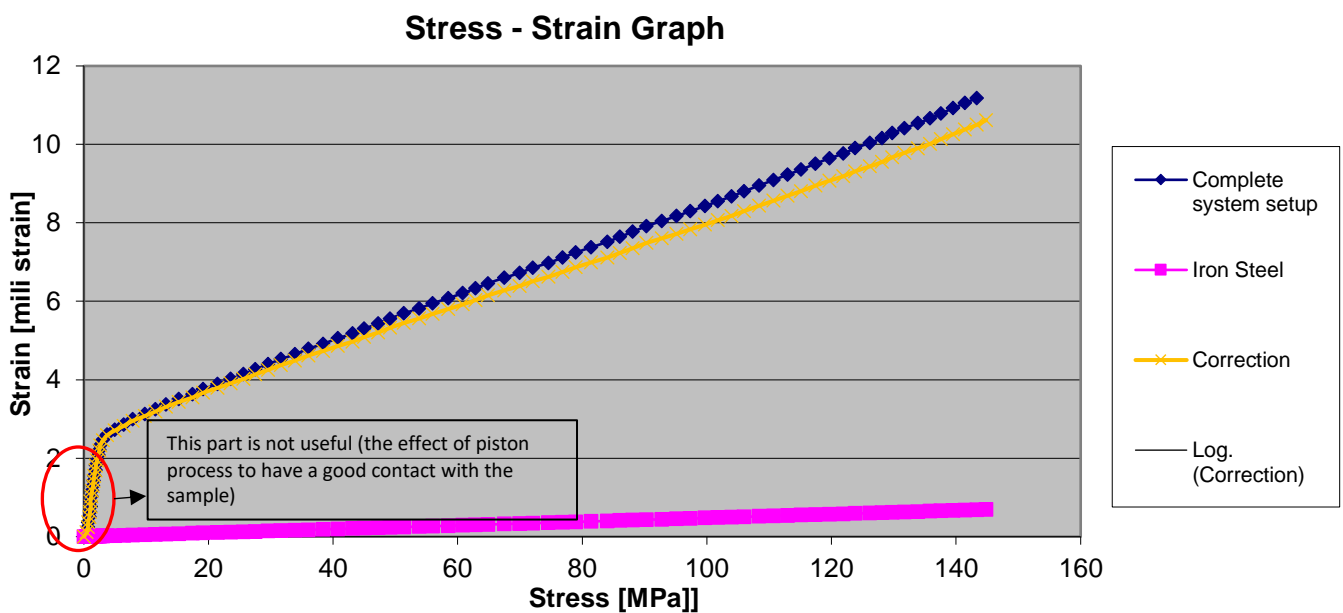
Graphic 3 Iron metal initial calibration chart with the deviator stress

The deviator stress in the initial phase of the calibration should be removed as it did not have the proper contact with the sample core. Therefore, the initial data range is removed from the Graphic 3.

Stress - Strain Graph
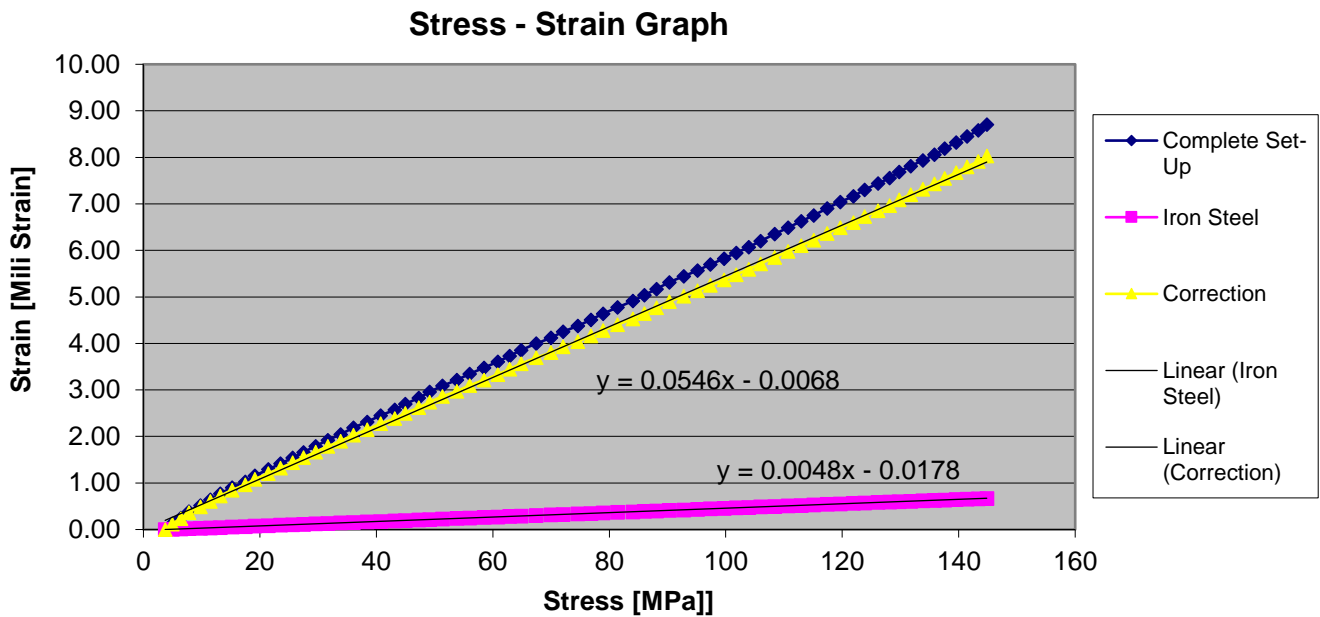
Graphic 4 Iron metal final calibration data

The calibration data above shows the strain (millistrain) as the y-coordinate and stress (MPa) as the x-axis. It is in the reverse way from the common stress-strain graph, therefore, the calibration equation from the graph should be reversed as well. The equation calibration that is used to correct the measure axial strain is $y = 210000x + 3.7282$ and it is applied in the data table.

a. Circumferential Extensometer Strain Calculation for the Radial Strain Correction

When the compression force was applied to the sample core, the core was not only deforming axially but also radially. In that situation, the extensometer only measured the change chord length between the center of the two end rollers ($L_f - L_i$). It does not measure the change of the core radius directly (MTS Manual Book). Therefore, the correction should be applied in the measured radial strain.
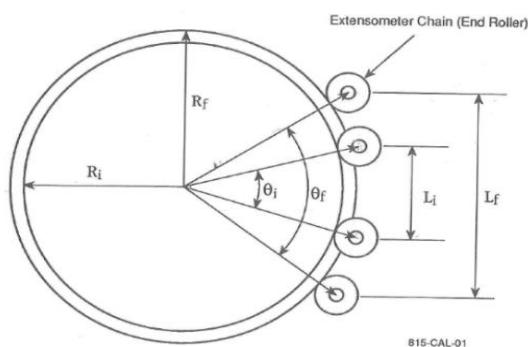
Figure 17 Extensometer chain

In this normal test analysis, iterative procedure is not used to obtain the exact values of change of core circumference. First step to do is to calculate the angle (θ_i)subtended by chord length and then calculate the change of core circumference (ΔC). The final formula of the change in the angle and the core circumferences can be seen below.

$$\theta_i = 2 \arcsin \frac{L_i}{2(R_i+r)} \quad \text{and} \quad \Delta C = \left[\frac{\Delta L \pi}{\sin\left(\frac{\theta_i}{2}\right) + \left(\pi - \frac{\theta_i}{2}\right)\cos\left(\frac{\theta_i}{2}\right)} \right]$$

Where L_i is the initial chord length, R_i is the initial radius of the core and r is the radius of the roller. After the ΔC is calculated, it is compared to the ΔL to find the radial strain correction factor and multiplied it to all the measured radial strain data. Some examples are showed below and the complete data can be seen in the appendix chapter.

				Circumferential Strain Correction									
				Reading from the result									
Core ID	Rock Type	Orientation	Li	Chain Initial	Chain final	Delta L	Ri	r	Li/(2(Ri+r))	tetha (θ) in radian	Circumference Change (ΔC)	% Difference	Speed
TPB01	Basalt (Tangkuban Perahu)	n/a	24.00	22.04	22.66	0.62	14.93	2.24	0.70	1.55	0.81	31.31	0.0009
TPB02	Basalt (Tangkuban Perahu)	n/a	23.20	22.01	22.28	0.27	14.90	2.24	0.68	1.49	0.35	28.63	0.0009
TPB03	Basalt (Tangkuban Perahu)	n/a	24.10	22.01	22.45	0.44	14.90	2.24	0.70	1.56	0.58	31.84	0.0009
TPB04	Basalt (Tangkuban Perahu)	n/a	23.30	21.98	22.08	0.11	14.87	2.24	0.68	1.50	0.14	29.11	0.0009

Table 2 Example of the calculation of the radial strain correction factor

In addition, several photographs were taken before and after the testing. It is being used to complement the CT-Scan result and some photographs could show the failure mode. The complete image can be seen in the appendix chapter.

2.7 XRD and XRF Analysis

X-ray Diffraction (XRD) and X-ray Fluorescence (XRF) methods are applied to identify the mineral phases and the whole chemistry (expressed in oxides) of the rocks used for the experiments of the thesis. The XRD patterns interpretation provide a semi-quantitative interpretation of the minerals constituting the samples (in weight %) while the XRF deliver the bulk chemistry (major oxides) of the whole sample.

The rocks were grinded in order to obtain the fine and homogeneous powder. The granite's orientation, in this thesis, is not relevant for the further analysis hence the rock was cored without orientation specification whereas basalt has its specific cooling processing form which the orientation is taken into account. The bulk rock of the basalt was formed mainly pentagonal (instead of hexagonal) columnar. Therefore, the powder from the basalt rock analyzed is from three sides: the center side (named as Y-plane orientation) and the boundary sides (named X-plane and Z-plane orientations).

In total, only granite Benin, basaltic andesite and andesite cores from Tangkuban Perahu are examined for the XRD and XRF analysis. Each core is stored in the oven under temperature around 40°C for at least a night prior delivery to the laboratories (3ME Delft and ITC Enschede). The focus on this examination is to see the difference of the material minerology-geochemistry before and after the heating treatment. Most of the cores showed different rock characteristics after the treatment based on their porosity and permeability measurement. Another concern is the core was plunged into a bowl of water after it is heated in order to create the thermal

shock. The contact of the rock material to the water is indicated affected the changing of the material structure (will be investigated by the CT-Scan) or component.

2.8 Brittleness Index

The Brittleness Index (BI) is being used to evaluate the hydraulic fracturing possibility. Brittleness is defined as the lack of ductility or its inverse (Hetenyi, 1966). The quantification method to determine the BI value has been published in many ways until today. There are 25 formulas listed (P.G. Ranjith, 2016) based on each test method and variable declaration. In this thesis, there are several ways in determining the BI values due to limited sample core availability, the list of the method can be seen below.

1. Rickman (2008) determined the brittleness index by using the Young's modulus (E) and Poisson's ratio (v) variables as the combination. The brittle rock condition is represented by the higher value of Young's modulus and lower value of Poisson's ratio, otherwise, the rock is considered as ductile (Rick Rickman, 2008) . The higher the brittleness index represent its easier application of the hydraulic fracturing on that specific rock.

$$BI_R = \frac{\frac{(E - E_{min})}{(E_{max} - E_{\min})} + \frac{(v - v_{\min})}{(v_{max} - v_{\min})}}{2}$$

E_{min} and E_{max} are the minimum and maximum Young's modulus value and the v_{min} and v_{max} are the minimum and maximum Poisson's ratio value for the specific cores. This formula needs more than 1 sample core to obtain the minimum and maximum value. Therefore, only granite Benin and basalt Eifel can apply this formula into further analysis. The basalt rock from Indonesia (including the andesitic basalt) and the basalt from the Iceland only have 1 rock per temperature shock difference, which causes the inefficient analysis by stating one sample core is absolutely easy to be fracture (BI equals to 1) and another sample core is impossible to be fractured (BI equals to 0).

2. Coates (1964), Hucka & Das (1974) and Bishop (1967) used the stress-strain curve to generate the BI values. The difference is Coatas and Hucka & Das used the elastic and plastic strain as the variables, meanwhile, the Bishop method used the peak and residual shear strength respectively. However, due to some sample cores exploded at the ultimate compressive strength (the core is thrown into pieces), it does not generate the residual shear strength. Therefore, the Bishop method will not be applicable for all sample cores. In the other side, some cores do not show the plastic condition where the strain rate is more than 2 µstrain/hour at a 50 percent of the uniaxial strength (Coates & Parsons, 1966) hence the Coates and Hucka & Das method cannot be applied on some sample cores. Due to most of the sample do not have big values of the reversible strain, the Coates formula is not used in this thesis. The BI formulas are listed below.

$$BI_C = \text{reversible strain}/\text{total strain} = BC/AC$$

$$BI_{HD1} = \varepsilon_{elastic}/\varepsilon_{total}$$

$$BI_B = \frac{\tau_{max} - \tau_{res}}{\tau_{max}}$$

Where BI_C is from the Coates method, BI_{HD} is from the Hucka & Das method and the BI_B is from the Bishop method. For the clearer interpretation, the image below illustrates which are the elastic-plastic strain and maximum-reversible strength from the strain-stress diagram of andesite sample Tangkuban Perahu TPD01.
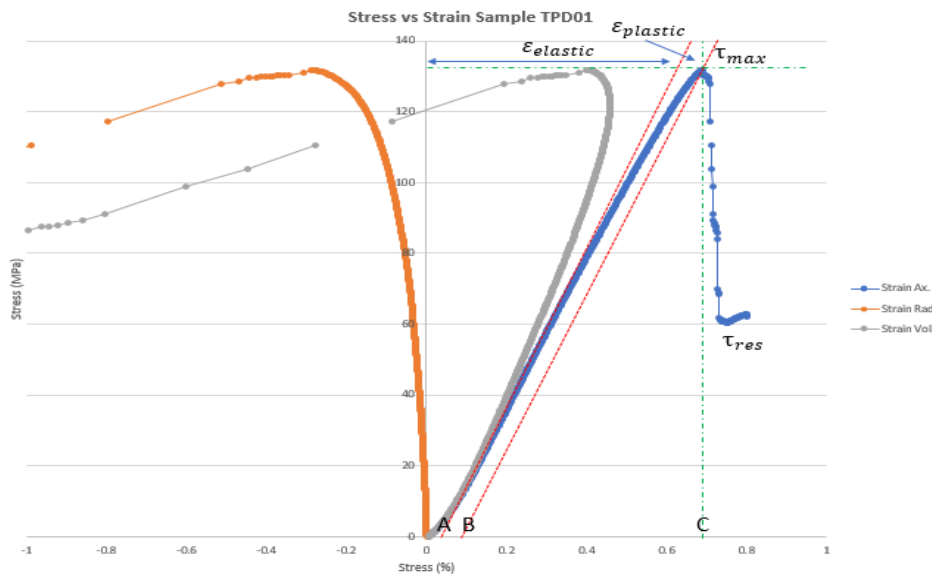
Figure 18 Stress strain curve examples from andesite

In the Hucka & Das method, ε_{total} is the total strain at failure ($\varepsilon_{plastic} + \varepsilon_{plastic}$). And in the Bishop method, τ_{max} and τ_{res} are the peak and residual peak strength.

3. Jarvie (2007) determined the Brittleness Index based on the composition of the rock minerology. It is obtained from the XRD result. Jarvie method focused on the ratio of quartz content over the total clay, carbonate and quartz itself. Despite the thesis 'objective to determine the brittleness index, the XRD was only conducted to see the difference between before and after heating treatment on the highest possible temperature used. Hence the data is not comprehensive due to two temperature conditions were tested (before and after heating treatment). However, due to variance of samples, the correlation can be observed and analyzed.

$$BI_J = \frac{Q}{Q + C + Cl}$$

Where BI_J is the Brittleness Index by Jarvie, Q is quartz, C is carbonate and Cl is the clay.

3. Results

3.1 Core Measurement

Each core is exposed to a particular heating temperature to create a thermal shock. The length and diameter of the core is measured by the digital caliper to see the core expansion / shrinkage due to thermal shock or mineral dissolved in the water. In addition, the density matrix is also analyzed from the matrix weight (by using the digital scale) and the matrix volume (from the pycnometer).

Core ID	Rock Type	Orientation	Temp. Exposed °C	Before Heating Treatment			After Heating Treatment		
				Length	Diameter	Density Matrix	Length	Diameter	Density Matrix
				mm	mm	gram/cc	mm	mm	gram/cc
TPB01	Basaltic Andesite (T.Perahu)	n/a	Room Temp.~20	62.59	29.85	2.68	n/a		
TPB02	Basaltic Andesite (T.Perahu)	n/a	200	60.01	29.81	2.67	60.01	29.80	2.69
TPB03	Basaltic Andesite (T.Perahu)	n/a	300	61.79	29.81	2.66	61.76	29.80	2.71
TPB04	Basaltic Andesite (T.Perahu)	n/a	400	60.43	29.78	2.66	60.33	29.74	2.72
TPD01	Andesite (T.Perahu)	n/a	Room Temp.~20	61.69	29.81	2.79	n/a		
TPD02	Andesite (T.Perahu)	n/a	200	61.50	29.83	2.78	61.49	29.83	2.87
TPD03	Andesite (T.Perahu)	n/a	300	61.29	29.80	2.81	61.29	29.80	2.84
TPD04	Andesite (T.Perahu)	n/a	400	61.23	29.81	2.80	61.26	29.82	2.85
TPD05	Andesite (T.Perahu)	n/a	500	61.13	29.81	2.80	61.15	29.82	2.84
IC01	Basalt Reynisfjara (Iceland)	n/a	Room Temp.~20	59.52	29.81	3.05	n/a		
IC02	Basalt Reynisfjara (Iceland)	n/a	200	61.42	29.81	3.07	61.43	29.79	3.06
IC03	Basalt Reynisfjara (Iceland)	n/a	300	61.49	29.80	3.06	61.69	29.80	3.06
IC04	Basalt Reynisfjara (Iceland)	n/a	400	61.85	29.79	3.06	61.84	29.79	3.07
IC05	Basalt Reynisfjara (Iceland)	n/a	500	61.41	29.80	3.06	61.41	29.79	3.07
TI009	Granite (Benin)	n/a	Room Temp.~20	59.81	29.77	2.64	n/a		
TI012	Granite (Benin)	n/a	Room Temp.~20	63.37	29.75	2.63	n/a		
TI004	Granite (Benin)	n/a	200	59.02	29.77	2.63	59.05	29.8	2.62
TI006	Granite (Benin)	n/a	200	59.97	29.79	2.63	59.02	29.80	2.63
TI001	Granite (Benin)	n/a	300	59.25	29.78	2.63	59.29	29.82	2.62
TI007	Granite (Benin)	n/a	300	60.42	29.8	2.63	60.47	29.82	2.63
TI003	Granite (Benin)	n/a	400	59.79	29.78	2.63	59.93	29.84	2.61
TI005	Granite (Benin)	n/a	400	60.01	29.78	2.64	60.01	29.86	2.62
TI002	Granite (Benin)	n/a	500	60.46	29.76	2.63	60.73	29.88	2.60
TI013	Granite (Benin)	n/a	500	62.26	29.75	2.63	62.45	29.85	2.60
A1X	Basalt (Eifel)	X-Plane	Room Temp.~20	61.91	29.72	3.00	n/a		
A4Z	Basalt (Eifel)	Z-Plane	Room Temp.~20	61.42	29.73	3.00	n/a		
A3X	Basalt (Eifel)	X-Plane	200	62.11	29.73	3.01	62.13	29.72	3.01
A5Z	Basalt (Eifel)	Z-Plane	200	61.97	29.72	3.01	61.97	29.71	3.00
C4AX	Basalt (Eifel)	X-Plane	300	60.38	29.71	3.03	60.38	29.73	3.01
A6Z	Basalt (Eifel)	Z-Plane	300	58.58	29.73	3.01	58.59	29.73	3.00
C5AX	Basalt (Eifel)	X-Plane	400	62.41	29.73	3.03	62.43	29.73	3.01
C1AZ	Basalt (Eifel)	Z-Plane	400	60.09	29.73	3.04	60.09	29.72	3.02
C5BX	Basalt (Eifel)	X-Plane	500	61.8	29.72	3.02	61.87	29.73	3.00
C2BZ	Basalt (Eifel)	Z-Plane	500	59.08	29.73	3.03	59.13	29.74	3.00

Table 3 General core measurement includes length, diameter and density

3.2 XRD and XRF Experiment

The XRD and XRF analysis of the mineral powder is done for basaltic andesite, andesite, pumice rock Tangkuban Perahu and granite Benin.

The experiment for granite Benin was done at the X-ray facilities at the department of Materials Science & Engineering, Delft University of Technology and Ruud Hendrikx is acknowledged for the X-ray analysis.

Meanwhile, the experiment for basalt basaltic andesite, andesite and pumice from Tangkuban Perahu (Indonesia) was done in ITC Lab. Caroline Lieven (ITC laboratory supervisor) and Chiel Welink (tutored by G.E. Damsma from Saxion Enschede) are acknowledged for the experiment report. The XRD analysis results of mineral powder for each rock (from 3ME TU Delft Lab and ITC Lab) are listed in the table below.

Sample	Compound Name	Compound Formula	Percentage
Granite - Benin	Quartz	$Si\ O_2$	28.37
	Albite	$Na\ Al\ Si_3\ O_8$	33.68
	Microcline	$K\ Al\ Si_3\ O_8$	37.95
Basaltic andesite Tangkuban Perahu - Indonesia	Plagioclase	$(Ca, Na)\ (Al, Si)_4\ O_8$	69.4
	Microcline	$K(AlSi_3O_8)$	29.2
	Goethite	$FeHO_2$	1.4
Andesite Tangkuban Perahu - Indonesia	Plagioclase	$(Ca, Na)\ (Al, Si)_4\ O_8$	59.7
	Anorthoclase	$Na,K(AlSi_3O_8)$	36.4
	Ilmenite	$FeTiO_3$	3.9
Pumice Tangkuban Perahu - Indonesia	Quarts	$Si\ O_2$	65.6
	Amorphous Silica	$(Na,Ca,K)_8(Si_6Al_6O_{24})(SO_4)_2(OH)_2H_2O$	26.2
	Rutile	TiO_2	8.2

Table 4 XRD result compilation

The figures below show the measured XRD patterns. The colored sticks assign each peak to a specific mineral phase occurring in the analyzed rock. The matching of each mineral phase with the measured peaks has been performed by using the library data base of the EVA Bucker diffraction Suite program. Some of small peaks could be identified (XRD result report) due to the background noise.
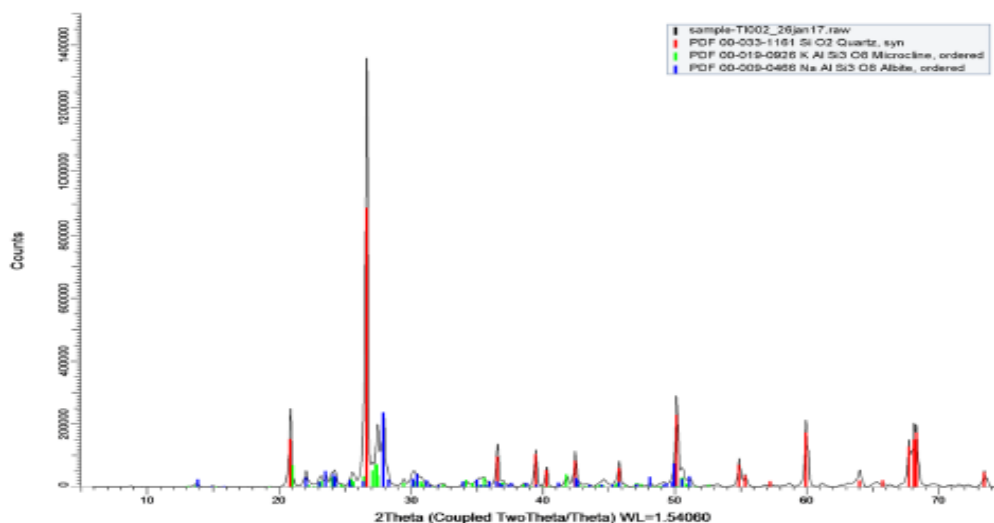
Figure 19 Diffractogram XRD granite Benin
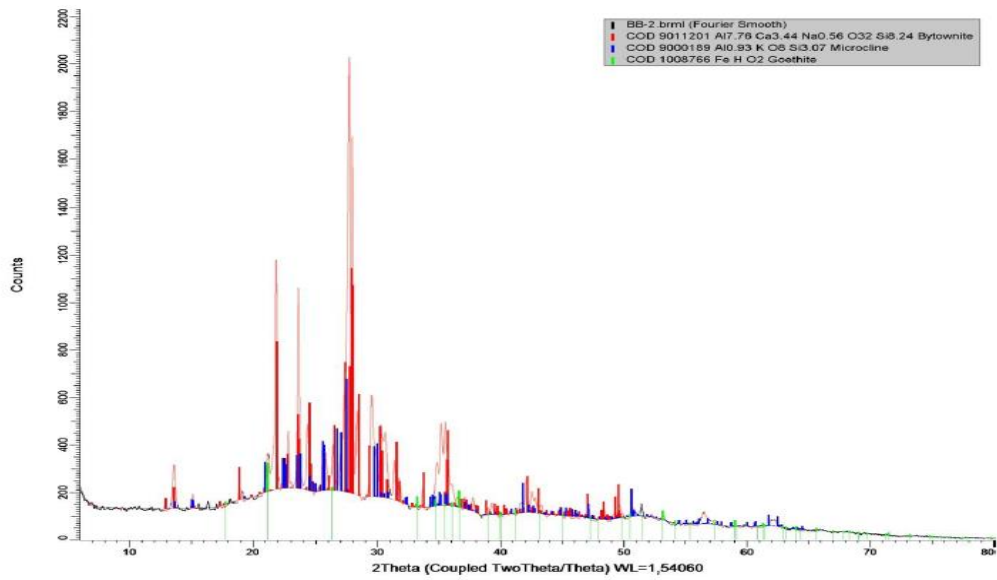
Figure 20 Diffractogram XRD basaltic andesite Tangkuban Perahu
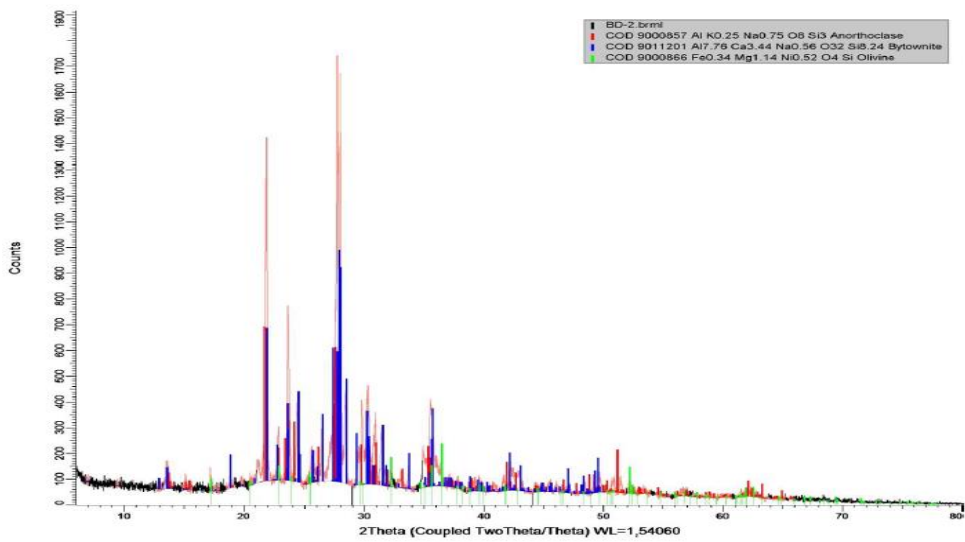
Figure 21 Diffractogram XRD andesite Tangkuban Perahu
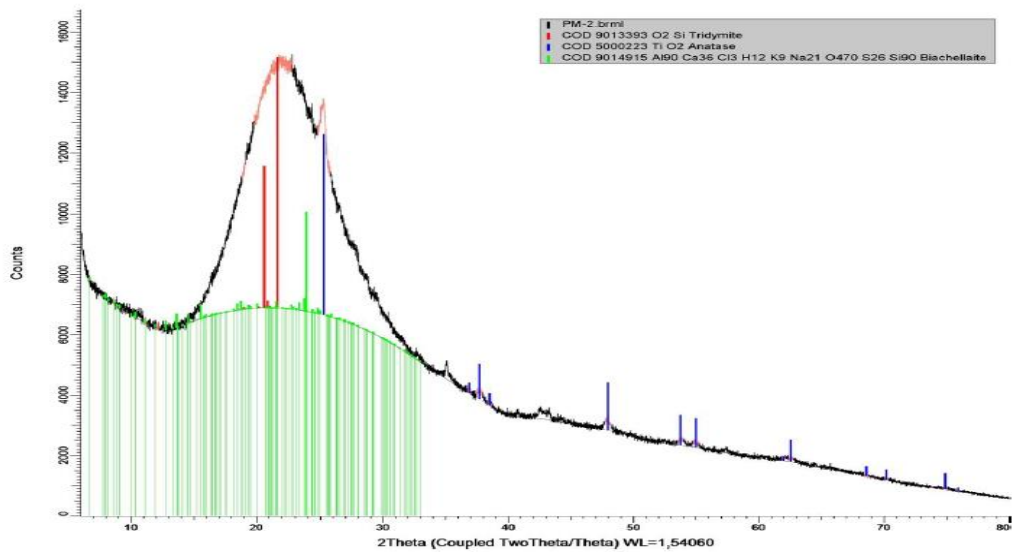
Figure 22 Diffractogram XRD pumice Tangkuban Perahu

The XRF analysis of granite Benin shows the mineral composition as below:

Granite - Benin	
Compound	Percentage
SiO2	75.474
Al2O3	11.451
Fe2O3	4.143
Na2O	4.122
K2O	2.368
NiO	0.861
CaO	0.736
SO3	0.252

Compound	B.Andesite	Andesite	Pumice
	Percentage	Percentage	Percentage
SiO2	53.37	62.23	109.89
MgO	3.59	3.92	0
FeO	7.97	7.62	0.99
AlO	15.85	18.96	4.19
P2O5	0.63	0.42	0.28
TiO2	0.97	0.68	1.95
CaO	5.5	7.9	0.29
K2O	2.66	1.42	0.79

Table 5 Compound percentage granite Benin (left) and all Tangkuban Perahu rocks (right)

The compound order between granite Benin and others is differentiated to ease the reading (the order is based on the original report from each institution).

3.3 Electron Microprobe Analyzer (EMPA)

Basaltic andesite, andesite and pumice rock from Tangkuban Perahu are the only rocks which was set up in the EMPA device. Each of the rock block has its own fracture characteristic and mineral composition which can be directly observed. Some of the features are selected in order to specify main points in the interpretation and the rest of the features are put in the appendix chapter. Dr. Franziska Wilke as the Electron Microprobe laboratory supervisor and Oona Appelt as the technical support are thanked for guiding the author in operating the machine and determining the specific points in the thin section to be examined.

1. Basaltic andesite – Tangkuban Perahu
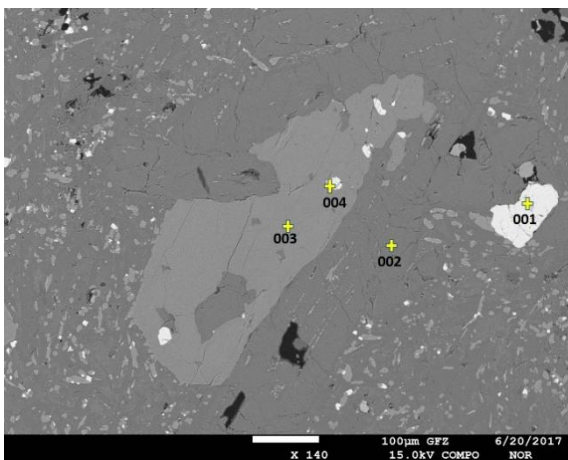
001: **Ilmenite** with MgO (1.81%), Al_2O_3 (2.87%), TiO_2 (18.40%), FeO (76.92%)

002: **Plagioclase** with CaO (15.89%), Na_2O (2.60%), Al_2O_3 (31.93%), SiO_2 (49.58%)

003: **Pyroxene** with CaO (20.04%), MgO (14.76%), Al_2O_3 (1.67%), SiO_2 (51.82%), FeO (11.71%)

004: **Ilmenite** with MgO (1.94%), Al_2O_3 (3.53%), TiO_2 (15.84%), FeO (78.69%)

Figure 23 Selected point 1 basaltic andesite Tangkuban Perahu

001: **Olivine** with MgO (21.17%), SiO$_2$ (34.4%), FeO (44.43%)

002: **Ilmenite** with MgO (1.77%), Al$_2$O$_3$ (2.57%), TiO$_2$ (20.58%), FeO (75.08%)

003: **Ilmenite** with MgO (1.00%), Al$_2$O$_3$ (2.10%), TiO$_2$ (23.11%), FeO (73.79%)
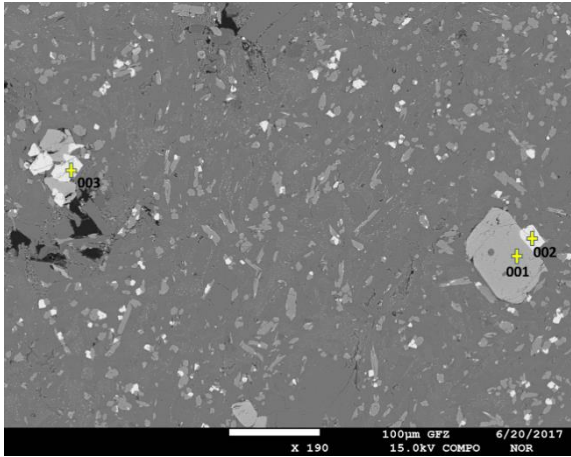
Figure 24 Selected point 2 basaltic andesite Tangkuban Perahu

2. Andesite – Tangkuban Perahu

001: **Ilmenite** with TiO$_2$ (19.08%), FeO (80.92%)

002: **Plagioclase** with CaO (11.11%), Na$_2$O (5.12%), Al$_2$O$_3$ (28.35%), SiO$_2$ (55.41%)

003: **Clay** with CaO (7.08%), MgO (8.59%), Al$_2$O$_3$ (19.22%), SiO$_2$ (39.99%), TiO$_2$ (3.25%), FeO (21.87%)

004: **Clay** with Al$_2$O$_3$ (46.85%), SiO$_2$ (53.15%)
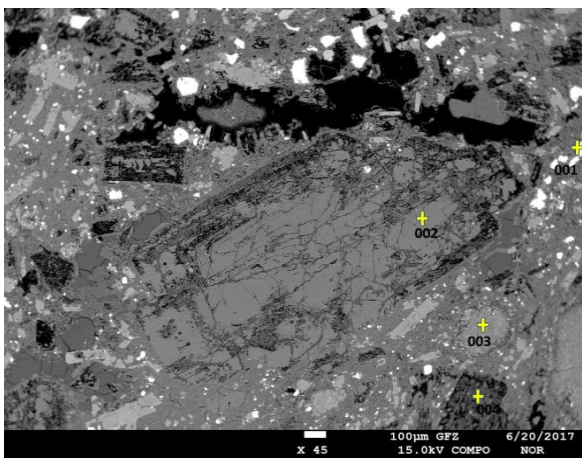
Figure 25 Selected point 1 andesite Tangkuban Perahu

001: **Plagioclase** with CaO (6.60%), Na$_2$O (6.81%), Al$_2$O$_3$ (24.05%), SiO$_2$ (61.39%), K$_2$O (1.14%)

002: **Pyroxene** with CaO (19.65%), MgO (15.19%), Al$_2$O$_3$ (2.08%), SiO$_2$ (51.77%), FeO (11.31%)

003: **Plagioclase** with CaO (12.42%), Na$_2$O (4.30%), Al$_2$O$_3$ (29.26%), SiO$_2$ (54.02%)

004: **Magnetic goethite** with MgO (1.89%), Al$_2$O$_3$ (2.55%), TiO$_2$ (3.15%), FeO (92.41%)
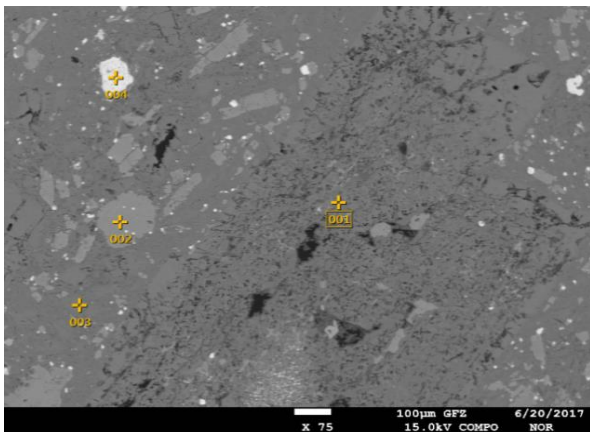
Figure 26 Selected point 2 andesite Tangkuban Perahu

001: **Pyroxene** with CaO (19.07%), MgO (13.72%), Al_2O_3 (3.44%), SiO_2 (50.59%), FeO (13.18%)

002: **Apatite** with CaO (53.03%), P_2O_5 (43.44%), Cl (1.38%)

003: **Clay / Altered Plagioclase** with CaO (7.99%), Na_2O (6.44%), Al_2O_3 (25.60%), FeO (59.97%)

004: **Ilmenite** with TiO_2 (29.38%), FeO (70.62%)
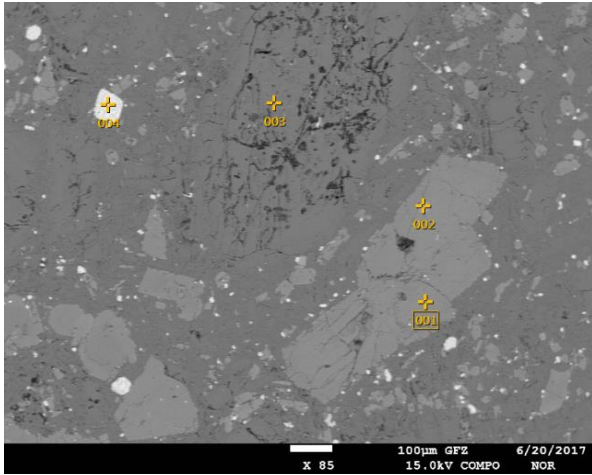
Figure 27 Selected point 3 andesite Tangkuban Perahu

3. Pumice – Tangkuban Perahu

001: **Quartz** with SiO_2 (100%)

002: **Rutile** with SiO_2 (17.75%), TiO_2 (82.25%)

003: **Mixture of Plagioclase and Quartz** with Na_2O (0.16%), Al_2O_3 (5.94%), SiO_2 (91.73%), K_2O (2.17%)
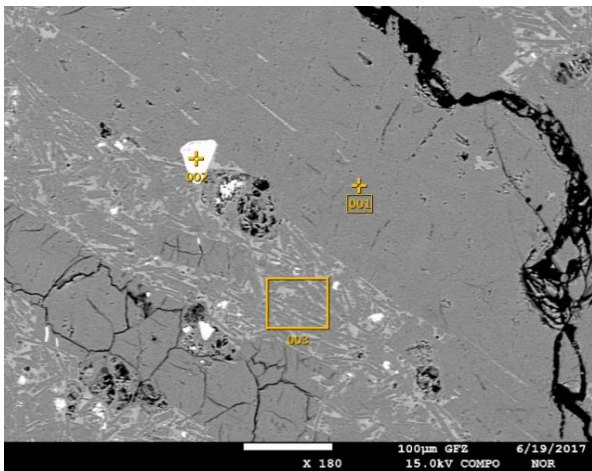
Figure 28 Selected point 1 pumice Tangkuban Perahu

001: **Quartz** with SiO_2 (100%)

002: **Rutile** with Al_2O_3 (0.56%), SiO_2 (5.78%), TiO_2 (93.66%)

003: **Rutile (or some Pyrite)** with Al_2O_3 (0.56%), SiO_2 (4.25%), P_2O_5 (1.50%), SO_3 (4.71%), TiO_2 (87.64%), FeO (1.34%)
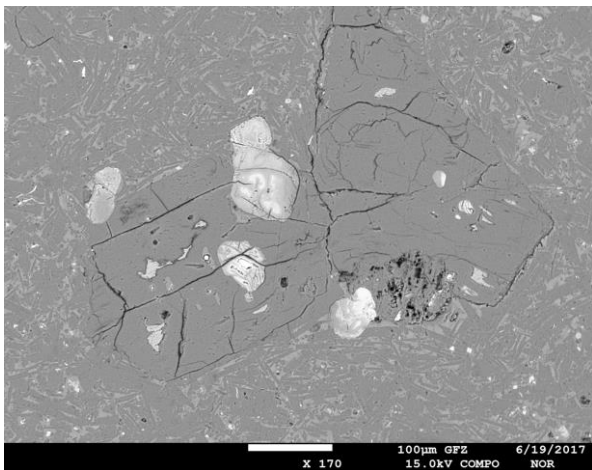
Figure 29 Selected point 2 pumice Tangkuban Perahu

3.4 Porosity and Permeability

3.4.1 Porosity Measurement Result

Porosity is measured by using the pycnometer device. The complete result of the porosity measurement for all basalt and granite rocks is showed in the table below.

Basalt block B Tangkuban Perahu					
Temperature	20	200	300	400	500
Porosity before Treatment	0.43	0.84	0.81	1.53	0.99
Porosity after Treatment		2.03	3.19	3.88	n/a
Difference:	**n/a**	**1.19**	**2.38**	**2.35**	**n/a**
Basalt block D Tangkuban Perahu					
Temperature	20	200	300	400	500
Porosity before Treatment	6.20	5.75	6.10	5.68	5.24
Porosity after Treatment		7.30	7.16	7.56	7.09
Difference:	**n/a**	**1.55**	**1.06**	**1.88**	**1.85**
Basalt Reynisfjara (Iceland)					
Temperature	20	200	300	400	500
Porosity before Treatment	14.06	14.69	14.09	14.36	13.89
Porosity after Treatment		14.61	14.36	14.72	14.18
Difference:	**n/a**	**-0.08**	**0.27**	**0.37**	**0.29**
Basalt Eifel X-Plane					
Temperature	20	200	300	400	500
Porosity before Treatment	0.38	0.29	0.61	0.48	0.38
Porosity after Treatment		0.71	1.02	1.42	1.40
Difference:	**n/a**	**0.42**	**0.41**	**0.95**	**1.02**
Basalt Eifel Y-Plane					
Temperature	20	200	300	400	500
Porosity before Treatment	0.33	0.18	0.19	0.37	0.15
Porosity after Treatment		0.42	0.92	1.11	1.41
Difference:	**n/a**	**0.24**	**0.73**	**0.74**	**1.27**
Basalt Eifel Z-Plane					
Temperature	20	200	300	400	500
Porosity before Treatment	0.39	0.30	0.35	0.47	0.58
Porosity after Treatment		0.71	1.27	1.50	1.41
Difference:	**n/a**	**0.41**	**0.92**	**1.03**	**0.83**
Granite Benin					
Temperature	20	200	300	400	500
Porosity before Treatment	0.25	0.32	0.28	0.44	0.35
Porosity after Treatment		1.75	1.60	2.24	1.91
Difference:	**n/a**	**1.43**	**1.33**	**1.79**	**1.56**

Table 6 Porosity before and after heating treatment

a. Tangkuban Perahu basaltic andesite and andesite rock (Indonesia)
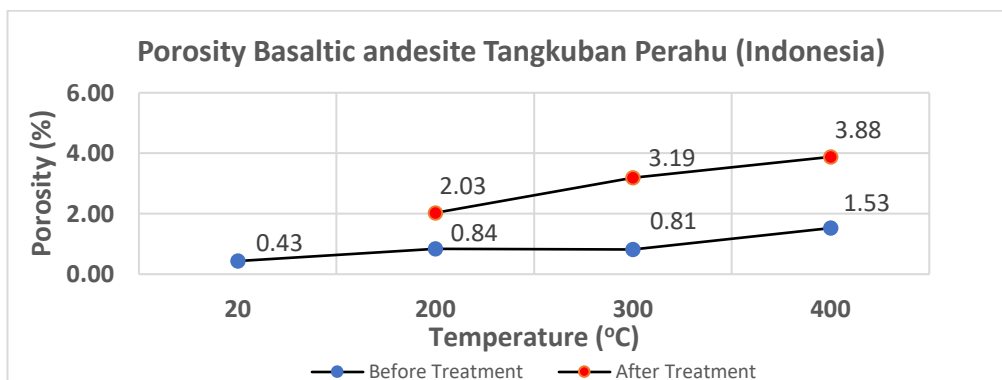
Graphic 5 Porosity basaltic andesite Tangkuban Perahu
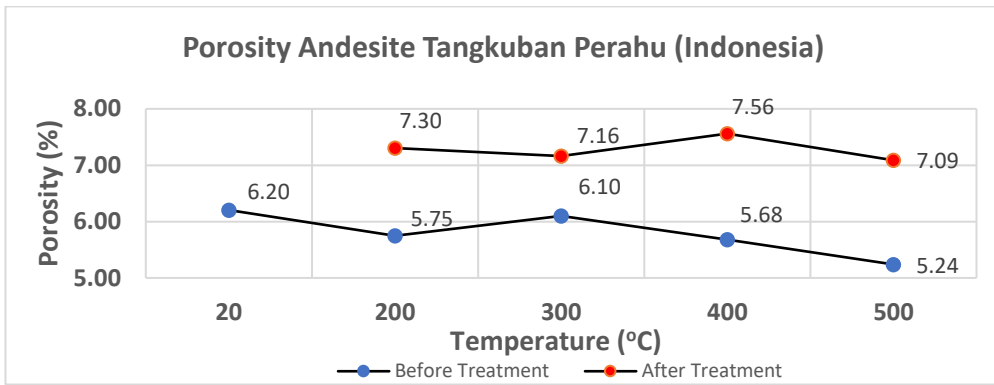
Graphic 6 Porosity andesite Tangkuban Perahu

b. Reynisfjara Beach (Iceland)
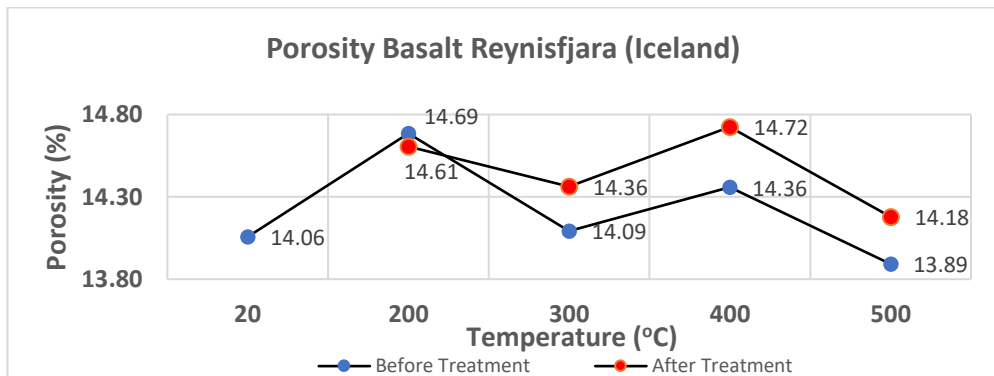
Graphic 7 Porosity basalt Reynisfjara (Iceland)

c. Eifel (Germany)
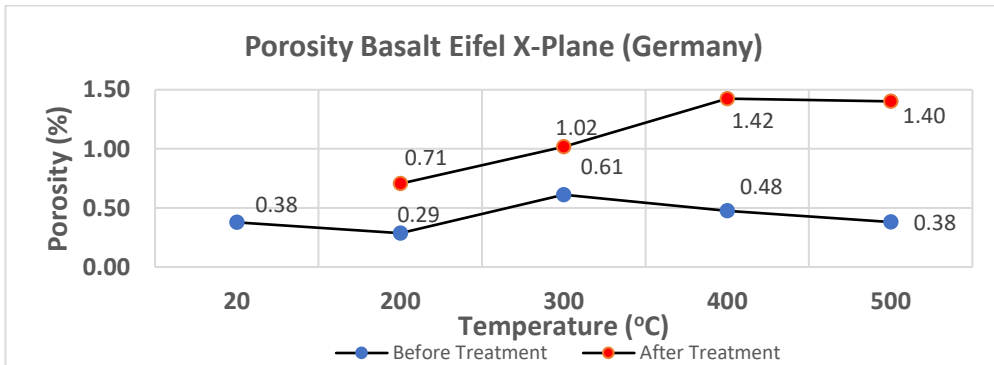
Graphic 8 Porosity basalt Eifel X-Plane Orientation
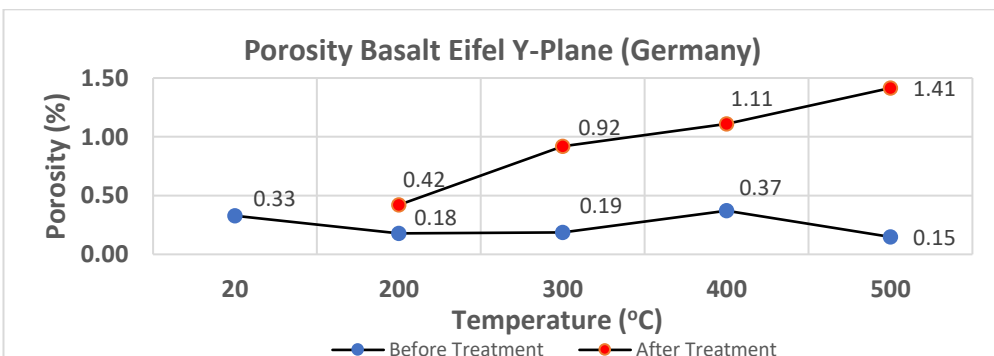
Graphic 9 Porosity basalt Eifel Y-Plane Orientation
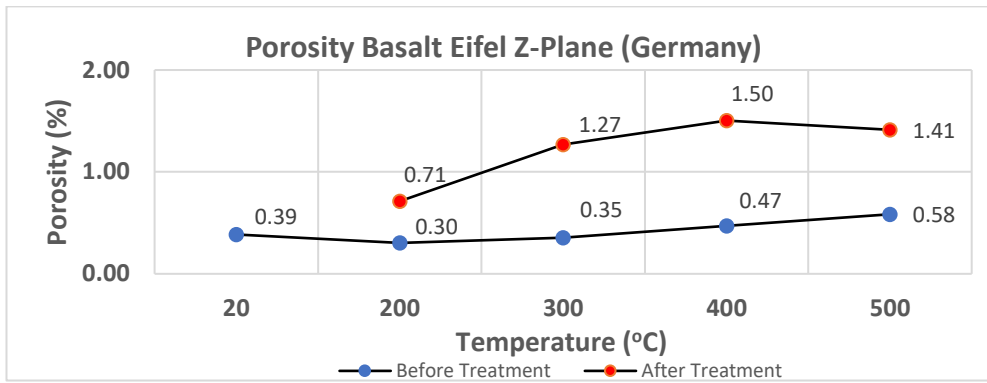
Graphic 10 Porosity basalt Eifel Z-Plane Orientation

d. Granite Benin (West Africa)
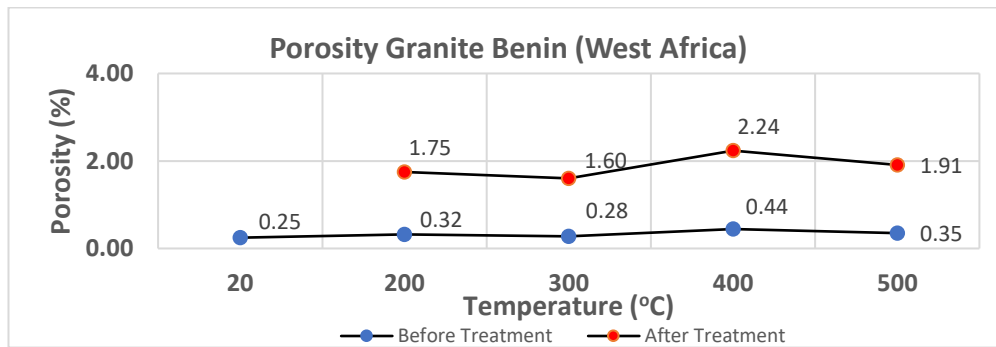
Graphic 11 Porosity granite Benin

3.4.2 Permeability Measurement Result

Permeability measurement used the different cores with different sizes. Its size is different with the core size for the previous porosity measurement. Initially, only 2 types of core had the permeability value before the heating treatment: Basalt Tangkuban Perahu Basaltic andesite and Basalt Reynisfjara. Other than those rocks, the permeability is below the detection limit. There was no flow observed in any type of valves and pressure drops.

Core ID	Length (cm)	Diameter (cm)	Area (cm2)	Large			Medium			Small			Notes
				0.25	0.5	1	0.25	0.5	1	0.25	0.5	1	(atm)
				25331.3	50662.5	101325	25331.3	50662.5	101325	25331.3	50662.5	101325	(Pa)
HTPB01	0.14	0.30	0.07	BDL	BDL	1.5	BDL	BDL	BDL	BDL	BDL	BDL	
HTPB02	0.15	0.30	0.07	BDL	BDL	1.5	BDL	BDL	BDL	BDL	BDL	BDL	
HTPB03	0.15	0.30	0.07	BDL	BDL	1	BDL	BDL	BDL	BDL	BDL	BDL	
HTPB04	0.16	0.30	0.07	BDL	BDL	1.5	BDL	BDL	BDL	BDL	BDL	BDL	
HTPB05	0.14	0.30	0.07	BDL	BDL	1	BDL	BDL	BDL	BDL	BDL	BDL	
HTPB06	0.16	0.30	0.07	BDL	BDL	1	BDL	BDL	BDL	BDL	BDL	BDL	(backup)
Block D Tangkuban Perahu													
HTPD01	0.12	0.30	0.07	BDL	BDL	BDL	BDL	BDL	BDL	BDL	BDL	BDL	
HTPD02	0.14	0.30	0.07	BDL	BDL	BDL	BDL	BDL	BDL	BDL	BDL	BDL	
HTPD03	0.14	0.30	0.07	BDL	BDL	BDL	BDL	BDL	BDL	BDL	BDL	BDL	
HTPD04	0.15	0.30	0.07	BDL	BDL	BDL	BDL	BDL	BDL	BDL	BDL	BDL	
HTPD05	0.14	0.30	0.07	BDL	BDL	BDL	BDL	BDL	BDL	BDL	BDL	BDL	
HTPD06	0.15	0.30	0.07	BDL	BDL	BDL	BDL	BDL	BDL	BDL	BDL	BDL	(backup)
Block Iceland													
HIC1	0.14	0.30	0.07	BDL	BDL	1	BDL	BDL	BDL	BDL	BDL	BDL	
HIC2	0.13	0.30	0.07	BDL	BDL	1	BDL	BDL	BDL	BDL	BDL	BDL	

Table 7 Flow pressure reading in mm for the cores before heating treatment (BDL means below detection limit of the Ruska permeameter)

However, after the heating treatment, andesitic basalt rock from Tangkuban Perahu Andesite also showed a significant result not only in the large three-way valve but also in the medium and small valves.

				Large			Medium			Small			Notes
After Heating Treatment (19 May 2017)													
Block B Tangkuban Perahu													
Core ID	Length (m)	Diameter (m)	Area (m2)	0.25	0.5	1	0.25	0.5	1	0.25	0.5	1	(atm)
				25331.3	50662.5	101325	25331.3	50662.5	101325	25331.3	50662.5	101325	(Pa)
HTPB01	0.14	0.30	0.07	No heating treatment applied									
HTPB02	0.15	0.30	0.07	BDL	BDL	1.5	BDL	BDL	BDL	BDL	BDL	BDL	
HTPB03	0.15	0.30	0.07	BDL	BDL	1.5	BDL	BDL	BDL	BDL	BDL	BDL	
HTPB04	0.16	0.30	0.07	BDL	BDL	1.5	BDL	BDL	BDL	BDL	BDL	BDL	
HTPB05	The rock was exploded in the oven												
Block D Tangkuban Perahu													
HTPD01	0.12	0.30	0.07	No heating treatment applied									
HTPD02	0.14	0.30	0.07	1	1	3	BDL	BDL	BDL	BDL	12	22	
HTPD03	0.14	0.30	0.07	1	2	4	BDL	BDL	BDL	BDL	BDL	31	
HTPD04	0.15	0.30	0.07	1	2	5	BDL	BDL	BDL	BDL	BDL	39	
HTPD05	0.15	0.30	0.07	1	1	2.5	BDL	BDL	BDL	BDL	BDL	22	
Block Iceland													
HIC1	0.14	0.30	0.07	No heating treatment applied									
HIC2	0.13	0.30	0.07	BDL	1	3	BDL	BDL	BDL	BDL	BDL	9	

Table 8 Flow pressure reading in mm for the cores after heating treatment

Even though the values on the table represents the direct reading from the air flow in the corresponding tube, it must be correlated with the flow graph provided by the instrument manual. In this case, there is also the minimum value that can be obtained from the flow graphics. For the air flow at 0.25, 0.5 and 1 atm, the minimum scale reading (in millimeter) that can be correlated to the air flow at mean pressure is 5mm. Therefore, the Andesite values from the Large valve could not be correlated to the air flow. By correlated the available data and calculated it based on the Darcy's Law (as mentioned in the method, previous chapter), there are several values available in millidarcy.

				Permeability value (milliDarcy)								
After Heating Treatment (19 May 2017)												
Block B Tangkuban Perahu												
Core ID	Length (m)	Diameter (m)	Area (m2)	Large			Medium			Small		
				25331.3	50662.5	101325	25331.3	50662.5	101325	25331.3	50662.5	101325
HTPB01	0.00	0.00	0.00	BDL	BDL	BDL	BDL	BDL	BDL	BDL	BDL	BDL
HTPB02	0.15	0.30	0.07	BDL	BDL	BDL	BDL	BDL	BDL	BDL	BDL	BDL
HTPB03	0.15	0.30	0.07	BDL	BDL	BDL	BDL	BDL	BDL	BDL	BDL	BDL
HTPB04	0.16	0.30	0.07	BDL	BDL	BDL	BDL	BDL	BDL	BDL	BDL	BDL
HTPB05	N/A	N/A	N/A	The rock was exploded in the oven								
Block D Tangkuban Perahu												
HTPD01	0.00	0.00	0.00	BDL	BDL	BDL	BDL	BDL	BDL	BDL	BDL	BDL
HTPD02	0.14	0.30	0.07	BDL	BDL	BDL	BDL	BDL	BDL	BDL	9.93	7.09
HTPD03	0.14	0.30	0.07	BDL	BDL	BDL	BDL	BDL	BDL	BDL	BDL	9.17
HTPD04	0.15	0.30	0.07	BDL	BDL	27.04	BDL	BDL	BDL	BDL	BDL	11.59
HTPD05	0.15	0.30	0.07	BDL	BDL	BDL	BDL	BDL	BDL	BDL	BDL	7.40
Block Iceland												
HIC1	0.00	0.00	0.00	BDL	BDL	BDL	BDL	BDL	BDL	BDL	BDL	BDL
HIC2	0.13	0.30	0.07	BDL	BDL	BDL	BDL	BDL	BDL	BDL	BDL	4.45

Table 9 Permeability values in mD for the cores after heating treatment

3.5 Static Elastic Moduli

The summary of the Young's modulus, Poisson's ratio and the ultimate strength is shown in the table below.

Core ID	Rock Type	Orientation	Temp. Exposed	Young's modulus	Poisson's ratio	Crack Initiation	Ultimate Strength
			ºC	GPa		MPa	MPa
TPB01	Basaltic andesite (T. Perahu)	n/a	Room Temp. 20	37.47	0.30	61.76	209.99
TPB02	Basaltic andesite (T. Perahu)	n/a	200	36.85	0.23	159.98	330.46
TPB03	Basaltic andesite (T. Perahu)	n/a	300	26.18	0.14	73.76	138.76
TPB04	Basaltic andesite (T. Perahu)	n/a	400	33.5	0.22	48.29	234.26
TPD01	Andesite (T. Perahu)	n/a	Room Temp. 20	21.41	0.25	83.68	131.82
TPD02	Andesite (T. Perahu)	n/a	200	25.28	0.22	79.18	142.78
TPD03	Andesite (T. Perahu)	n/a	300	25.10	0.21	62.69	125.29
TPD04	Andesite (T. Perahu)	n/a	400	19.30	0.13	43.34	133.64
TPD05	Andesite (T. Perahu)	n/a	500	20.50	0.17	48.56	121.80
IC01	Basalt Reynisfjara (Iceland)	n/a	Room Temp. 20	27.23	0.29	135.61	171.23
IC02	Basalt Reynisfjara (Iceland)	n/a	200	23.29	0.26	74.83	141.03
IC03	Basalt Reynisfjara (Iceland)	n/a	300	19.14	0.23	24.11	103.23
IC04	Basalt Reynisfjara (Iceland)	n/a	400	21.94	0.15	46.45	143.11
IC05	Basalt Reynisfjara (Iceland)	n/a	500	17.88	0.22	40.13	93.77
TI009	Granite (Benin)	n/a	Room Temp. 20	14.44	0.27	132.85	160.55
TI012	Granite (Benin)	n/a	Room Temp. 20	31.56	0.18	33.15	104.43
TI004	Granite (Benin)	n/a	200	15.55	0.19	106.34	121.39
TI006	Granite (Benin)	n/a	200	28.24	0.21	228.51	228.51
TI001	Granite (Benin)	n/a	300	23.97	0.29	110.50	132.34
TI007	Granite (Benin)	n/a	300	24.23	0.28	186.16	186.16
TI003	Granite (Benin)	n/a	400	22.39	0.2	197.61	197.61
TI005	Granite (Benin)	n/a	400	18.01	0.19	134.60	134.60
TI002	Granite (Benin)	n/a	500	16.14	0.1	107.13	107.13
TI013	Granite (Benin)	n/a	500	4.28	0.26	69.88	73.46
A1X	Basalt (Eifel)	X-Plane	Room Temp. 20	25.3	0.19	175.01	283.00
A4Z	Basalt (Eifel)	Z-Plane	Room Temp. 20	54.52	0.48	384.73	384.73
A3X	Basalt (Eifel)	X-Plane	200	9.5	0.36	63.01	177.74
A5Z	Basalt (Eifel)	Z-Plane	200	50.92	0.45	211.39	288.59
C4AX	Basalt (Eifel)	X-Plane	300	9.11	0.18	111.08	146.01
A6Z	Basalt (Eifel)	Z-Plane	300	47.6	0.27	150.37	261.22
C5AX	Basalt (Eifel)	X-Plane	400	53.77	0.14	197.13	229.00
C1AZ	Basalt (Eifel)	Z-Plane	400	40.07	0.5	140.37	207.66
C5BX	Basalt (Eifel)	X-Plane	500	27.48	0.11	109.58	109.58
C2BZ	Basalt (Eifel)	Z-Plane	500	32.01	0.28	67.63	139.14

Table 10 Summary of the static elastic moduli variables

Most of the rocks are represented by 1 core for each temperature due to the availability limitation of the rock. The granite rock has 2 cores for each heating treatment and the basalt rock from Eifel is set to three planes in order to see the isotropic characteristic (in this thesis only 2 planes are tested). Each core is tested in the representative temperature which starts from the room temperature (stable around 20°C) and progressively increase from 200, 300, 400 and 500°C. The compilation of all the sample cores is showed below and followed by each type of rock category and each temperature category.
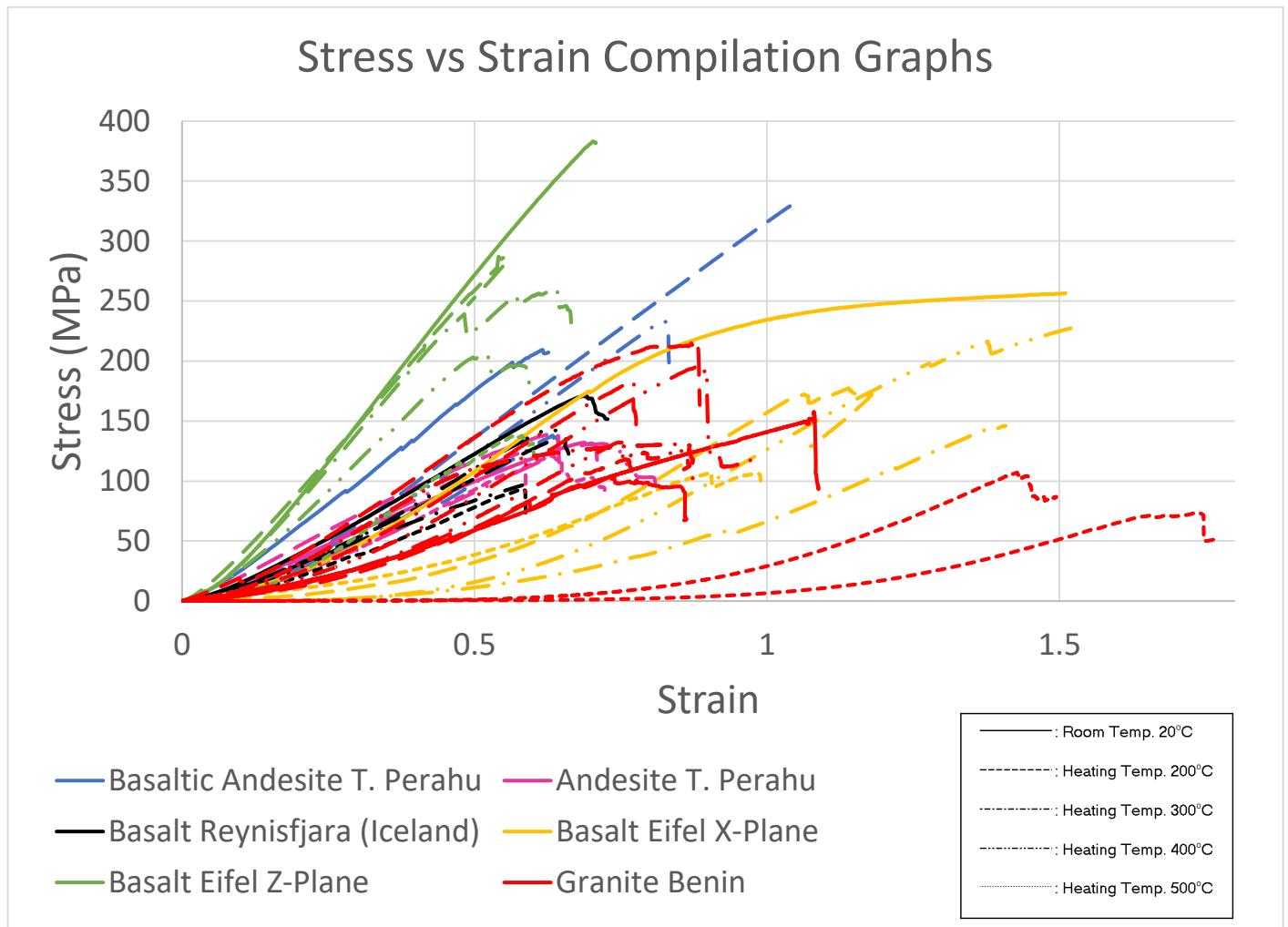
Graphic 12 The compilation of the stress-strain curves from all the rock

The stress vs strain plots can be categorized based on the rock types and the heating temperatures to see the variations of each type of rocks. To see how each of the heating temperatures affect the rock mechanic properties, the stress vs strain plots from each type of rock will be showed in the discussion chapter.

The data tables below show each rock type static elastic moduli. For basalt Eifel, the values between different planes can be compared to see the isotropy of the rock.

BASALTIC ANDESITE - Tangkuban Perahu				
Core ID	Temperature (°C)	Young's Modulus	Poisson's Ratio	Crack Initiation	Ultimate Strength
TPB01	20	37.47	0.30	61.76	209.99
TPB02	200	36.85	0.23	159.98	330.46
TPB03	300	26.18	0.14	73.76	138.76
TPB04	400	33.50	0.22	48.29	234.26

Table 11 Basaltic andesite Tangkuban Perahu static elastic moduli

ANDESITE - Tangkuban Perahu				
Core ID	Temperature (°C)	Young's Modulus	Poisson's Ratio	Crack Initiation	Ultimate Strength
TPD01	20	21.41	0.25	83.68	131.82
TPD02	200	25.28	0.22	79.18	142.78
TPD03	300	25.10	0.21	62.69	125.29
TPD04	400	19.30	0.13	43.34	133.64
TPD05	500	20.50	0.17	48.56	121.80

Table 12 Andesite Tangkuban Perahu static elastic moduli

BASALT Reynisfjara - Iceland				
Core ID	Temperature (°C)	Young's Modulus	Poisson's Ratio	Crack Initiation	Ultimate Strength
IC01	20	27.23	0.29	135.61	171.23
IC02	200	23.29	0.26	74.83	141.03
IC03	300	19.14	0.23	24.11	103.23
IC04	400	21.94	0.15	46.45	143.11
IC05	500	17.90	0.22	40.13	93.77

Table 13 Basalt Reynisfjara static elastic moduli

GRANITE Benin - West Africa				
Core ID	Temperature (°C)	Young's Modulus	Poisson's Ratio	Crack Initiation	Ultimate Strength
TI009	20	17.20	0.06	91.69	160.55
TI012	20	13.14	0.12	33.15	104.43
TI004	200	21.67	0.07	106.34	121.39
TI006	200	33.15	0.11	228.51	228.51
TI001	300	24.77	0.08	41.19	132.34
TI007	300	29.72	0.12	186.16	186.16
TI003	400	27.86	0.07	197.61	197.61
TI005	400	23.92	0.09	134.60	134.60
TI002	500	16.05	0.03	107.13	107.13
TI013	500	12.05	0.04	69.88	73.46

Table 14 Granite Benin static elastic moduli

BASALT Eifel X-Plane (Germany)				
Core ID	Temperature (°C)	Young's Modulus	Poisson's Ratio	Crack Initiation	Ultimate Strength
A1X	20	35.12	0.12	175.01	283.00
A3X	200	14.96	0.06	63.01	177.74
C4AX	300	10.12	0.02	37.34	146.01
C5AX	400	26.17	0.07	197.13	229.00
C5BX	500	17.02	0.05	109.58	109.58

Table 15 Basalt Eifel x-plane static elastic moduli

BASALT Eifel Z-Plane (Germany)				
Core ID	Temperature (°C)	Young's Modulus	Poisson's Ratio	Crack Initiation	Ultimate Strength
A4Z	20	61.47	0.21	384.73	384.73
A5Z	200	53.89	0.16	211.39	288.59
A6Z	300	52.89	0.12	150.37	261.22
C1AZ	400	45.85	0.15	140.37	207.66
C2BZ	500	30.62	0.19	67.63	139.14

Table 16 Basalt Eifel z-plane static elastic moduli

Average value of each temperature heating treatment for granite Benin can be seen on the table below.

GRANITE Benin - West Africa				
Temperature (^{o}C)	Young's Modulus	Poisson's Ratio	Crack Initiation	Ultimate Strength
20	15.17	0.09	62.42	132.49
200	27.41	0.09	167.43	174.95
300	27.24	0.10	113.68	159.25
400	25.89	0.08	166.11	166.10
500	14.05	0.03	88.51	90.30

Table 17 Average granite Benin static elastic moduli

To see the static moduli of different type of rocks in one visualization, each value is normalized and the trendline is applied.
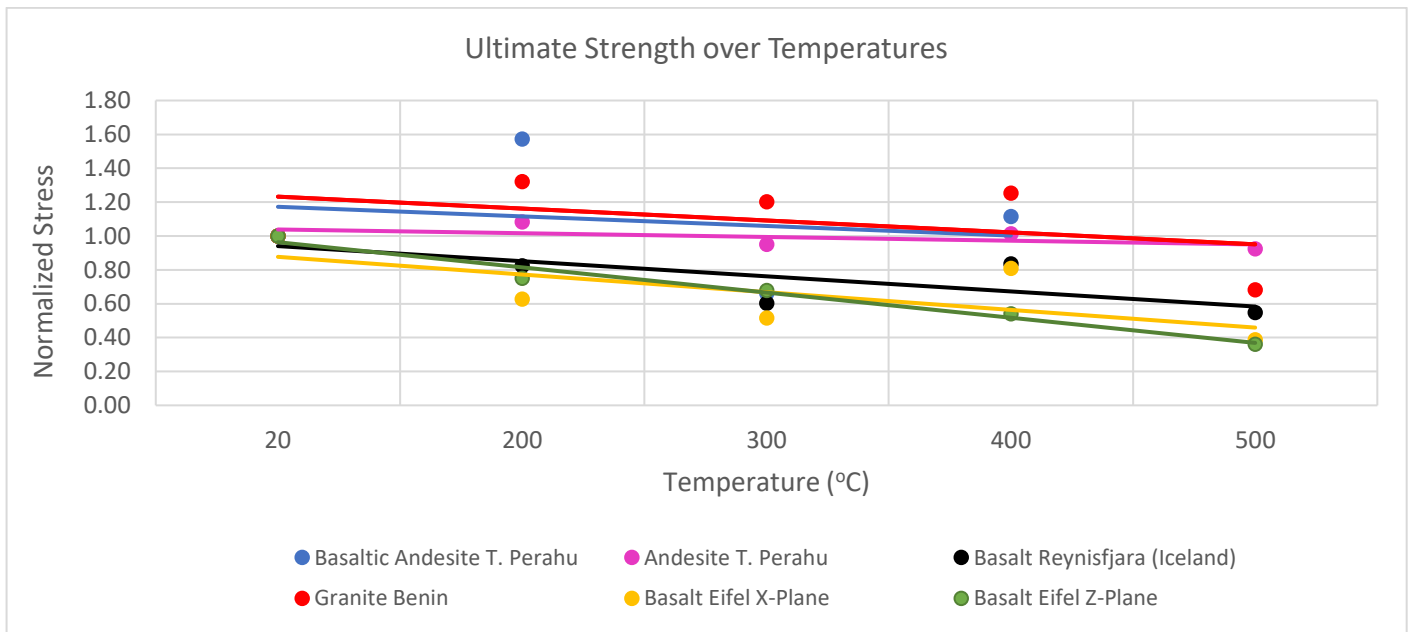
Graphic 13 Ultimate Compressive Strength (UCS) for all cores
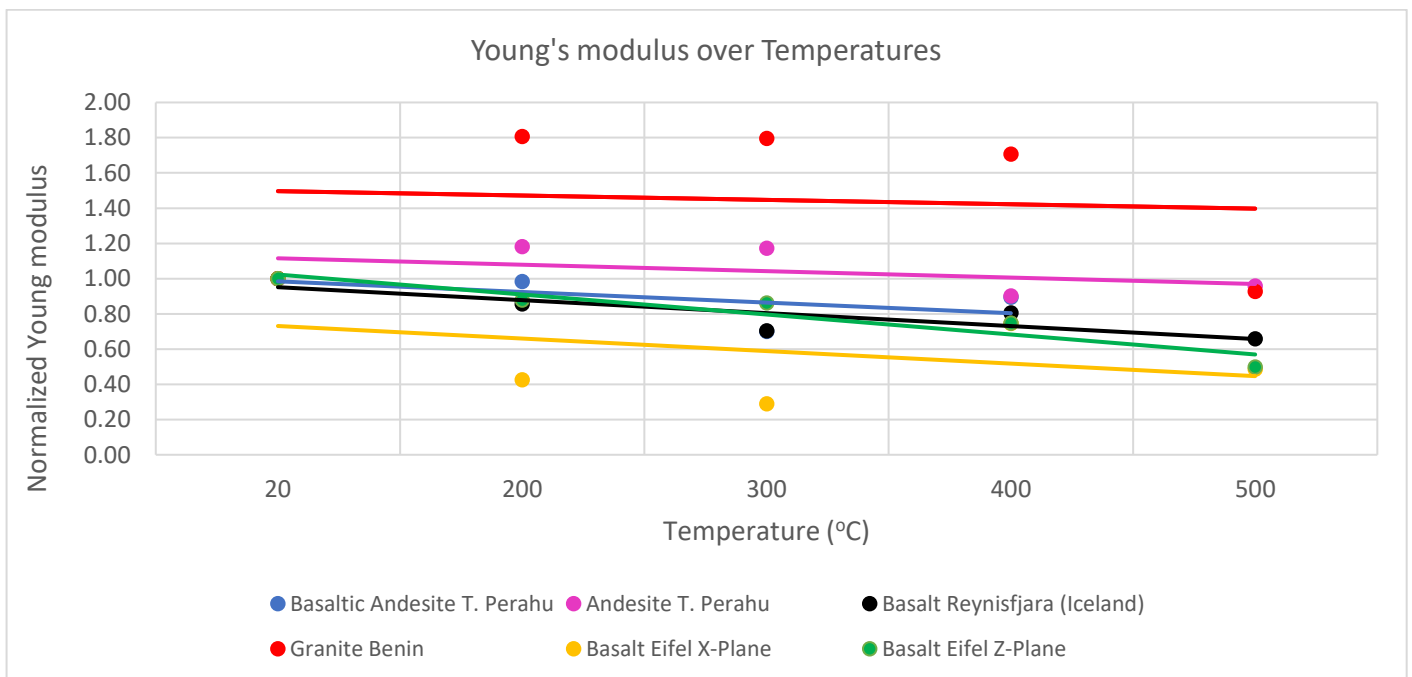
Graphic 14 Young's modulus for all cores
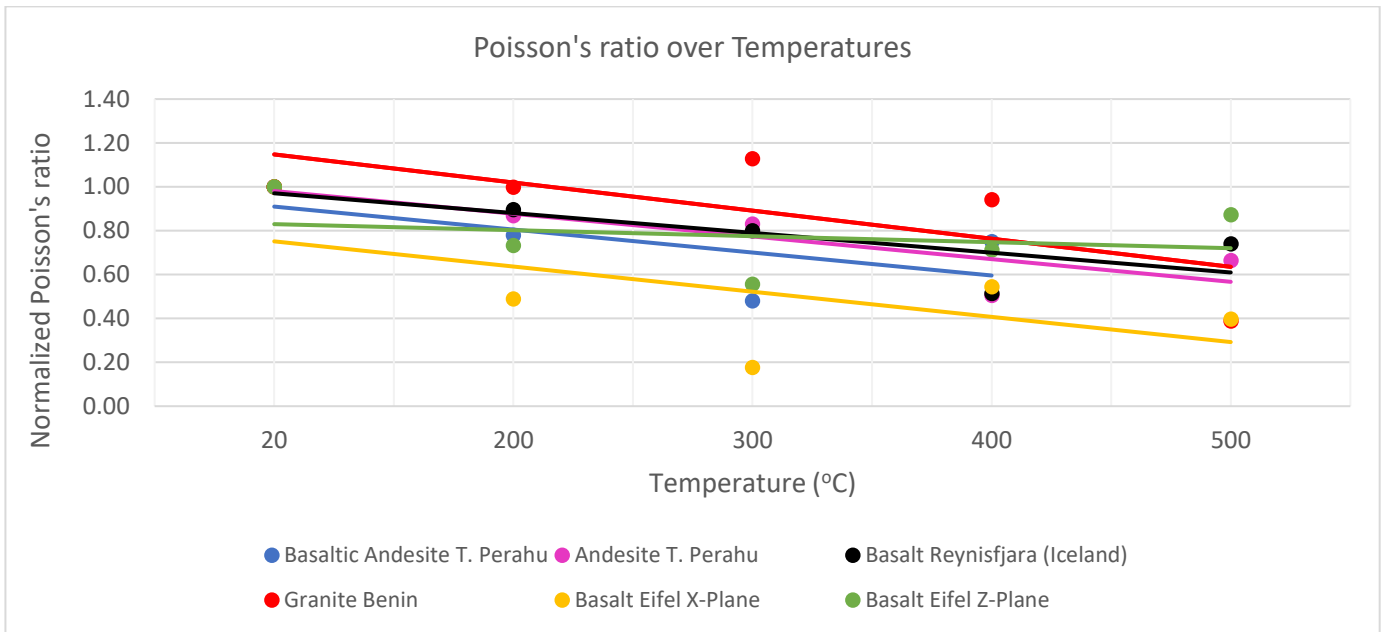
Graphic 15 Poisson's ratio for all cores

The basalt rock from Eifel, with its columnar-shaped bulk rock, is intrigued to be observed its isotropic characteristic. Therefore, the general graphs above are narrowed into basalt Eifel static moduli only. The graphs below show the ultimate strength, Young's modulus and Poisson's ratio of the basalt Eifel.
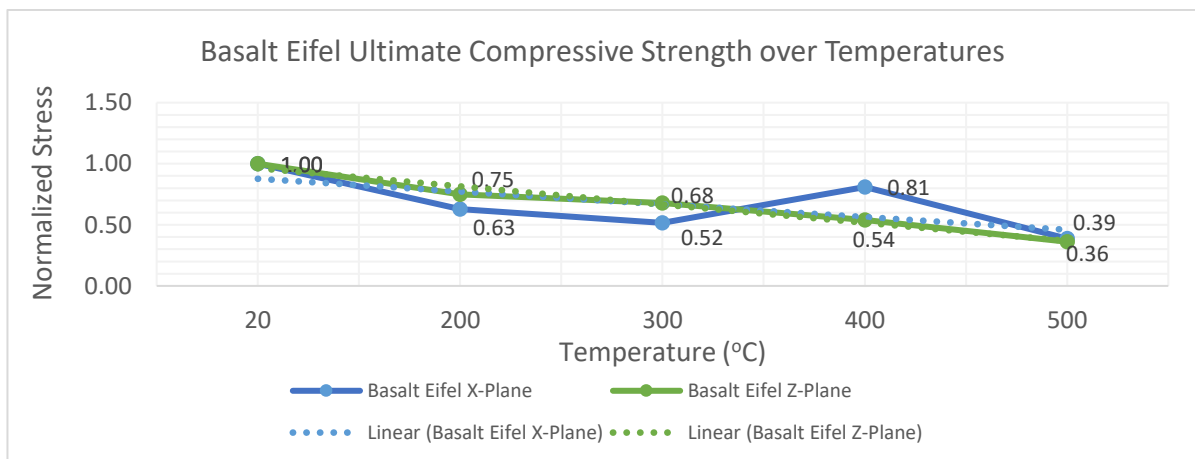
Graphic 16 Ultimate Compressive Strength particularly for Basalt Eifel
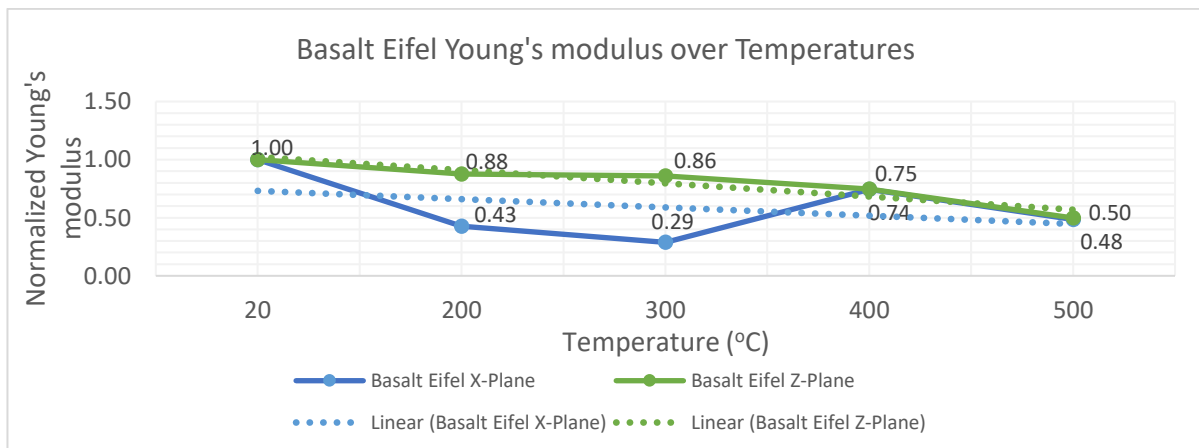
Graphic 17 Young's modulus particularly for Basalt Eifel
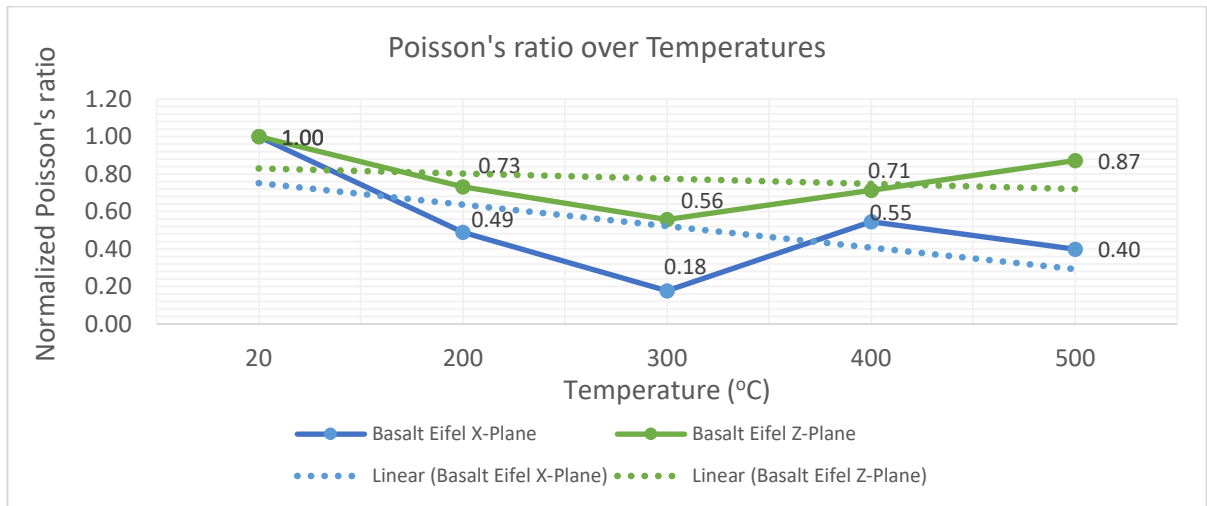
Graphic 18 Poisson's ratio particularly for Basalt Eifel

In addition, the isotropic characteristic of the rock depends on many factors and one of them is the variability. To see the characteristic variability of each rock, it requires a lot of data samples but the source availability does not allow to picture the trend in the clearer interpretation.

3.6 CT-Scan Result

The core porosity visualization is done by using the Avizo software series 9.3. In this visualization, only basalt rock has been performed to be visualized. Granite Benin scan files are still need to be restructured in order to observe the microfractures. However, based on the quick look, the core detection is quite difficult. Therefore, it is decided to focus on the basaltic rocks of Tangkuban Perahu and Eifel.
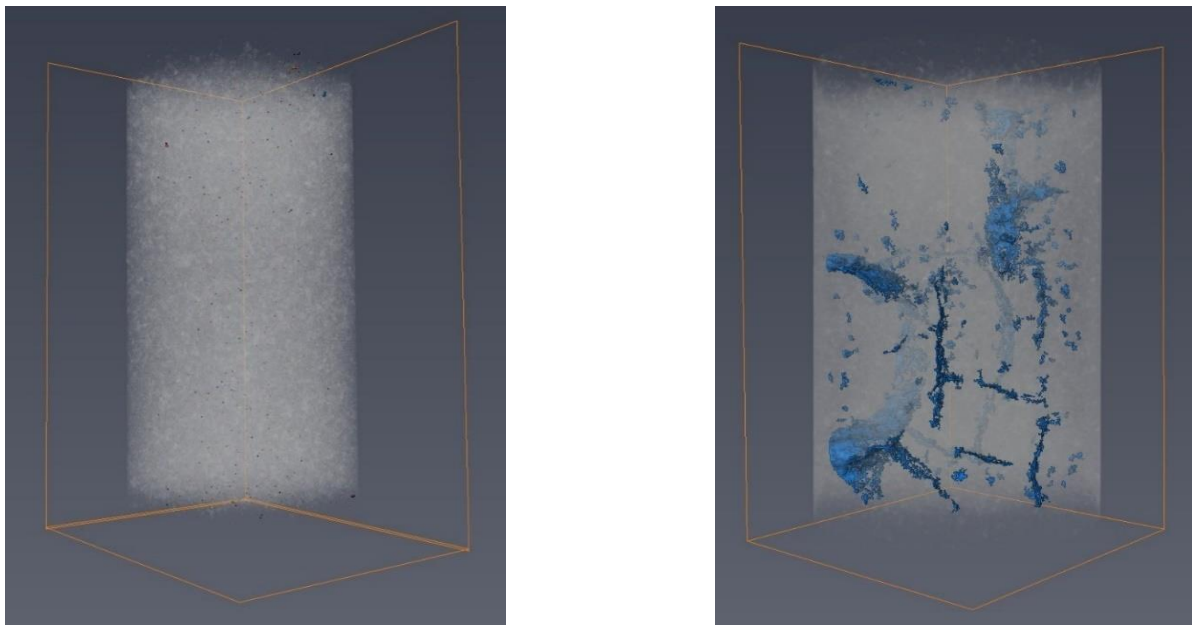
Figure 30 Core TPB6 before heating treatment (left) and after heating treatment (right)
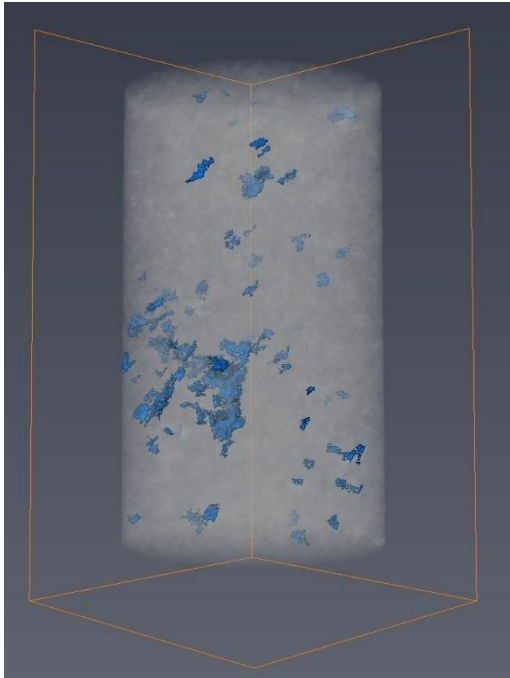
Figure 31 Core TPD5 before heating treatment (left) after heating treatment (right)
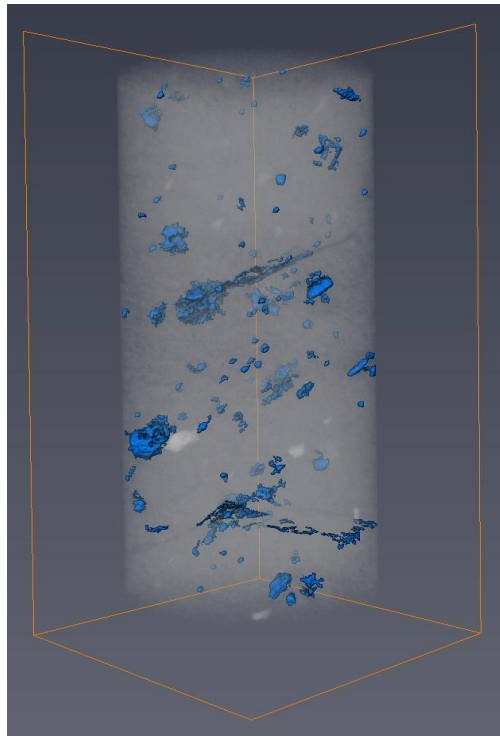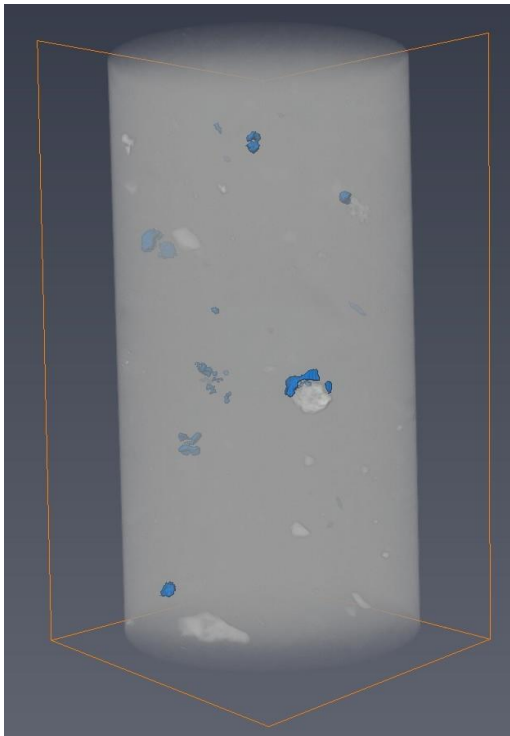
Figure 32 Core AY2 (Eifel) before heating treatment (left) and after heating treatment (right)

All the cores were heated to 500°C to observe its effect to a high thermal shock condition. The colormaps of the porosity is changed into a colorful one when the pores are proceeded to the label analysis. Prior that, the color is stick to the binary color (which only showed by one color, in this case is blue). The author will fix this issue soon by reupload the files into the Avizo.

Another scan results from the small cores (the two mini cores to observe the difference between outer and inner core side) are showed in the discussion chapter to ease the explanation.

3.7 Brittleness Index

As mentioned in the method chapter, all rocks cannot be analyzed with the same BI method due to core availability. Rickman method requires a set of cores to have a minimum and maximum value of Young's modulus and Poisson's ratio. In this case, only granite Benin and basalt Eifel are determined with 2 sample cores on the same heating temperature and have total 10 sample cores representative from each rock.

Three methods of the Brittleness Index calculation are used for the basalt Tangkuban Perahu basaltic andesite, andesite and basalt Reynisfjara. Some obstacles are faced in order to determine visually the parameters used to calculate the BI. During the UCS testing for the Tangkuban Perahu B, the radial extensometer was thrown away and the rock broke into pieces. This resulted the reversible stress (which is used by the Bishop method) could not be measured.

Core ID	Temp. Exposed	Brittleness Index				Notes
	°C	BI (Rickman)	BI (Coates)	BI (Huckas and Das)	BI (Bishop)	
TPB01	Room Temp.~20	1.00	0.95	0.97	N/A	extensometer thrown away
TPB02	200	0.80	0.97	0.99	N/A	extensometer thrown away
TPB03	300	0.15	N/A	N/A	N/A	εelastic>εplastic, extensometer thrown away, no record of τres
TPB04	400	0.00	N/A	N/A	N/A	εelastic>εplastic, extensometer thrown away, no record of τres
TPD01	Room Temp.~20	0.68	0.92	0.94	0.54	τres at 60.79
TPD02	200	0.87	0.90	0.91	0.29	τres at 101.77
TPD03	300	0.81	0.89	0.95	0.22	τres at 97.93
TPD04	400	0.00	N/A	N/A	N/A	εelastic>εplastic, no record of τres
TPD05	500	0.26	N/A	N/A	N/A	εelastic>εplastic, no record of τres
IC01	Room Temp.~20	1.00	0.97	0.98	N/A	no record of τres
IC02	200	0.68	0.97	0.98	N/A	no record of τres
IC03	300	0.36	0.92	0.94	0.05	the τres is predicted because of the compaction of particles, τmax (103.23MPa) and τres (98.33MPa) is not significantly different.
IC04	400	0.22	N/A	N/A	N/A	εelastic>εplastic, no record of τres
IC05	500	0.23	N/A	N/A	0.25	εelastic>εplastic

Table 18 Brittleness Index for Tangkuban Perahu and Reynisfjara rocks

4. Discussion

4.1 Petrography of the rocks

To know the rock type, the minerology analysis of the collected rocks should be discussed first. Most of the rocks are basaltic rocks which are considered as he effusive-volcanic rocks. The granite rock is different to the others because it is an intrusive-plutnic rock. However, to classify the igneous rocks and to name the sample rocks accurately, some criteria can be used such as:

4.1.1 The presence of the major minerals that form the rock

Olivine mineral has been detected in the basaltic rocks (Eifel and Tangkuban Perahu). In the EMPA observation of the basaltic andesite Tangkuban Perahu, we observed the existence of the olivine but not as the major constituent of the rock. The EMPA measurement showed a composition characterized by plagioclase, pyroxene, olivine and ilmenite. On one hand, the XRD analysis shows the basaltic andesite contained mainly plagioclase and followed by microcline and goethite. On the other, the andesite Tangkuban Perahu rock contains a higher amount of plagioclase followed by anorthoclase and ilmenite. In addition, no olivine was observed in andesite.

Table XRD semi-quantitative analysis

Sample	Crystallinity percentage	Compound name	Compound formula	Weight percent
BB (Block B)	64,1	Bytownite	$(Ca,Na)(Al,Si)_4O_8$	69,4
		Microcline	$K(AlSi_3O_8)$	29,2
		Goethite	$FeHO_2$	1,4
BD (Block D)	80,3	Bytownite	$(Ca,Na)(Al,Si)_4O_8$	59,7
		Anorthoclase	$Na,K(AlSi_3O_8)$	36,4
		Ilmenite	$FeTiO_3$	3,9

Source: Welink, 2017

Table 19 XRD semi-quantitative analysis

4.1.2 Color appearance of the collected sample rock

Bowen's reaction series exhibit the order cooling magma crystallization. It distinguishes the minerals that were formed before or after cooling magma process, which defines the minerals into mafic or felsic minerals. Mafic (magnesium and ferrum) minerals have darker color compared to the felsic (feldspar and silica-quartz) minerals that show light color (Lutgens, Tarbuck, & G., 2014).

Figure 33 Dark color basaltic andesite Tangkuban Perahu (left) and light color andesite Tangkuban Perahu (right)

The color difference of the two rocks is very obvious. Basaltic andesite core has dark color and the andesite has light color. Those rocks were taken at the same location and it was suspected that the andesite was exposed to a high alteration condition hence this sample may contain higher iron (Fe) amount. In order to obtain more accuracy of the two rocks differences, the chemical composition investigation (XRF and EMPA) have been conducted in the laboratory.

4.1.3 Chemical composition investigation from XRD, XRF and EMPA analysis

From the XRD and XRF, the minerology composition and whole rock chemistry can be obtained. From the XRD analyses the mineral weight fraction of the sample can be semi-quantitatively interpreted while the bulk chemistry of the rock can be obtained from XRF. The quantitative analysis is measured from the rock that was crushed into powder, which allocate only the particular part of the rock. Therefore, the chosen piece of rock should be the most representative part in the core. Basalt rock from Tangkuban Perahu consists of plagioclase in majority. The results from the XRF analysis allow to classify the rock based on the amount of silica (SiO_2) and the sum of major alkali (Na_2O+K_2O). The classification is usually based on the diagram of the chemical classification. However, K_2O has not been measured on the samples investigated in this work. Thus, the classification is based on the amount of the mineral fraction, the rock texture and only partially on the chemistry.
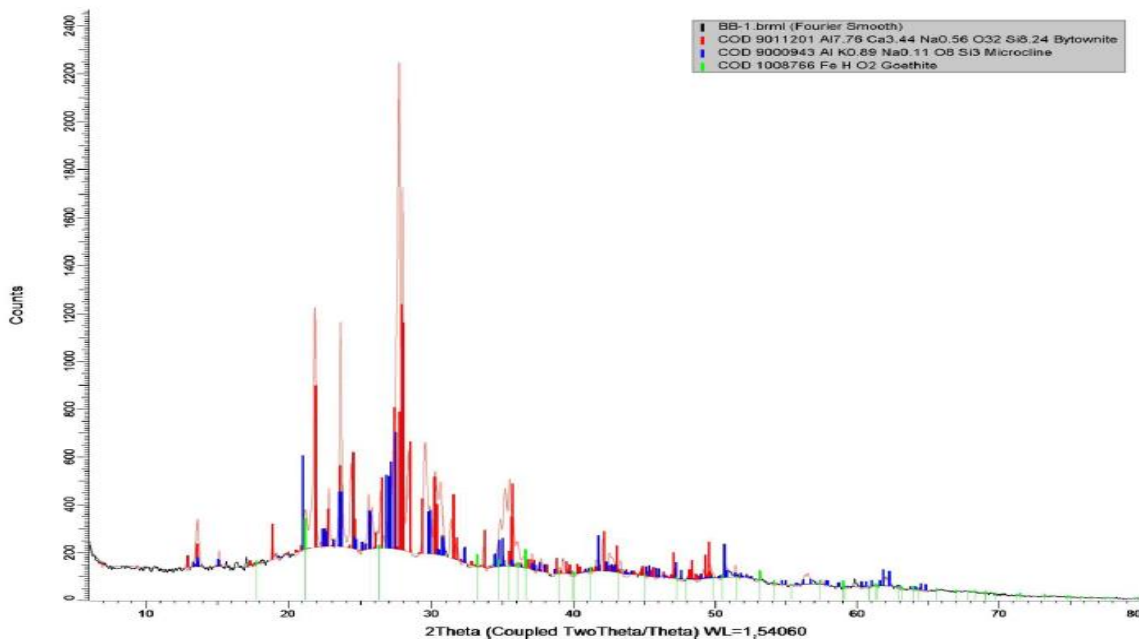
Figure 34 Diffractogram basaltic andesite Tangkuban Perahu
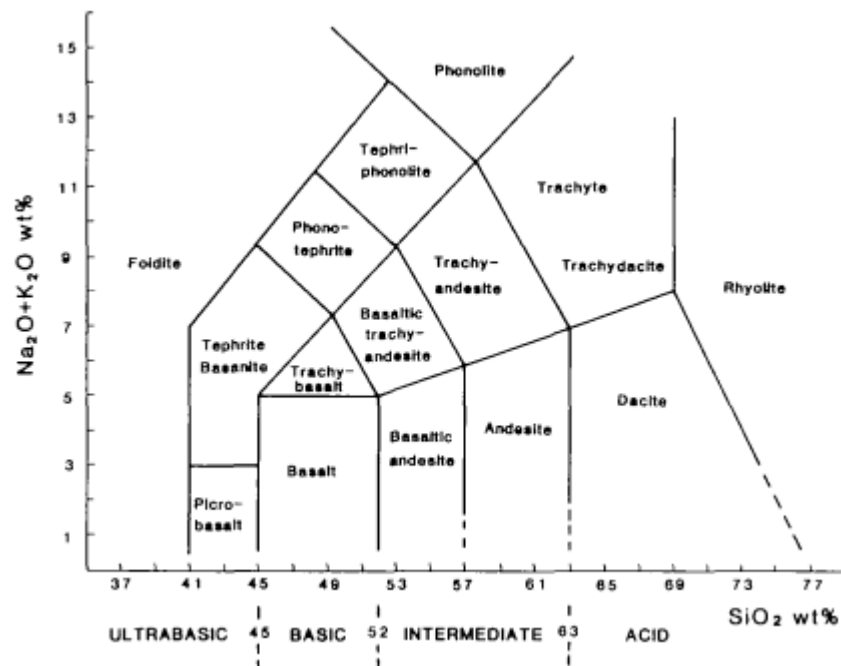
Figure 35 Chemical Classification of volcanic rocks proposed by Le Bas et.al (1986, page 747)

The x-axis represents the silica amount and the y-coordinate represents the sum of sodium and potassium oxide. Due to lack of the sodium oxide in the XRF element results, the combination of silica and potassium oxide indicates the classification of the rocks but not as the absolute result. Basaltic andesite Tangkuban Perahu rock, with 53.37% silica and 2.66% potassium oxide, is considered as the basaltic andesite. Andesite Tangkuban Perahu rock, with 62.23% silica and 1.42% potassium oxide, is considered as the andesite. Further XRF measurement are planned to complete the interpretation with sodium oxide.

In the correlation between minerals and microfractures, microcracks is significantly affected by the amount of the quartz in the rock due to its large thermal expansivity (Kranz, 1983). The XRF experiment only provide the silica oxide belonging to all SiO_2 nearing phases of the sample, not as a quartz mineral. Therefore, the quartz indicator cannot be used to compare the porosity of the whole rocks.

To ease the reading, in the following chapters and subchapters, basaltic andesite will be written as basaltic andesite Tangkuban Perahu and andesite will be written as andesite Tangkuban Perahu.

4.2 The thermal shock effects to various types of rocks

4.2.1 Increase porosity and permeability values after heating treatment

Increase porosity values due to thermal shock event

Porosity, the pore volume within a rock that can contain fluids, can be originated from the existed pores (like the Reynisfjara basalt) or fractures from the initial cooling (lava cooling). The thermal induced microcracks are the result of the differential thermal expansion between grains' thermoelastic moduli and thermal

conductivities (Kranz, 1983). The microcracks also contribute to the porosity increase. In the beginning, basalt Eifel and granite Benin were tested by a three-cycles heating method (see chapter 2.5). This method did not increase porosity significantly (some cores have porosity decrease over multiple thermal shocks), thus the procedure is returned to the one-cycle heating method. This unstable measurement might be affected by some factors (helium pressure and chamber temperature change). Due to small different value, these factors are negligible.

In general result, the porosity increases from 1.02 times (basalt Reynisfjara) to 85.5 times (basalt Eifel) after the heating treatment. The range value sounds tremendous, however, it only changes from 0.15% to 1.27% porosity of basalt Eifel and from 14.09% to 14.36% porosity value of basalt Reynisfjara. Higher thermal shock effect (exposed to higher temperature) created more porosity to all rocks due to microfractures creation and extension to other existed microfractures.

In a particular event, some cores (basaltic andesite Tangkuban Perahu, basalt Reynisfjara, basalt Eifel Z-plane and granite Benin) exhibit lower porosity value at 500°C compared to 400°C exposure. Two reasons this case happened:

a. At 500°C some matrix is restructured and cause either some voids filled by matrix or disconnection of the interconnected pores (generate more isolated pores).

b. The porosity value is still in the range of variability. It means by having more cores to be heated at the same temperature, one can be certain about the range of the valid porosity value (currently is still not manageable since only 1 core for every measurement).

Basaltic andesite Tangkuban Perahu did not have the porosity measurement at 500°C as the core exploded inside the oven. Based on the micro-CT scan result, a big fracture plane existed inside thus the trapped air pressure might expand when it is heated to high temperature. A quick high-temperature exposure might also be considered as the reason because the core experienced rapid temperature change from room temperature to the aimed heating temperatures (200 to 500°C).

Increase permeability values due to thermal shock

Most of the observed increased permeability values are found in the andesite rock Tangkuban Perahu. To see the proper trend between porosity and permeability, minimum numbers of data should be available. Due to the limitation, the porosity-permeability analysis is only available for andesite Tangkuban Perahu (5 small cores). It does not give a clear relation between porosity and permeability under different heating experiment. In addition, the porosity values are also bigger compared to the values from the full cylinder cores. It might be

due to calibration file used in the medium chamber instead of the large one (different chamber pressure sensitivity).

Core ID	Permeability (mD)	Porosity (%)
HTPD01	0.00	10.09
HTPD02	7.09	9.10
HTPD03	9.17	10.15
HTPD04	11.59	9.81
HTPD05	7.40	9.79

Table 20 Porosity-Permeability andesite Tangkuban Perahu
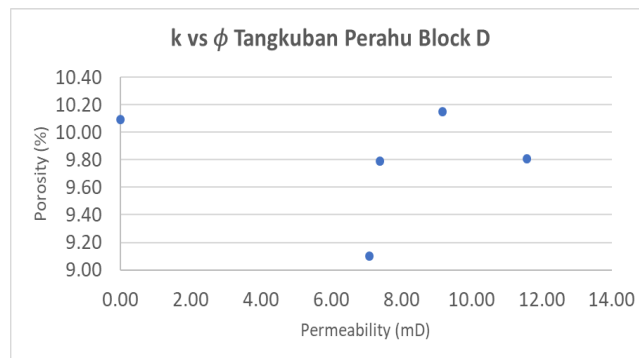
Graphic 19 Porosity-Permeability andesite Tangkuban Perahu

The prior and after heating treatment results show that the treatment enhanced the permeability values. Initially, the permeability of all sample rocks could not be detected. The estimation of minimum detectable permeability value by Ruska gas permeameter (for the length and diameter size of 15 mm and 30 mm) is around 2.6 millidarcy. It comes from the most minimum air flow at 0.25 atm and based on the most minimum scale reading that can be noted (8 mm). Below that value, the permeability is considered as undetectable.

Servo-controlled semi-steady-flow permeameter is used in the evaluation of some basalts in another paper and it can detect the very low permeability value such as 1.5×10^{-16} m^2 (0.15 millidarcy) for the Etnean basalt and 9×10^{-21} m^2 (9×10^{-6} millidarcy) for the Seljadur basalt (S. Vinciguerraa, 2005). By looking the permeability result after heating treatment below, it follows the linear trend from 200 to 400°C but failed to show higher permeability value at 500°C (even though it shows higher porosity value). As it mentioned before, more cores can give a more predictable result. One core for one heating experiment could not give a solid representative of the treatment result.

Increase permeability value after the heating treatment might be caused by:

a. Increasing fluid pathways due to creation or extended microfractures.

b. Isolated pores are connected to the existed interconnected pores.

c. Some minerals may be dissolved by the water and generate the fluid pathways.

d. The heating experiment removes or restructured the clay-bound-water or the clay from the basalt. Andesite Tangkuban Perahu is considered as the altered basalt rock based on its appearance. Based on the mineral composition evaluation by EMPA, there is some detected clay that consists of mostly silica and alumina. Oven-dried core porosity includes the hydration or clay-bound water removal (Eslinger & Pevear, 1988). In addition, drying the core in high temperature can destroy the delicate clay structure (Kodikara, 1999).
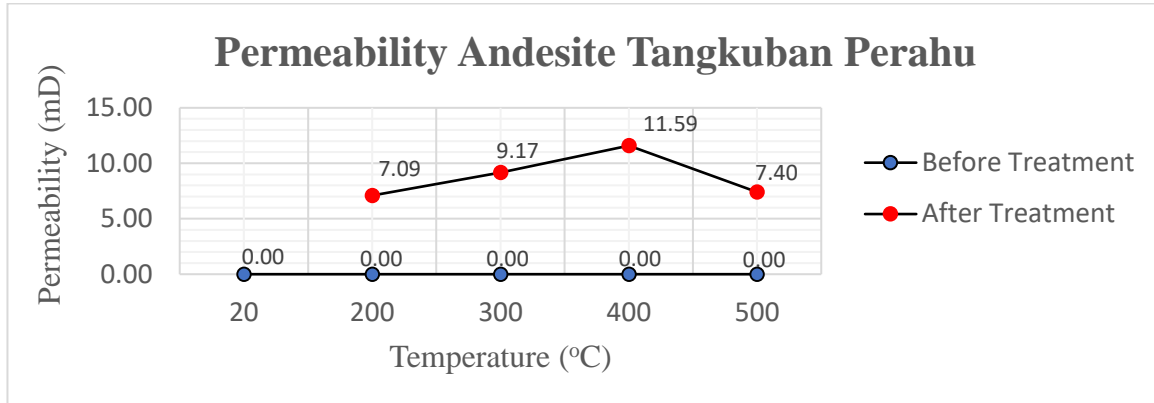
Graphic 20 Permeability values before and after treatment for andesite Tangkuban Perahu

4.2.2 Decrease static elastic moduli over higher thermal shock effect

Stress and Strain

Stress and strain are the main parameters that were measured from the practical experiment. In the stress-strain illustration graphic, every zone distinguishes the crack closure, the maximum point of the elastic condition, stable and unstable crack growth and the peak/post-peak region. The data selection relies on the qualitative interpretation, which is based on the line slope interpretation, to determine the static moduli. All of the cores in this experiment either showing the strong or tough characteristic. Over the higher thermal shock exposure, all rocks show less strong characteristic. No core has the ductile characteristic because none of them has a decreased stress gradually over the progressive strain after reached the stress-strain peak.

Thermal shock effect of all rocks in a particular heating temperature

To compare every rock and to see the strength order among them, the stress-strain graphs of all sample rocks are plotted at same temperature by considering all rocks are exposed to the same heating temperature. Every rock has its own inconsistent strength order over the temperature. One type of rock may show to be the weakest amongst all rocks but in a certain temperature it becomes one of the toughest rock.

The stress-strain graphics below shows the rock characteristic in the original condition from 20 to 500°C. Basalt Eifel Z-plane is considered to be the strongest rock. Contrary to its X-Plane cores, statistically it is showed to be the least strength rock amongst the others (even though its original condition were not as weak

as the heated conditions). The other rocks generally have similar stress-shear trend that are getting less strong with higher temperature.
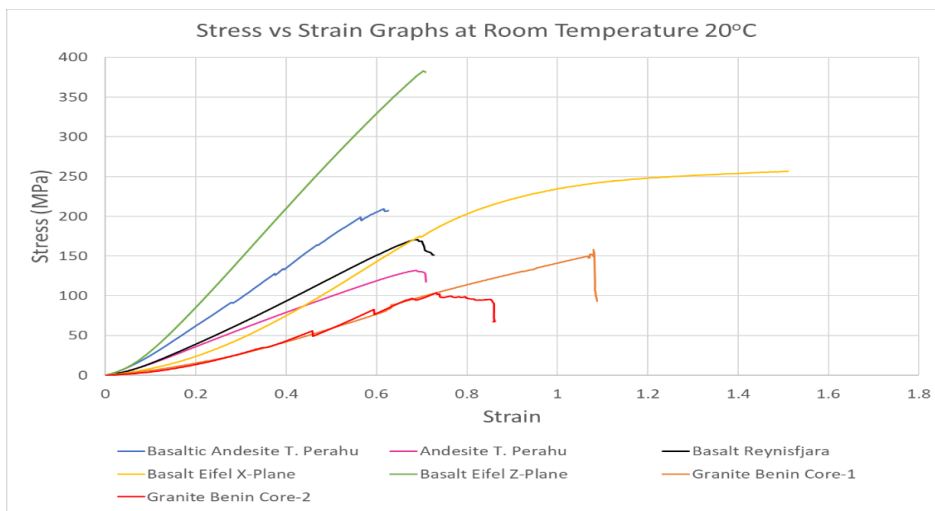
Graphic 21 Stress strain graphs for different type of rock under room temperature 20ºC
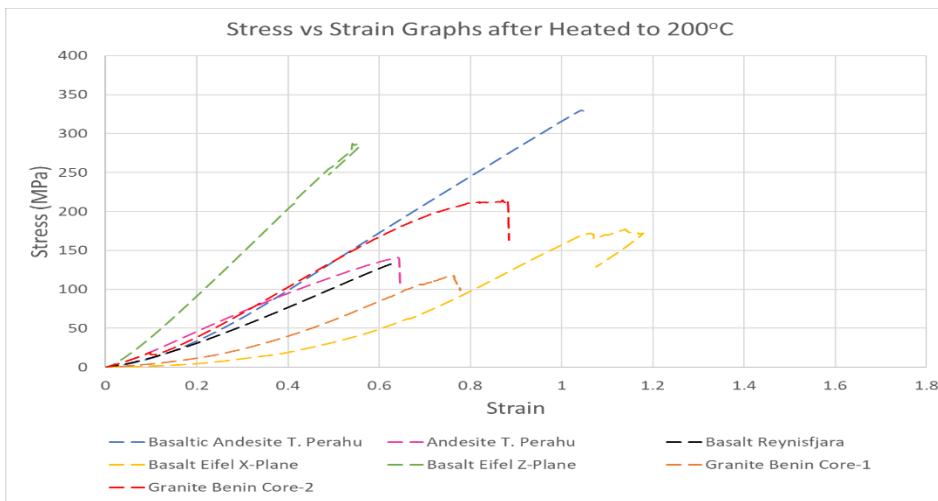
Graphic 22 Stress strain graphs for different type of rock under heating temperature 200ºC
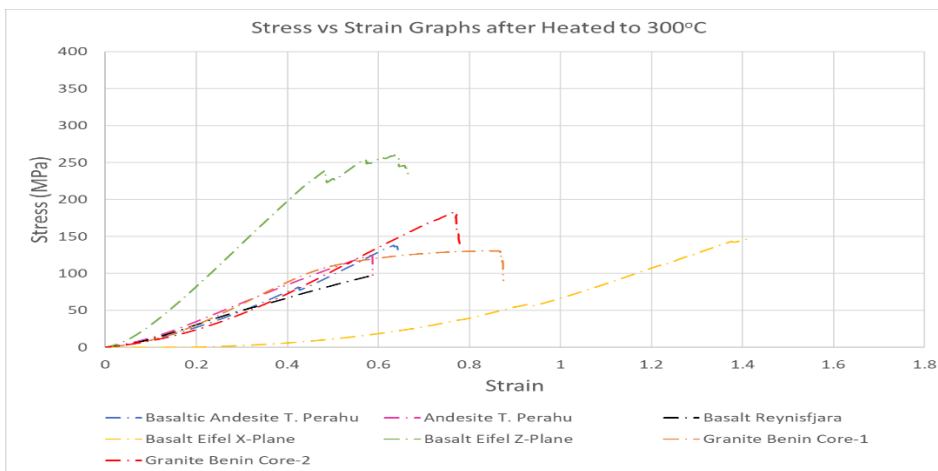
Graphic 23 Stress strain graphs for different type of rock under heating temperature 300ºC
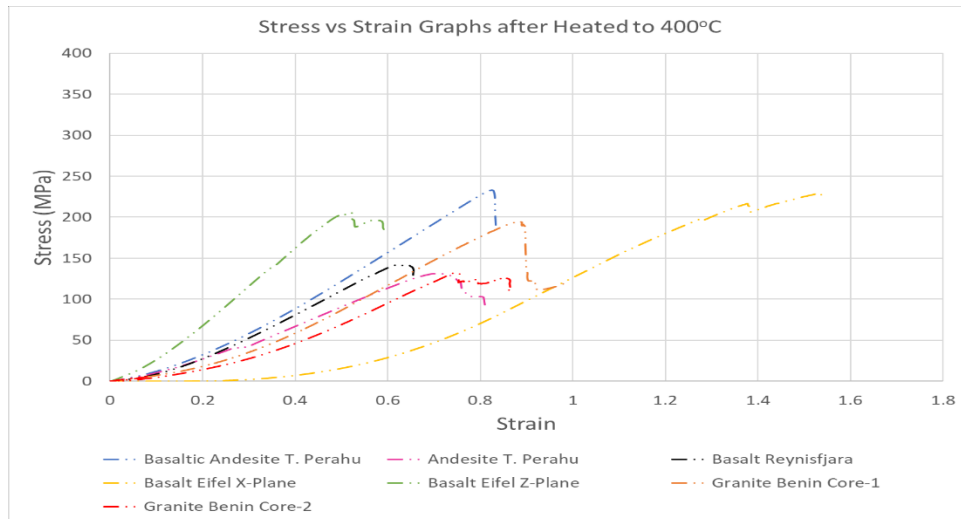
Graphic 24 Stress strain graphs for different type of rock under heating temperature 400ºC
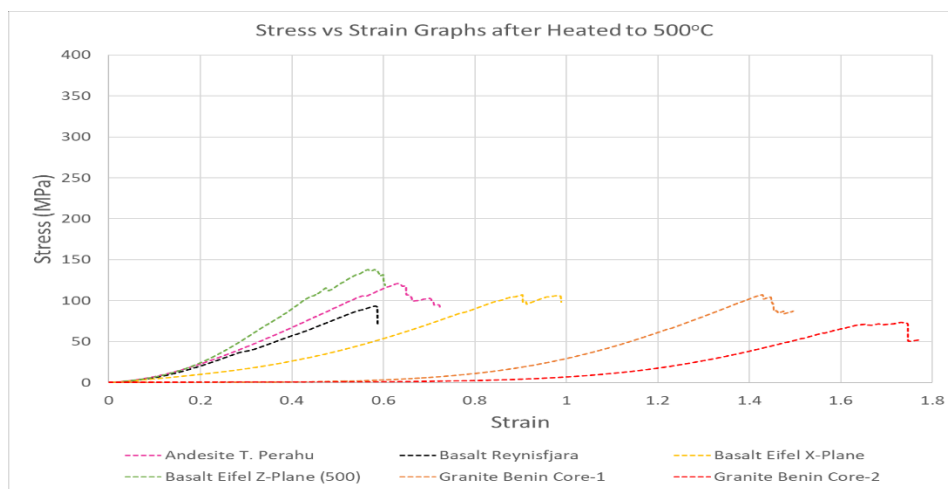
Graphic 25 Stress strain graphs for different type of rock under heating temperature 500ºC

Thermal shock effect of each rock in all heating temperature

After the rocks have been compared to each other, the next evaluation is to see each rock's exposure to five heating temperatures. Each of the graph below will show how strong of the rock in the initial condition and its strength decline over the progressive heating temperature. Basaltic andesite Tangkuban Perahu, considered as the second strongest rock in this thesis, is a good example of how the heating exposure creates the changes in the rock strength. Over the higher heating temperature, the stress-strain slope decreases and the ultimate compressive stress is lower. All the stress-strain curves are generally linear to the maximum strain and terminated in the fracture without a well notified plastic zone which characterize a brittle rock type. In conclusion, the higher the heating temperature the less strong the rock is.
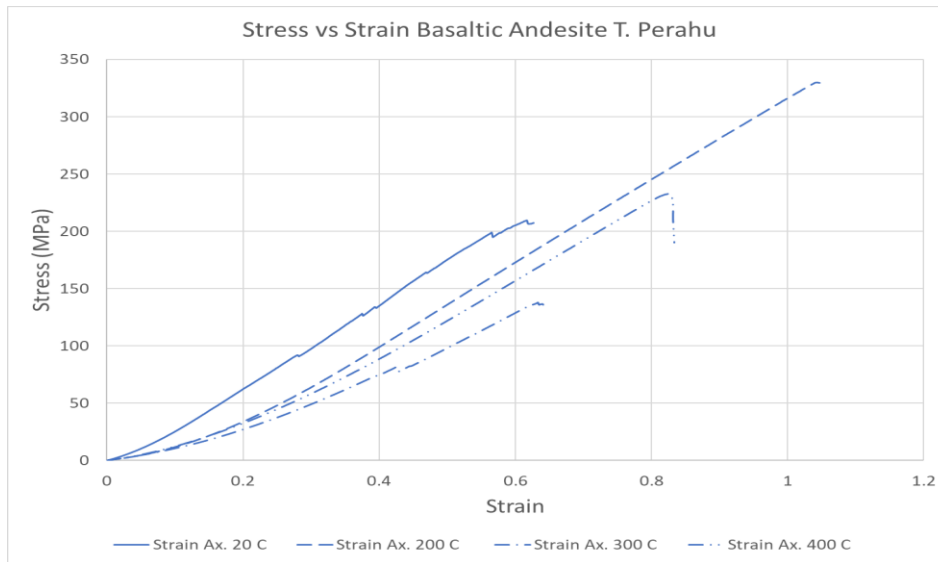
Graphic 26 Stress strain graphs of various thermal shock from basaltic andesite Tangkuban Perahu

During the UCS experiment, the procedure is finished in a single action which means there is no elasticity check during the middle of the experiment. Once the strain increased, the experiment was kept until it reached the ultimate compressive strength. Most of the rocks exhibit the linear stress-strain characteristic, and some cores exhibited a bursting condition, without any plastic condition was observed.

The andesite Tangkuban Perahu also showed the same trend condition, except the core without heating treatment due to variability. As only one core is tested, the result may more deviate from the prediction. One solution to prove the variability is by testing multiple cores with the same heating treatment. A large number of cores should be tested to get the correct range or trend. In the basalt rock from Reynisfjara (Iceland), the order of the heating temperature trend is reversed between 200ºC and 300ºC but it may be caused by the heterogeneity of the material.
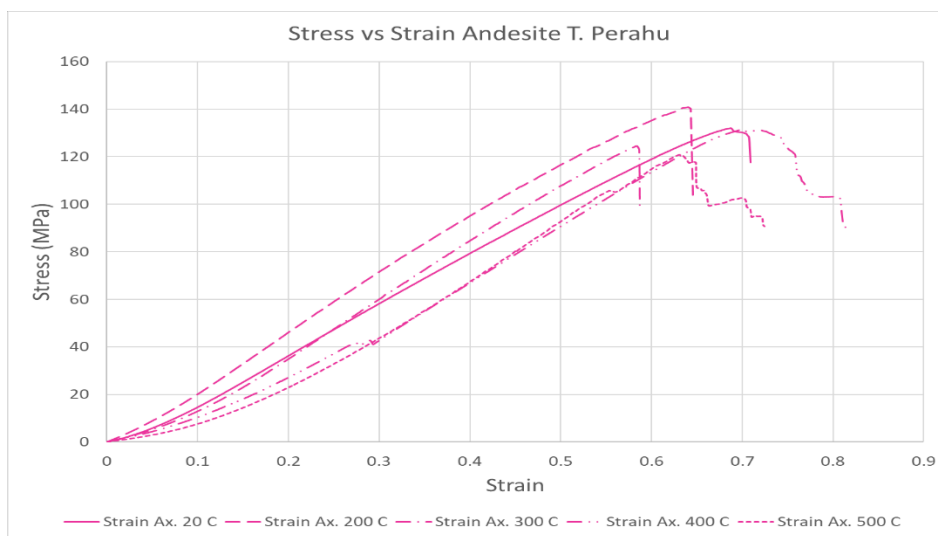
Graphic 27 Stress strain graphs of various thermal shock from andesite Tangkuban Perahu
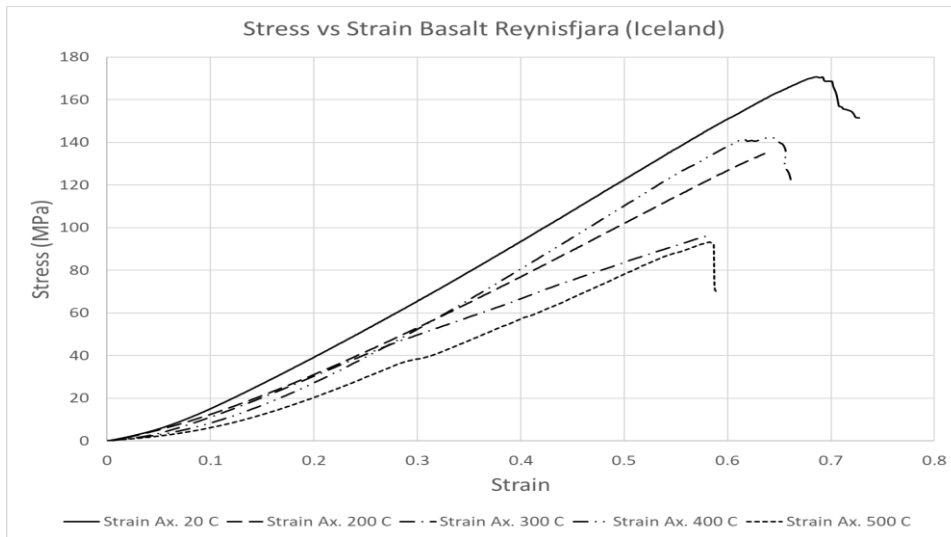
Graphic 28 Stress strain graphs of various thermal shock from basalt Reynisfjara – Iceland
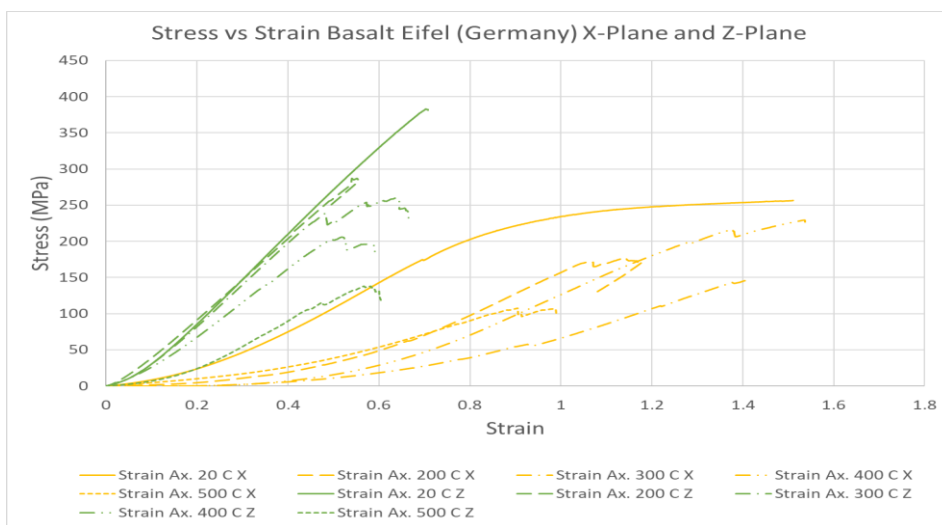
Graphic 29 Stress strain graphs of various thermal shock from basalt Eifel (X and Z plane)
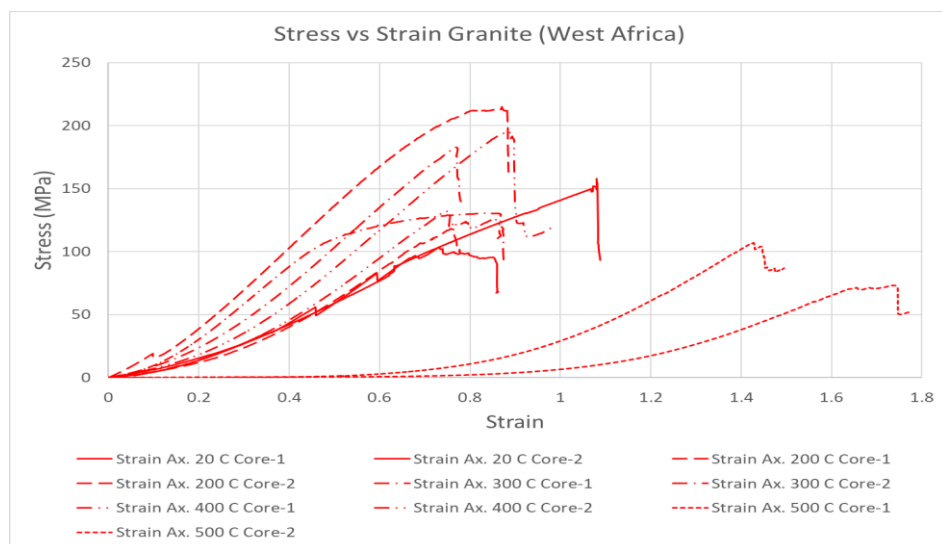
Graphic 30 Stress strain graphs of various thermal shock from granite Benin

However, it seems only the first core from the X-plane experienced this event and no other cores experienced the same. It is because during the UCS test the core was too strong (we can also compare it with the 20ºC core

from Z-Plane) and deformed the iron cups (top and bottom) of seismic transducers. That is the main reason of the absence of sonic acquisition measurement for the Tangkuban Perahu and Reynisfjara basalt (and decided to terminate for all rocks). Hence, the dynamic moduli are not analyzed in this thesis. Based on the evaluation of each heating temperature and each type of rocks, the inconsistent result might be affected by:

1. The heterogeneity of the starting material. The cores that are made from the same bulk rock may visually look homogenous but the structure and mineral composition might be different (such as a complex composition of granite) on a micro scale.

2. The variability of the micro fracture network formed during the heating treatment. Some cores may have the natural microfracture before the experiment and some may not. The microfracture that is created by the thermal shock should be more in the core that has initial natural microfracture.

These factors affect the variability from the same rock and should be assessed more in the micro-CT scan visualization and EMPA result discussion.

Young's modulus and Poisson's ratio

The influence of the thermal process is measured directly from the deformation due to application of known force (uniaxial compression). The in-situ stress application results, Young's modulus and Poisson's ratio, are used to evaluate the stress distribution, deformation easiness and toughness of the rock sample. In order to calculate the Young's modulus, the stress and the axial stress value should be obtained. The value given from the UCS record is the force. The area of the core is added into the stress (σ) calculation (F =P/A). In other variable, the axial strain (ε) value is obtained from the change of the length over the initial length ($\Delta L/Lo$). Thereafter, the Young's modulus is written as below.

$$E = \frac{Stress}{Strain} = \frac{F/A}{\Delta L/L}$$

Poisson's ratio is a ratio of the radial strain over the axial strain.

$$v = \frac{\varepsilon_{radial}}{\varepsilon_{axial}}$$

The ultimate compressive strength measured is the latest value obtained before the core is totally deformed or damaged. Most of the value can be seen from the generated graph, except one basalt core that was stopped before it reaches the ultimate strength due to the safety distance of the LVDT (basalt Eifel X-plane core 20°C). Apart from the three variables previously mentioned, the crack initiation is also predicted from the graph analyses.

The results show both Young's modulus and Poisson's ratio are getting lower over the higher thermal shock exposures. In the graphs that show the changing of the stress-strain slope over the thermal shock exposure, it was obvious that the slope decreases. The quick interpretation of Young's modulus can be determined by the slope. In the low strain situation, the rock material still obeys the Hooke's Law hence the stress (σ) is proportional to strain (ε) with Young's modulus (E) as the constant.

$$\sigma = E\varepsilon \quad or \quad E = \sigma/\varepsilon$$

All the cores are still in the category of strong rock but it is getting less as it exposed to higher thermal shock. In the graph interpretation (in chapter 3), it does not only plot the straight line to find the constant E because the crack may initiate and bring the stress-strain curve into the plastic flow (non-linearity started to happen).

There are two possible reasons of E value decreases over the higher thermal shock.

1. The stress is less required over the same axial strain generated. Having said that, the effect of the microcracks on the elastic properties of rock is getting higher and the cores are getting less strong.

2. Some types of rock (granite Benin and basalt Eifel) exhibited a subtle longer length of core (0.01-0.07 mm) after the heating treatment. The equation of the axial strain consists of the change of length and the initial length. When the change of length is higher the axial strain is higher too and the Young's modulus will be lower.

The second reason was not very convinced to be the main reason due to only two types of rocks possess the effect (basalt Eifel and granite Benin).

The other static elastic parameter is the Poisson's ratio (v), the comparison of the radial strain over the axial strain. The v value is also obtained from the slope of the stress-strain graph but it requires two slopes from stress-strain axial and stress-strain radial. The normalized Poisson's ratio also shows the decreasing v value over the higher thermal shock exposure.

$$\frac{Stress_{axial}/Strain_{axial}}{Stress_{radial}/Strain_{radial}} = \frac{Strain_{radial}}{Strain_{axial}}$$

Basaltic andesite Tangkuban Perahu shows the most significant reduced v value and basalt Eifel Z-plane in contrary has the least (its 500ºC treatment result is quite similar to the non-heated core). Two reasons of why all the types of the rock show a lower value of Poisson's ratio:

1. Microfractures distribution in the sample core affect the stiffness of the core and form the core into more brittle condition. The cylinder core starts to ruptures radially earlier by the same amount of the axial strain generated (basalt TPB is the perfect example of the reduction of v value).

2. Some minerals inside the sample core were heated when the cores were exposed to higher temperature. It might create a fissure space inside the core and increase the brittleness of the cores.

In conclusion, both E and v values decrease when the heating temperature increases. Both moduli are mainly affected by the microfractures created during the heating treatment. Further visualization of the microfractures will be delivered in the micro-CT scan and EMPA result analysis.

4.3 Visualization of the microfracture characterization

There are two ways to observe the microfractures in this thesis: CT-Scan visualization and the Electron Microprobe Analyzer (EMPA). The CT-Scan generated the three-dimensional image that contains the position and density of the absorbing object (Phoenix X-Ray Computed Tomography poster). The micro-CT scan resolution used in this thesis is initially 60 µm and changed to 30 µm for the 3D image construction. The observed microfractures could be partially detected from the visualization by using the Avizo software because the smallest detected pores volumes are still in the mm^3 unit.

4.3.1 Micro-CT scanner result shows higher porosity image but do not show microfractures

Intensity range plays a major rule in detecting the pores. Big pores are easy to be detected and some of them can visualize the image of their connection to other pores which created the interconnected pores. The micro pores are also detected but it does not show any microfractures. In addition, it can be biased as the noise when the intensity is adjusted to a very small pixel size. As we focused on visualizing the microfracture induced by the thermal shock experiment, it is quite difficult to rely on micro-CT scan result to observe the microfractures.
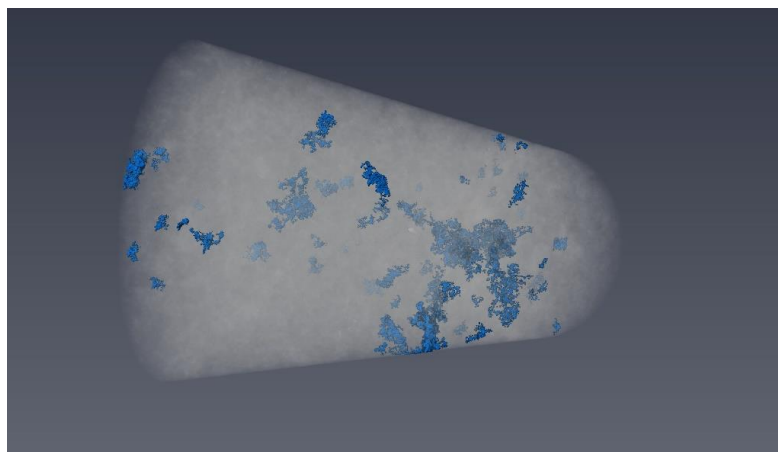
Figure 36 Porosity image example of andesite Tangkuban Perahu

4.3.2 Mini cores visualization shows higher porosity in the outside part of the core

Further smaller cores have been analyzed by using the micro-CT scan. The cylinder cores are drilled from a quarter sized core to have more detail scanning image construction (see chapter 2.4). The image of the porosity is visualized and quantified by calculating the porosity of the three sections (two sections of the outer cylinder and one section of the inner cylinder).

By positioning the core vertically (figures below), the porosity for each section is listed below:

Porosity of small core B upper section/middle section/lower section: 0.56% / 0.05% / 0.17%

Porosity of small core D upper section/middle section/lower section: 0.18% / 0.02% / 0.06%

The total length of the small core is divided into three sections (the upper, middle and lower orientation section) and the porosity of each section is calculated by dividing the pores volume in each section over the third of the total volume. It is obvious from these cores that the inner core does not have higher porosity compared to the outer sections. It means, the microcracks or microfractures exists more on the outside of the core than in the inner part of the core.

Figure 37 Pore distribution small core B Tangkuban Perahu (left) and small core D Tangkuban Perahu (right)

4.3.3 Visualization by Electron Microprobe Analyzer (EMPA) shows the microfractures

Because we are interested in the microfractures investigation, we have decided to analyze the cores at the Electron Microprobe Analyzer. It works by having an electron beam hitting the sample's surface and the intensities are measured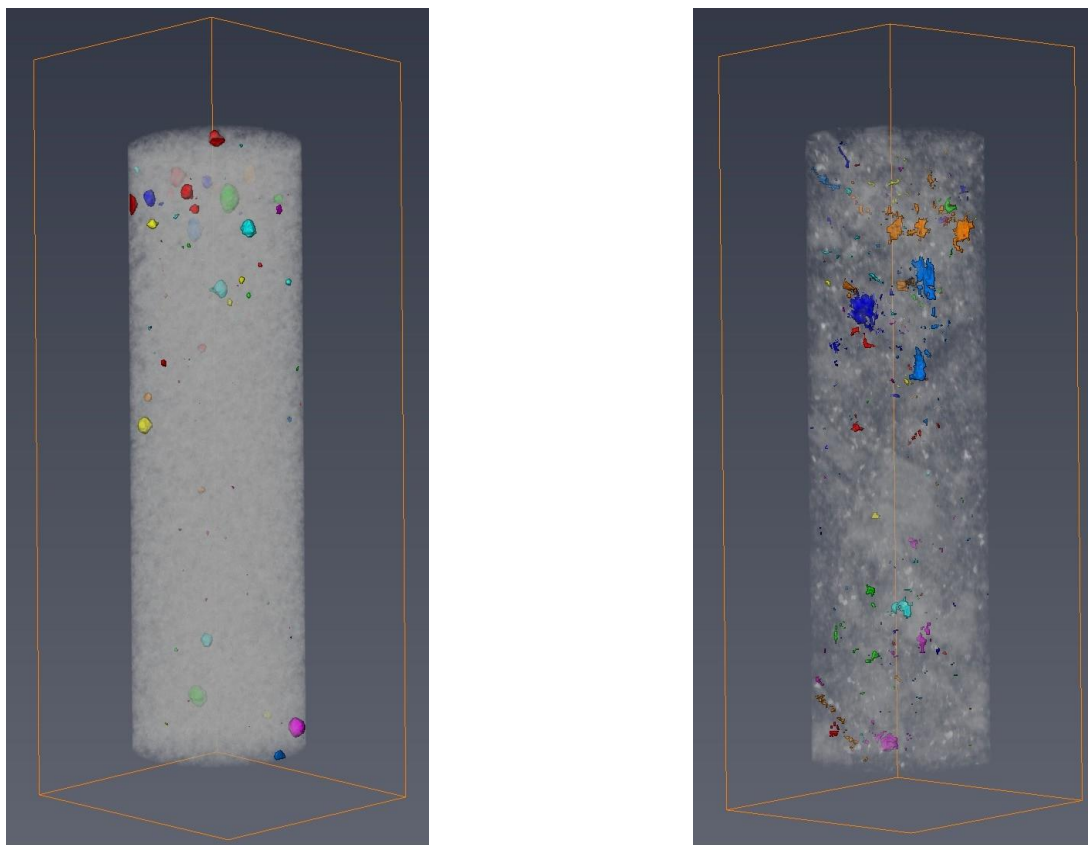 with wavelength or energy dispersive spectrometers (GFZ Potsdam, 2017). In practical words, the thin section is placed into a sample holder put inside a specific chamber of the electron microprobes. With the observation tools of the device, the specific spot to be analyzed can be located. Beside very detailed image acquirement, the EMPA allow to determine the exact chemical composition of each single mineral by performing point analysis. The instrument should be always calibrated on well-characterized standards according to the mineral phases that will be investigated. In this work, no point analysis have been conducted using a standard but only EBS measurement on spots-areas have been performed. The high resolution of the EMPA (few micro) is very useful in visualizing the microfractures. The detected cracks are mostly the trans granular cracks (running across the grains) and the intragranular cracks (within grains) with width around 1-5 µm. The definition of the trans granular and intragranular is based on the journal by Kranz in 1983. It is quite difficult to distinguish the intergranular cracks (between minerals) in the image because of its tiny size and difficulties to difference it with the grain borders. Below is the EMPA image from andesite, the red square shows the trans granular cracks and the yellow square shows the intragranular cracks. Another core from Tangkuban Perahu, TPB core, also shows the intragranular cracks and trans granular cracks. The blue square shows the trans granular cracks and the yellow square shows the intragranular cracks. The width of the intragranular cracks is qualitatively less than 1µm and the length is way less than the diameter of the grain, which suits the intragranular definition from Kranz (1983) in his journal.
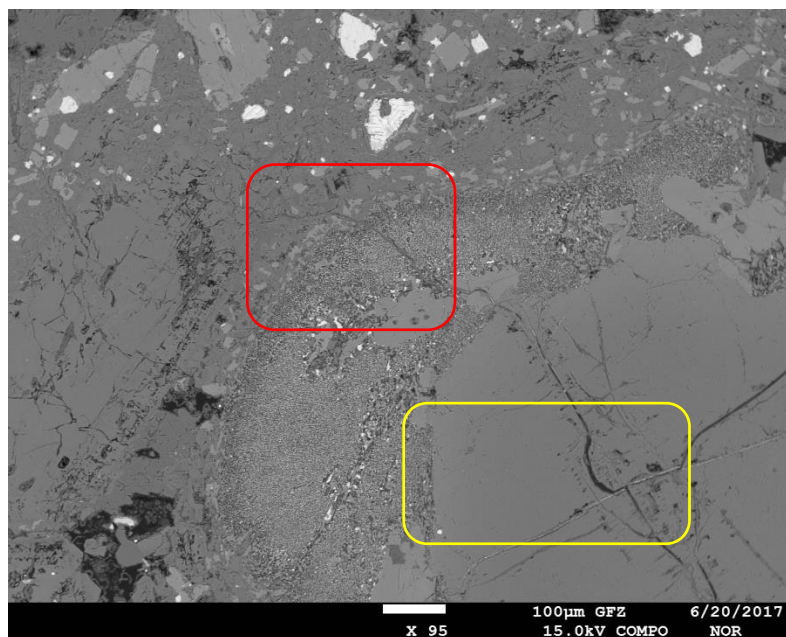

Figure 38 Image acquired at the EMPA of andesite Tangkuban Perahu point 15
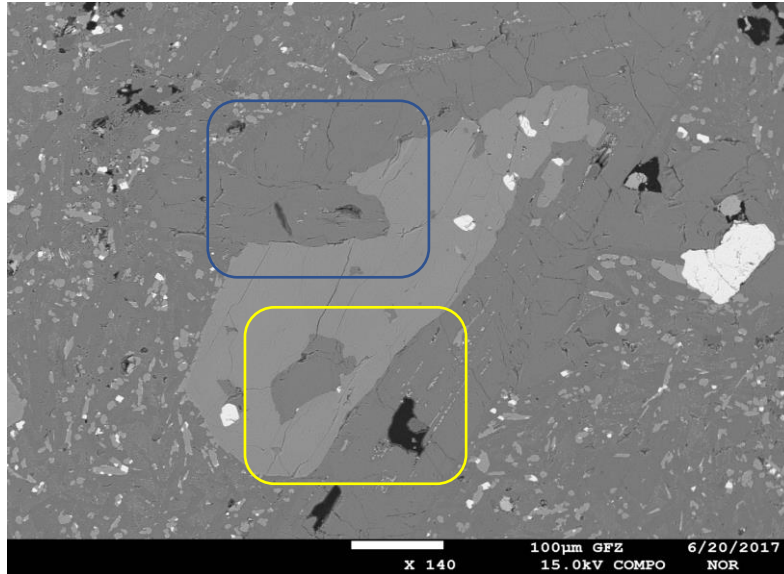
Figure 39 Image acquired at the EMPA of basaltic andesite Tangkuban Perahu point 2

The direction of the stress-induced microcracks mostly oriented within 30° of the macroscopic maximum stress direction (Kranz, 1983). The andesite Tangkuban Perahu microfractures image above show the trends in all direction. The thin section from the andesite is from a core that was heated at 500^oC and was taken out vertically from the center of the core. Another core from the same rock that was heated to the same temperature experienced the UCS test and show the microfracture direction following the compression stress direction. However, to prove the statement from Kranz above, the core compression stress should also be applied to the core that has the thin section (this core only experienced the heating experiment). For further investigation of the microcracks, the linear crack density (LCD) can be used to know the number of cracks from some specific lines by using the scanning electron microscope (Sousa, 2004). However, the particular scanning to obtain LCD is not conducted during this thesis period. The practical objective of the EMPA is only to acquire images of the microfractures to identify the mineral forming the rocks and its composition. The first objective is accomplished and the second objective will be explained in the next sub-chapter.

Figure 40 Andesite Tangkuban Perahu core before UCS test (left) and after UCS test (right)

4.4 Implication of the thermal shock effect to the sample cores

4.4.1 Brittleness Index application that shows the cores generally become less strong

All the core results present the lower value of Young's modulus and lower value of Poisson's ratio over the higher heating temperature. These static moduli affect the BI calculation. Qualitatively, the BI values are decreased over the higher heating temperature (even though each of the point does not literally follow the trend line) and represent the less strong characteristic of the rock when it is exposed to the higher thermal shock. High BI value indicates the quartz rich lithology and low BI indicates clay rich lithology which quartz' character is stiffer than clay in the aggregate material (Jorg V. Herwanger, 2015). Quantitatively, based on the four methods, strong rocks have a high chance to not giving any reversible stress during the UCS test or strain elastic is more than the strain plastic which leads to an absence of BI values. In conclusion, the BI calculation in this thesis needs more cores to have the more valid result. With this core limitation, the result only shows a broad range of BI and should not be used as the solid variable in determining the brittleness characteristic of the rock.

4.4.2 Thermal induced microfractures in the geothermal fields

The creation of the thermal induced microfractures supported the hydrofracturing process in the Enhanced Geothermal System (EGS) scenario. By injecting the gallons of water from the surface at a high rate, the water temperature was kept at a low-temperature level to create the thermal shock that opens up the cracks in the formation rock. It increases the fluid pathways in micro size and likely to increase the permeability of the rocks. Moreover, the injected fluid should not contain chemicals as only temperature matters (such as chemical used along with water during the stimulation process) and only water is used.

In the other side, the operating/developed geothermal fields in Indonesia also have a reservoir temperature range from around 240 to 330°C (Amir Fauzi, 2000). By investigating the thermal creation in the wide temperature shock range, the analysis of the microfractures creation is wider and show more trend towards the thermal shock implication. Each geothermal area also has different rock characteristics, such as Tangkuban Perahu area that has basaltic andesite, andesite and pumice rock in one field. Thus, by having more different sample rocks and looking the thesis result, each rock can be correlated based on their mechanical properties to see their characteristic under thermal shock application.

5. Conclusion and Recommendations

5.1 Conclusions

Based on some practical series, there are some points can be concluded:

1. The porosity values after the heating treatment are higher than before heating treatment. The increased range starts from 1.02 times (basalt Reynisfjara) to 85.5 times (basalt Eifel Y-plane) increased value. It is a very significant increased porosity value of basalt Eifel, however, it only changes from 0.15% porosity to 1.27% porosity. In contrary, the 1.9% increase porosity value of basalt Reynisfjara is coming from 14.09% porosity to 14.36% porosity value. Basalt Reynisfjara has the biggest porosity amongst all and basalt Eifel Y-plane has the smallest one.

2. Before any heating treatment, most of the cores had undetectable permeability value with low porosity value (some of them have small permeability value, but could not put in the Ruska gas permeameter graph). Only andesite Tangkuban Perahu and basalt Reynisfjara gives a significant increase value of permeability. Basalt andesite show 7-11 millidarcy permeability value and the basalt Reynisfjara show around 4.45 millidarcy.

3. Basaltic andesite Tangkuban Perahu is a good example of how the heating exposure creates the changes in the rock strength. Over the higher heating temperature, the stress-strain slope decreases and the ultimate compression stress is lower. All the stress-strain curves are generally linear to the maximum strain and terminated in the fracture without any well-notified plastic zone which characterized a brittle rock type.

4. The inconsistent result of each rock's strain-stress curve might be affected by the heterogeneity of the starting material and the variability of the micro fracture network formed during the heating treatment.

5. Two reasons of E value is getting lower over the higher thermal shock: over the same axial strain generated the stress required is less and some types of rock (granite Benin and basalt Eifel) exhibited a subtle longer length of the core (0.01-0.07 mm) after the heating treatment. However, the second reason was not very convinced to be the main reason due to only two types of rocks possess the effect.

6. All types of the rock show lower value of Poisson's ratio over the higher thermal shock. There are two reasons behind this phenomenon: microcracks distribution in the sample core affect the stiffness of the core and some heated minerals might create a fissure space inside the core (and increase the brittleness of the cores).

7. Qualitatively, the BI values are decreased over the higher heating temperature and represent the less strong characteristic of the rock when it is exposed to the higher thermal shock. Quantitatively, the BI calculation need more cores to have a more valid result.

8. The micro-CT scan resolution used in this thesis is initially 60 µm and changed to 30 µm for a faster 3D image construction. The observed microfractures could not be particularly detected from the visualization by using the Avizo software because the smallest detected pores volumes are still in the mm^3 unit and it could not give the visualization of the microfractures.

9. EMPA could give more insights about the microfractures in the cores. The detected cracks are mostly the trans granular cracks (running across the grains) and the intragranular cracks (within grains) with width around 1-5 µm.

10. The small size cores show that the inner core does not have higher porosity compared to the outer sections. It means, the microcracks or microfractures exists more on the outside of the core than in the center of the core.

11. EMPA allows to detect the major forming minerals in the rocks, such as plagioclase and to validate the XRD results. Moreover, the device allows detecting mineral phases which are low concentrated in the rock.

12. Based on the chemical composition, basaltic andesite Tangkuban Perahu rock, with 53.37% silica is considered as basaltic andesite. Andesite Tangkuban Perahu rock, with 62.23% silica is considered as andesite rock.

13. Many subsurface complexity factors are not included in the experiment such as the heterogeneity in the subsurface, the geometry/structure/fault, shallow subsurface compaction, background stress distribution and the pressure change during the operations.

5.2 Recommendations

1. Further XRF measurement should be planned to analyze the sodium oxide. The classification of volcanic rock can be completed by having silica combined with sodium and potassium oxide.

2. Generally, the more number of cores will give more valid representative result in analyzing properties, such as porosity and permeability. In addition, the stress-strain analysis and BI calculation will be significantly improved by more sample results.

3. It is suggested to use the servo controlled semi-steady-flow permeameter to measure the permeability of the very strong rock with very low porosity value like the basaltic rock. Therefore, the undetectable permeability value can be detected.

4. The heating experiment needs a longer procedure, it is better to put the core in the oven at low temperature to avoid an unnecessary thermal shock when it is put inside the oven in the beginning. Practically, after the

oven was used for 200ºC, it continued to heat until 300ºC based in the system. The core that was prepared for 300ºC heating treatment exposed the thermal shock from room temperature to 200ºC immediately.

5. On some experiments, the crack initiation stress even cannot be noticed due to the strength of the sample cores. The strain rate that was mostly used in this experiment is 0.0009/s, lower speed may give more noticeable crack initiation event.

6. Some very strong rock could not give the reversible stress, which leads to an absence of some BI method. There are around 24 BI methods that well recognized, some methods should be investigated further so it can give the clearer interpretation.

7. If possible, the measurement of the bulk volume of each core should be done by the Avizo visualization. All the scanned cores never show a perfect cylinder, thus the volume calculation (which lead to the porosity value) and the length measurement (which can lead to the E evaluation) are valid.

8. For further investigation of the microcracks, the linear crack density (LCD) can be used to know the number of cracks from some specific lines by using the scanning electron microscope.

6. Appendix

Appendix 1: Circumferential Strain Correction Factor Calculation

Circumferential Strain Correction

| Core ID	Rock Type	Orientation	Li	Reading from the result: Chain Initial	Chain final	Delta L	Ri	r	Li/(2(Ri+r))	tetha (θ) in radian	Circumference Change (ΔC)	% Difference	Speed
TPB01	Basalt (Tangkuban Perahu)	n/a	24.00	22.04	22.66	0.62	14.93	2.24	0.70	1.55	0.81	31.31	0.0009
TPB02	Basalt (Tangkuban Perahu)	n/a	23.20	22.01	22.28	0.27	14.90	2.24	0.68	1.49	0.35	28.63	0.0009
TPB03	Basalt (Tangkuban Perahu)	n/a	24.10	22.01	22.45	0.44	14.90	2.24	0.70	1.56	0.58	31.84	0.0009
TPB04	Basalt (Tangkuban Perahu)	n/a	23.30	21.98	22.08	0.11	14.87	2.24	0.68	1.50	0.14	29.11	0.0009
TPD01	Andesitic Basalt (T.Perahu)	n/a	22.70	22.01	22.25	0.24	14.91	2.24	0.66	1.45	0.30	26.94	0.0009
TPD02	Andesitic Basalt (T.Perahu)	n/a	23.70	22.05	22.19	0.14	14.92	2.24	0.69	1.52	0.19	30.27	0.0009
TPD03	Andesitic Basalt (T.Perahu)	n/a	23.50	21.97	22.11	0.14	14.90	2.24	0.69	1.51	0.18	29.66	0.0009
TPD04	Andesitic Basalt (T.Perahu)	n/a	23.90	22.02	22.20	0.17	14.91	2.24	0.70	1.54	0.23	31.05	0.0009
TPD05	Andesitic Basalt (T.Perahu)	n/a	22.80	22.05	22.34	0.29	14.91	2.24	0.66	1.45	0.38	27.26	0.0009
IC01	Basalt Reynisfjara (Iceland)	n/a	23.50	21.95	22.17	0.22	14.91	2.24	0.69	1.51	0.29	29.61	0.0009
IC02	Basalt Reynisfjara (Iceland)	n/a	23.40	21.98	22.21	0.22	14.90	2.24	0.68	1.50	0.29	29.31	0.0009
IC03	Basalt Reynisfjara (Iceland)	n/a	23.60	22.01	22.48	0.47	14.90	2.24	0.69	1.52	0.60	30.02	0.0009
IC04	Basalt Reynisfjara (Iceland)	n/a	23.40	21.97	22.14	0.18	14.90	2.24	0.68	1.50	0.23	29.31	0.0009
IC05	Basalt Reynisfjara (Iceland)	n/a	23.40	22.00	22.19	0.19	14.90	2.24	0.68	1.50	0.25	29.31	0.0009
TI009	Granite (Benin)	n/a	22.75	22.04	22.42	0.38	14.89	2.24	0.66	1.45	0.48	27.19	0.0007
TI012	Granite (Benin)	n/a	22.56	21.96	23.24	1.28	14.88	2.24	0.66	1.44	1.62	26.62	0.0007
TI004	Granite (Benin)	n/a	22.79	22.18	22.82	0.63	14.90	2.24	0.66	1.45	0.81	27.27	0.0007
TI006	Granite (Benin)	n/a	22.35	22.20	23.01	0.81	14.90	2.24	0.65	1.42	1.02	25.89	0.0007
TI001	Granite (Benin)	n/a	22.54	22.07	22.26	0.19	14.91	2.24	0.66	1.43	0.25	26.43	0.0007
TI007	Granite (Benin)	n/a	22.43	22.10	22.16	0.07	14.91	2.24	0.65	1.43	0.08	26.09	0.0007
TI003	Granite (Benin)	n/a	22.86	22.23	22.28	0.05	14.92	2.24	0.67	1.46	0.07	27.41	0.0007
TI005	Granite (Benin)	n/a	22.80	22.20	22.26	0.06	14.93	2.24	0.66	1.45	0.08	27.18	0.0007
TI002	Granite (Benin)	n/a	22.88	22.36	22.38	0.01	14.94	2.24	0.67	1.46	0.02	27.39	0.0007
TI013	Granite (Benin)	n/a	22.84	22.39	23.19	0.80	14.93	2.24	0.67	1.46	1.01	27.30	0.0007
A1X	Basalt (Eifel)	X-Plane	22.13	21.92	22.14	0.22	14.86	2.24	0.65	1.41	0.28	25.37	0.0007
A3X	Basalt (Eifel)	X-Plane	22.41	21.88	24.35	2.47	14.86	2.24	0.66	1.43	3.12	26.24	0.0007
C4AX	Basalt (Eifel)	X-Plane	22.29	21.92	23.22	1.30	14.86	2.24	0.65	1.42	1.63	25.86	0.0007
C5AX	Basalt (Eifel)	X-Plane	22.05	22.00	22.35	0.35	14.86	2.24	0.64	1.40	0.44	25.13	0.0007
C5BX	Basalt (Eifel)	X-Plane	22.35	22.01	22.03	0.02	14.87	2.24	0.65	1.42	0.03	26.01	0.0007
A4Z	Basalt (Eifel)	Z-Plane	17.44	21.94	22.04	0.10	14.87	2.24	0.51	1.07	0.11	14.13	0.0007
A5Z	Basalt (Eifel)	Z-Plane	17.41	21.95	22.54	0.59	14.86	2.24	0.51	1.07	0.67	14.10	0.0007
A6Z	Basalt (Eifel)	Z-Plane	17.54	22.01	24.72	2.71	14.86	2.24	0.51	1.08	3.10	14.34	0.0007
C1AZ	Basalt (Eifel)	Z-Plane	17.70	21.99	22.46	0.46	14.86	2.24	0.52	1.09	0.53	14.65	0.0007
C2BZ	Basalt (Eifel)	Z-Plane	17.69	22.02	22.77	0.74	14.87	2.24	0.52	1.09	0.85	14.61	0.0007

Basaltic andesite rock Tangkuban Perahu

Andesite rock Tangkuban Perahu
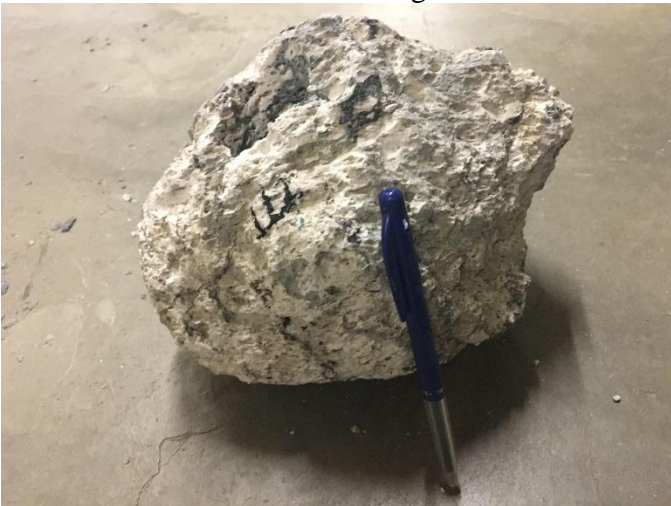
Pumice rock Tangkuban Perahu
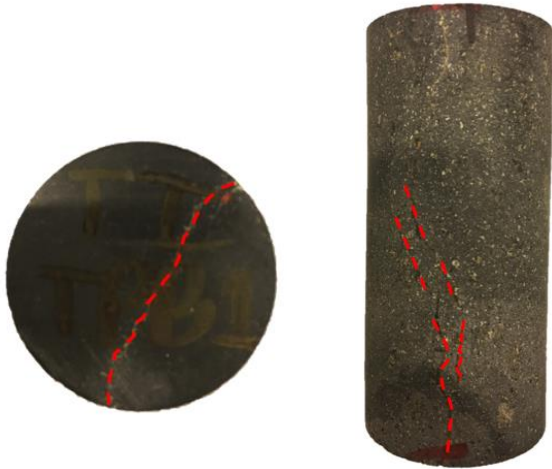

Basalt rock Eifel - Germany
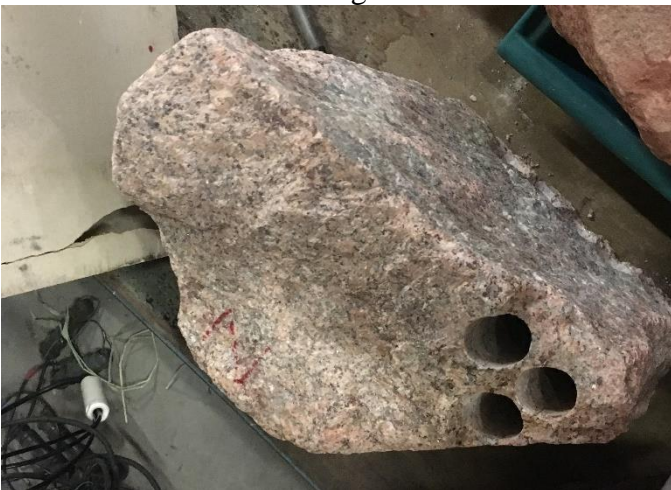
Granite rock Benin
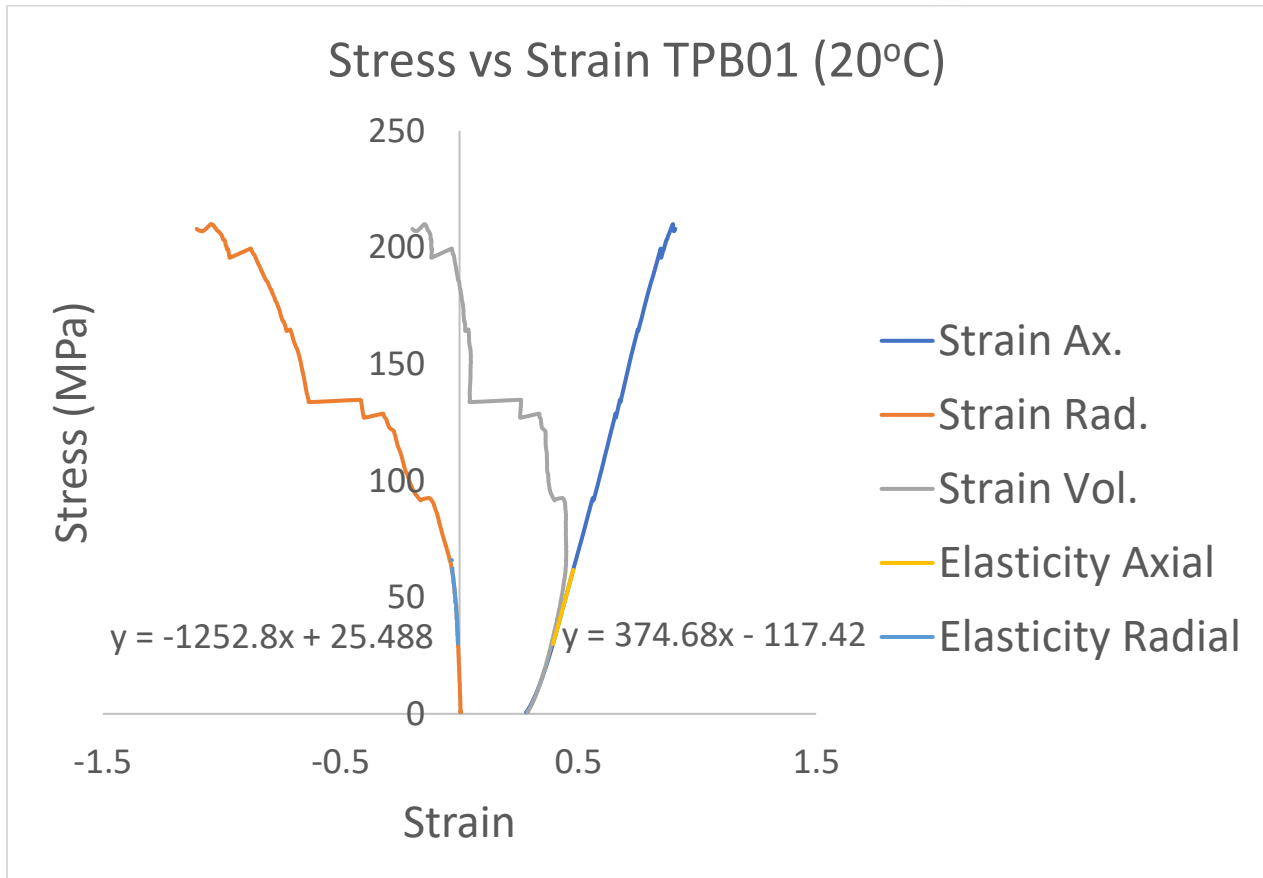

Basalt rock Reynisfjara - Iceland

TANGKUBAN PERAHU (INDONESIA) – BASALTIC ANDESITE
1. TPB01

BEFORE UCS TEST	AFTER UCS TEST

Stress vs Strain TPB01 (20°C)

$y = -1252.8x + 25.488$

$y = 374.68x - 117.42$

Legend:
— Strain Ax.
— Strain Rad.
— Strain Vol.
— Elasticity Axial
— Elasticity Radial

Test Data
Test: Uniaxial Compressive Strength
Test Date: 18-May-2017

Test Result
Crack Initiation: 61.76 MPa
Ultimate Compressive Strength: 209.99 MPa
Young's modulus: 37.47 GPa
Poisson's ratio: 0.30
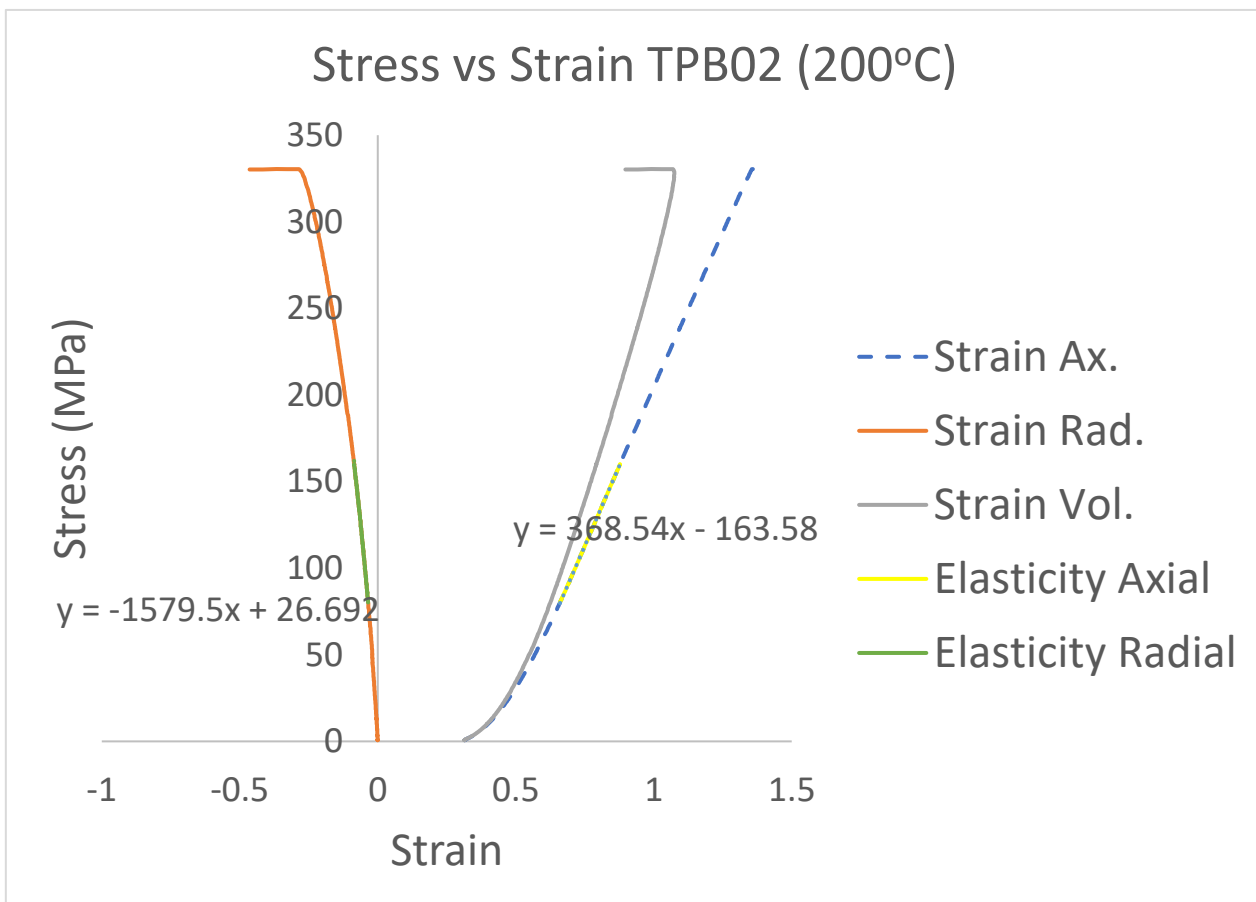Remark: Totally damaged

Core Data
ID: TPB01
Rock Type: Basaltic andesite
Location: Tangkuban Perahu (Indonesia)
Length: 62.59mm
Diameter: 29.85mm
Matrix Density: 2.68 gram/cc

2. TPB02

BEFORE UCS TEST

AFTER UCS TEST

Stress vs Strain TPB02 (200°C)

$$y = 368.54x - 163.58$$

$$y = -1579.5x + 26.692$$

Legend:
- – – – Strain Ax.
- —— Strain Rad.
- —— Strain Vol.
- —— Elasticity Axial
- —— Elasticity Radial

Test Data
Test: Uniaxial Compressive Strength
Test Date: 18-May-2017

Test Result
Crack Initiation: 159.98 MPa
Ultimate Compressive Strength: 330.46 MPa
Young's modulus: 36.85 GPa
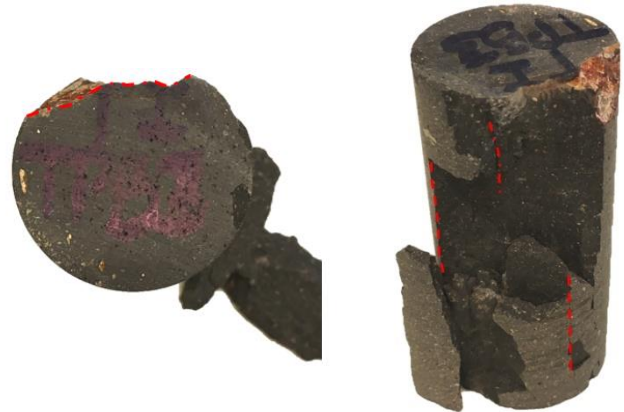Poisson's ratio: 0.23
Remark: Totally damaged

Core Data
ID: TPB02
Rock Type: Basaltic andesite
Location: Tangkuban Perahu (Indonesia)
Length: 60.01mm
Diameter: 29.8mm
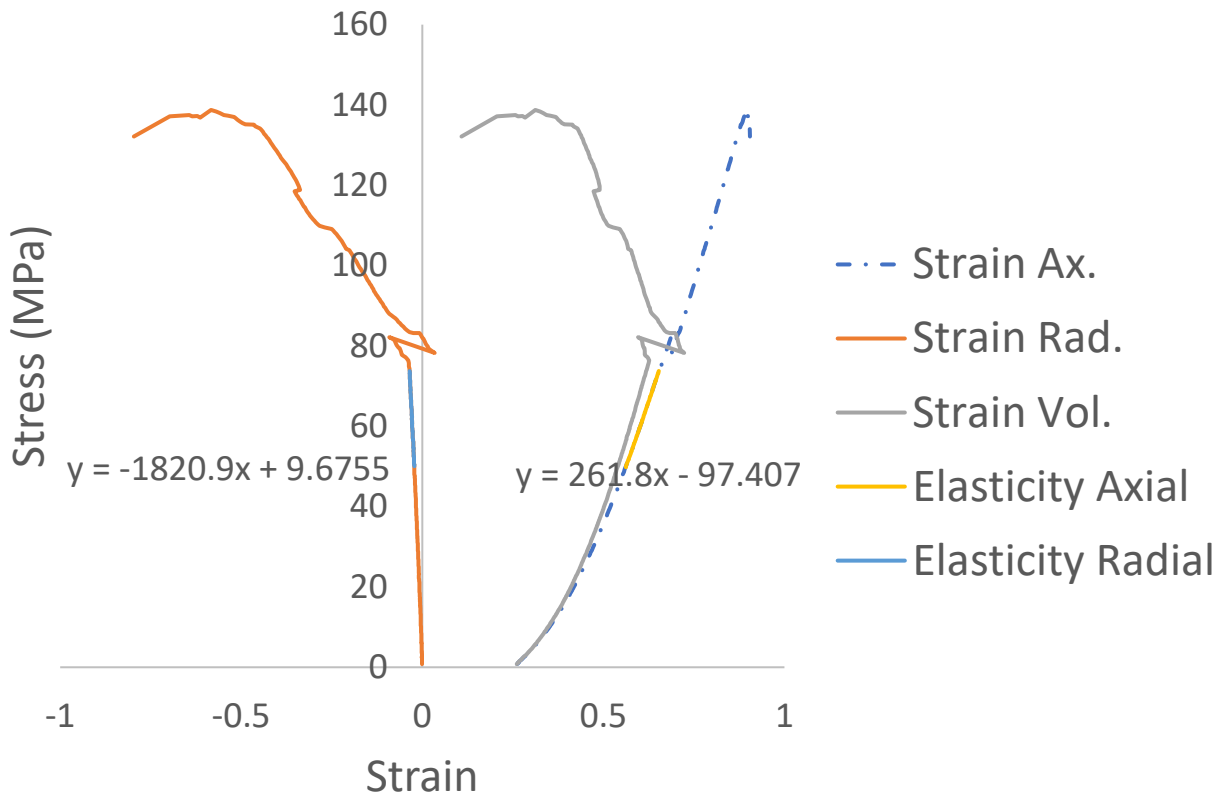Matrix Density: 2.69 gram/cc

3. TPB03

BEFORE UCS TEST

AFTER UCS TEST

Stress vs Strain TPB03 (300°C)

$y = -1820.9x + 9.6755$

$y = 261.8x - 97.407$

- Strain Ax.
- Strain Rad.
- Strain Vol.
- Elasticity Axial
- Elasticity Radial

Test Data
Test: Uniaxial Compressive Strength
Test Date: 18-May-2017

Test Result
Crack Initiation: 73.76 MPa
Ultimate Compressive Strength: 138.76 MPa
Young's modulus: 26.18 GPa
Poisson's ratio: 0.14
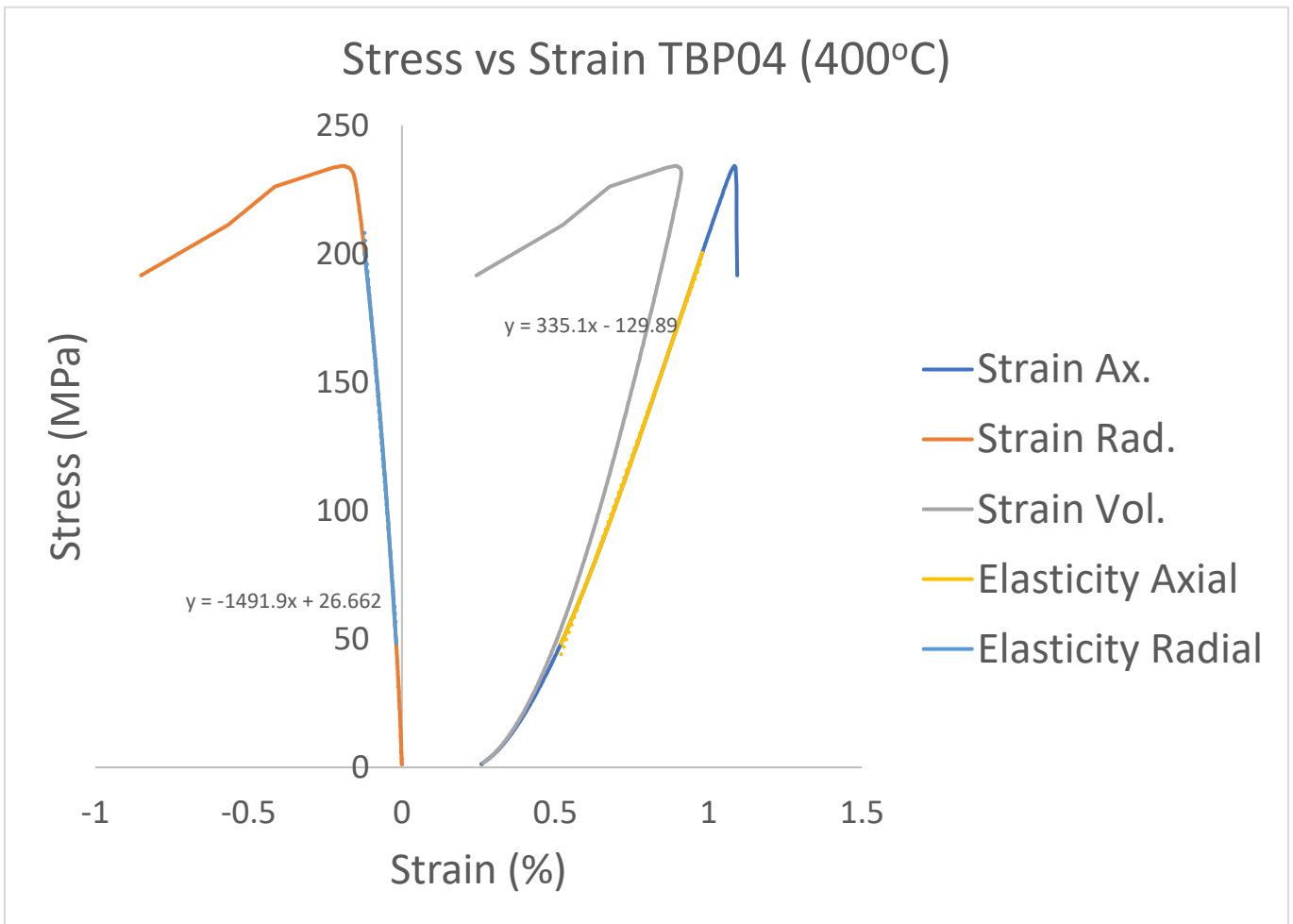Remark: Partial damaged (one side vertically)

Core Data
ID: TPB03
Rock Type: Basaltic andesite
Location: Tangkuban Perahu (Indonesia)
Length: 61.76mm
Diameter: 29.8mm
Matrix Density: 2.71 gram/cc

4. TPB04

BEFORE UCS TEST   **AFTER UCS TEST**

Stress vs Strain TBP04 (400°C)

$y = 335.1x - 129.89$

$y = -1491.9x + 26.662$

Legend:
- Strain Ax.
- Strain Rad.
- Strain Vol.
- Elasticity Axial
- Elasticity Radial

Test Data
Test: Uniaxial Compressive Strength
Test Date: 18-May-2017

Test Result
Crack Initiation: 48.29 MPa
Ultimate Compressive Strength: 234.26 MPa
Young's modulus: 33.51 GPa
Poisson's ratio: 0.22
Remark: Vertically damaged

Core Data
ID: TPB04
Rock Type: Basaltic andesite
Location: Tangkuban Perahu (Indonesia)
Length: 60.33mm
Diameter: 29.74mm
Matrix Density: 2.72 gram/cc

5. TPB05

BEFORE HEATING TREATMENT

AFTER HEATING TREATMENT

Core Data
ID: TPB05
Rock Type: Basaltic andesite
Location: Tangkuban Perahu (Indonesia)
Length: 60.92 mm
Diameter: 29.84 mm
Matrix Density: 2.63 gram/cc

Notes: The core exploded inside the oven at unknown temperature. The oven was opened after 2.5 hours heating at 500ºC.
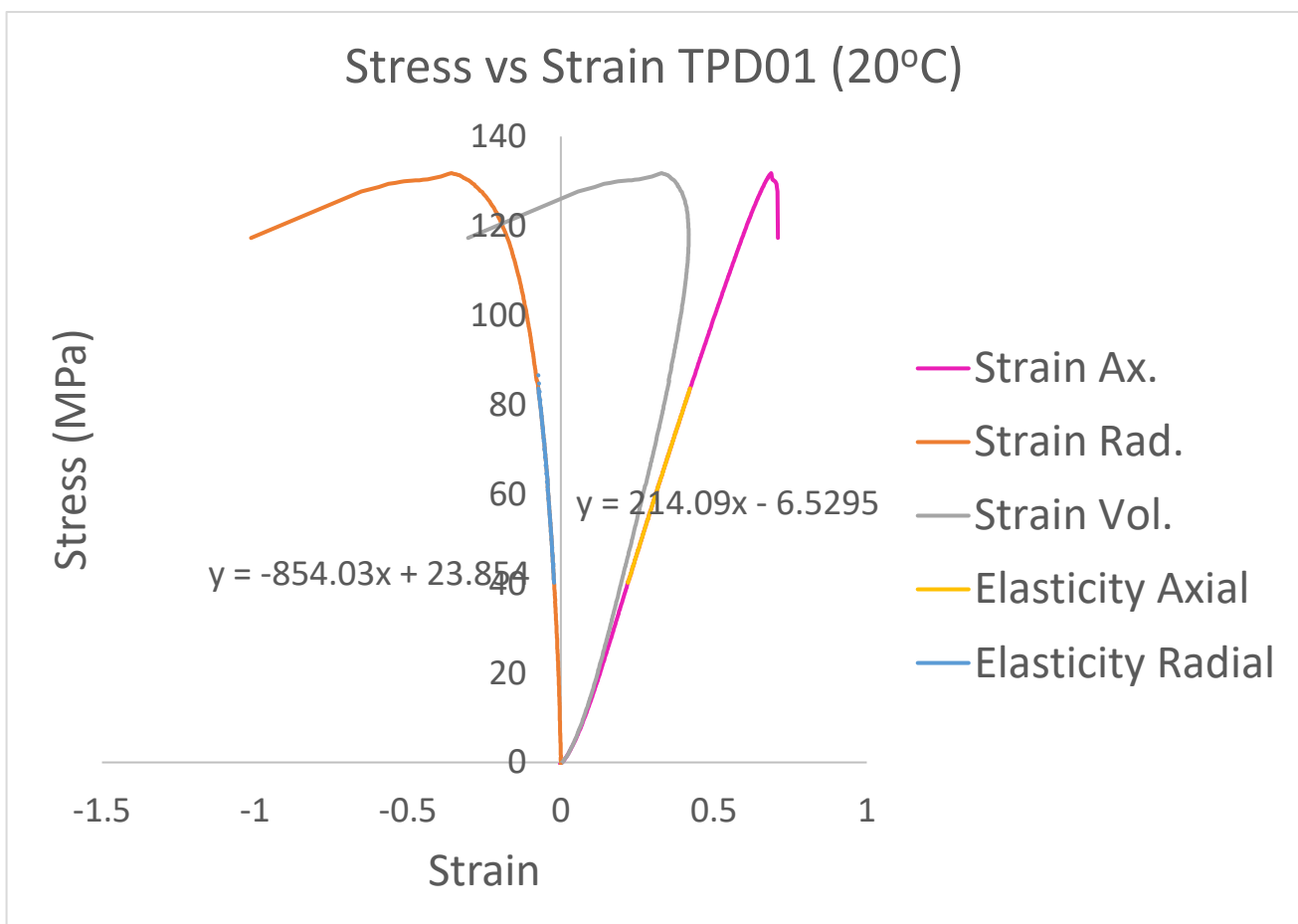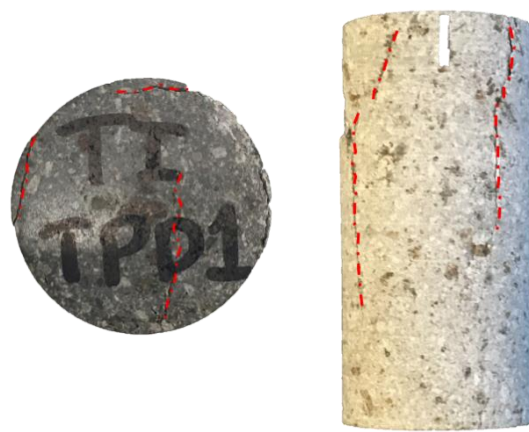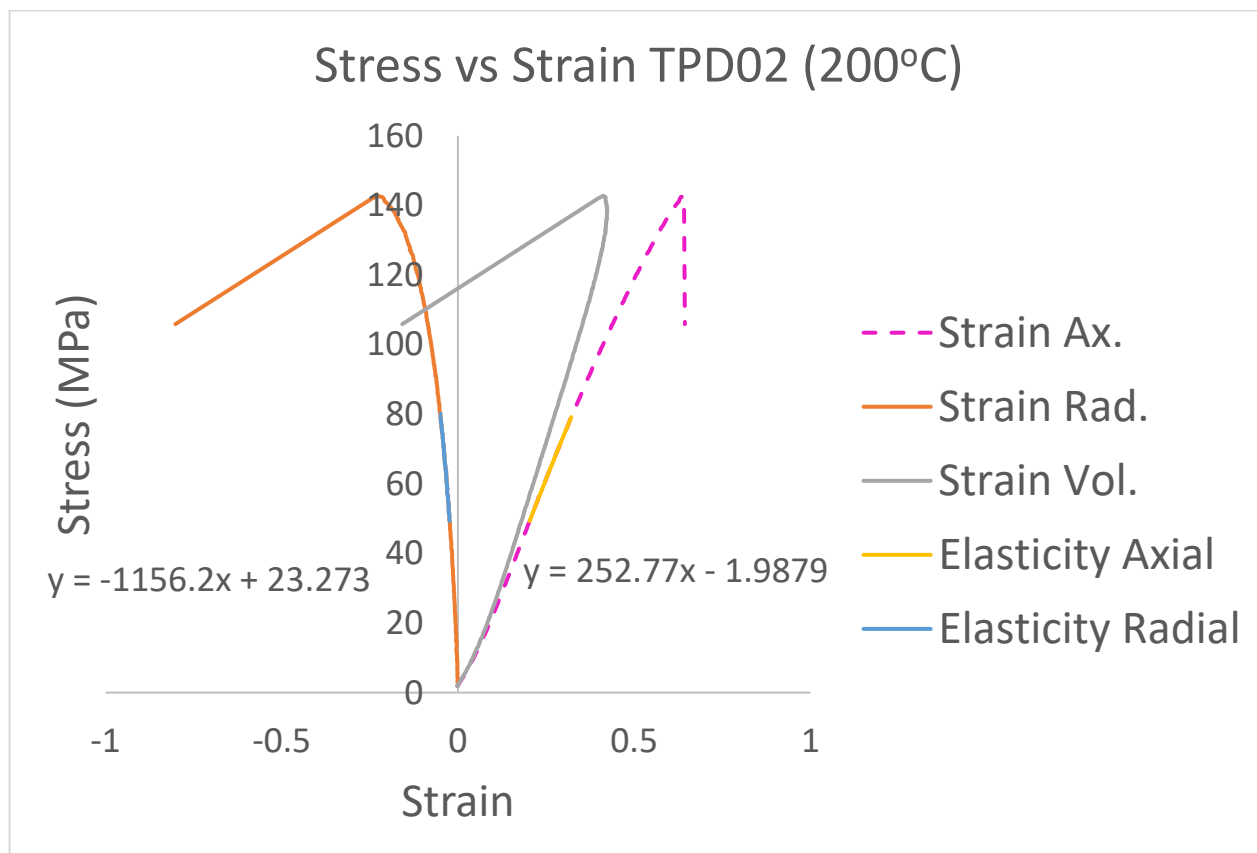
TANGKUBAN PERAHU (INDONESIA) – ANDESITE
1. TPD01

BEFORE UCS TEST	AFTER UCS TEST

Stress vs Strain TPD01 (20°C)

$y = -854.03x + 23.854$

$y = 214.09x - 6.5295$

Legend:
- Strain Ax.
- Strain Rad.
- Strain Vol.
- Elasticity Axial
- Elasticity Radial

Test Data
Test: Uniaxial Compressive Strength
Test Date: 18-May-2017

Test Result
Crack Initiation: 83.68 MPa
Ultimate Compressive Strength: 131.82 MPa
Young's modulus: 21.41 GPa
Poisson's ratio: 0.25
Remark: -

Core Data
ID: TPD01
Rock Type: Andesitic Basalt
Location: Tangkuban Perahu (Indonesia)
Length: 61.69 mm
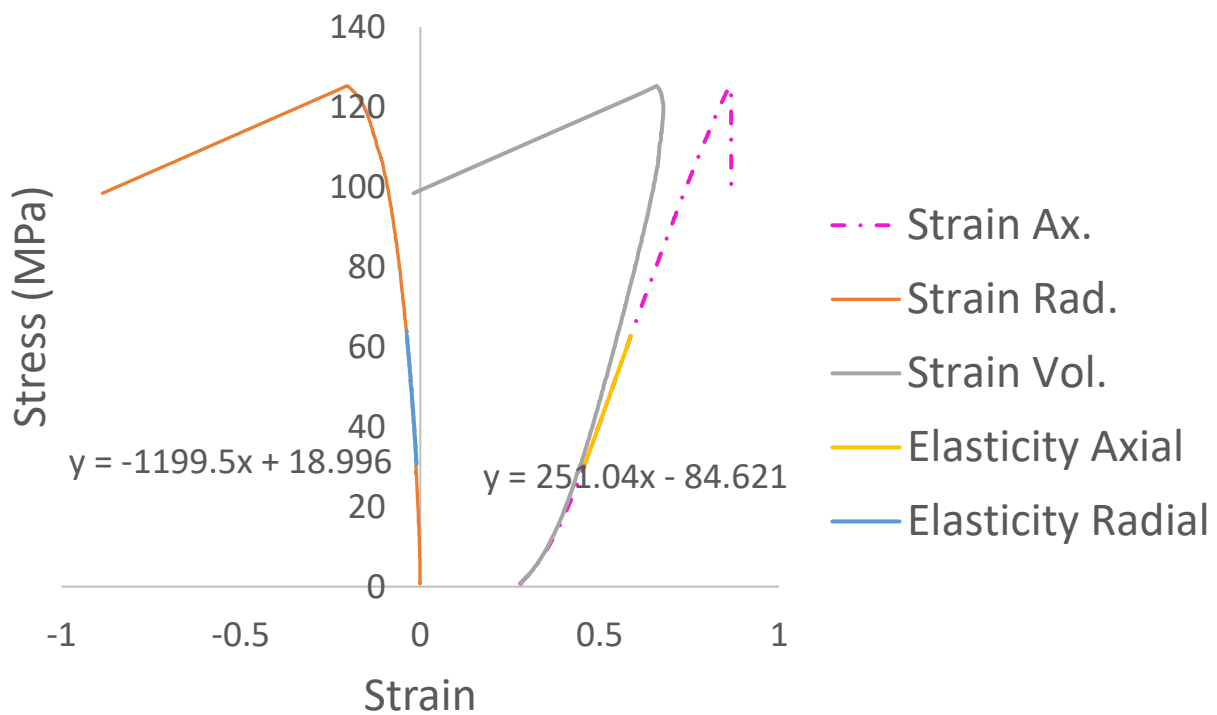Diameter: 29.81 mm
Matrix Density: 2.79 gram/cc

2. TPD02

BEFORE UCS TEST

AFTER UCS TEST

Stress vs Strain TPD02 (200°C)

$y = -1156.2x + 23.273$

$y = 252.77x - 1.9879$

Legend:
- Strain Ax.
- Strain Rad.
- Strain Vol.
- Elasticity Axial
- Elasticity Radial

Test Data
Test: Uniaxial Compressive Strength
Test Date: 18-May-2017

Test Result
Crack Initiation: 79.18 MPa
Ultimate Compressive Strength: 142.78 MPa
Young's modulus: 25.28 GPa
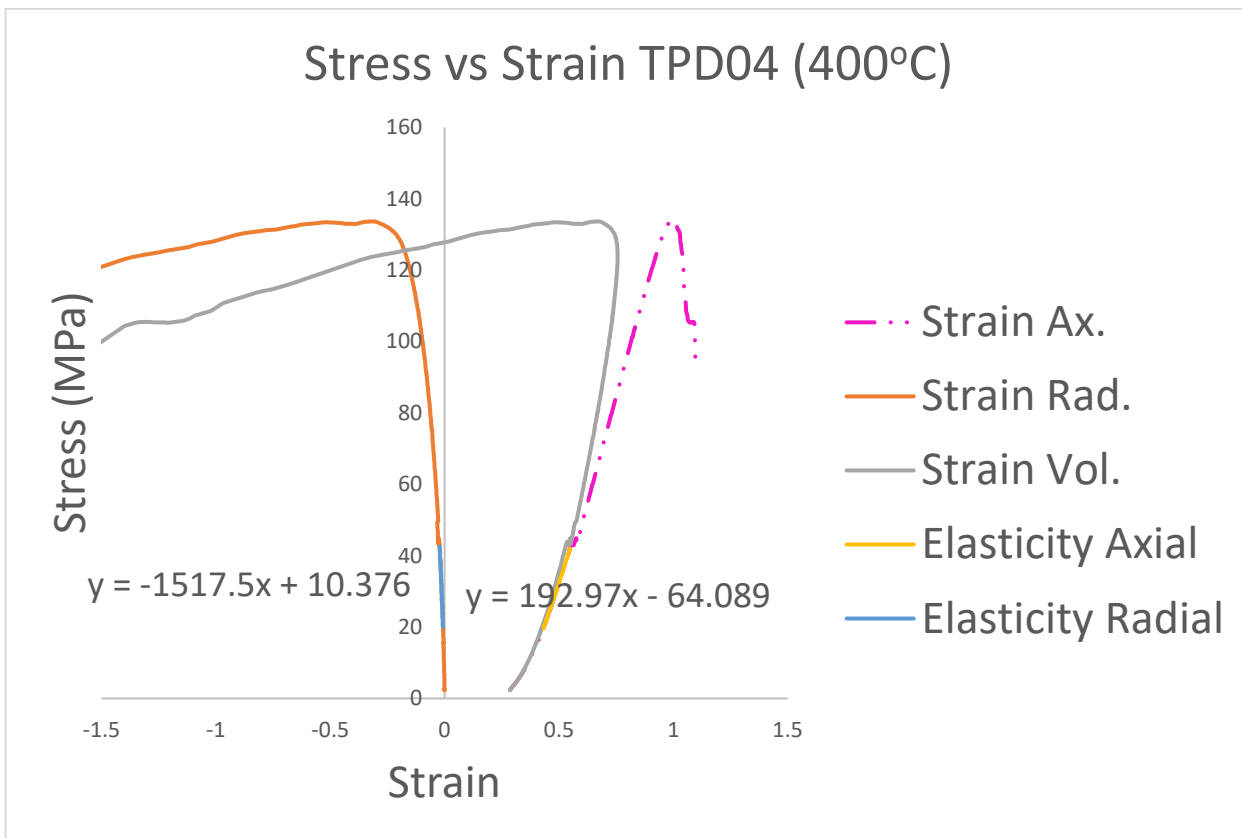Poisson's ratio: 0.22
Remark: -

Core Data
ID: TPD02
Rock Type: Andesitic Basalt
Location: Tangkuban Perahu (Indonesia)
Length: 61.49 mm
Diameter: 29.83 mm
Matrix Density: 2.87 gram/cc

3. TPD03

BEFORE UCS TEST

AFTER UCS TEST

Stress vs Strain TPD03 (300°C)

y = -1199.5x + 18.996

y = 251.04x - 84.621

- – · – Strain Ax.
- —— Strain Rad.
- —— Strain Vol.
- —— Elasticity Axial
- —— Elasticity Radial

Stress (MPa) vs Strain

Test Data
Test: Uniaxial Compressive Strength
Test Date: 18-May-2017

Test Result
Crack Initiation: 62.29 MPa
Ultimate Compressive Strength: 125.29 MPa
Young's modulus: 25.10 GPa
Poisson's ratio: 0.21
Remark: -

Core Data
ID: TPD03
Rock Type: Andesitic Basalt
Location: Tangkuban Perahu (Indonesia)
Length: 61.29 mm
Diameter: 29.80 mm
Matrix Density: 2.84 gram/cc

4. TPD04

BEFORE UCS TEST

AFTER UCS TEST

Stress vs Strain TPD04 (400°C)

$y = -1517.5x + 10.376$

$y = 192.97x - 64.089$

Legend:
- Strain Ax.
- Strain Rad.
- Strain Vol.
- Elasticity Axial
- Elasticity Radial

Test Data
Test: Uniaxial Compressive Strength
Test Date: 18-May-2017

Test Result
Crack Initiation: 43.34 MPa
Ultimate Compressive Strength: 133.64 MPa
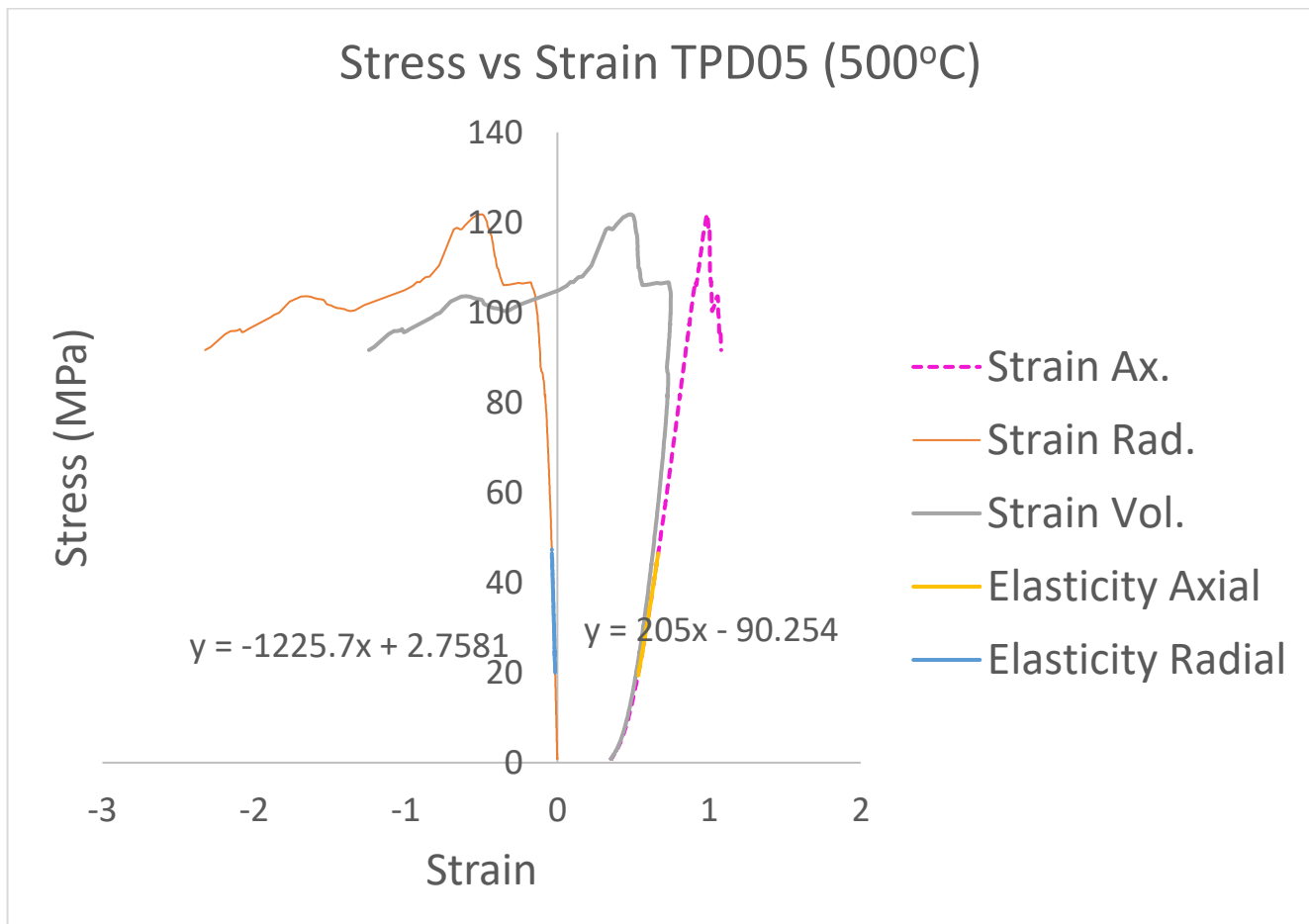Young's modulus: 19.3 GPa
Poisson's ratio: 0.13
Remark: -

Core Data
ID: TPD04
Rock Type: Andesitic Basalt
Location: Tangkuban Perahu (Indonesia)
Length: 61.26 mm
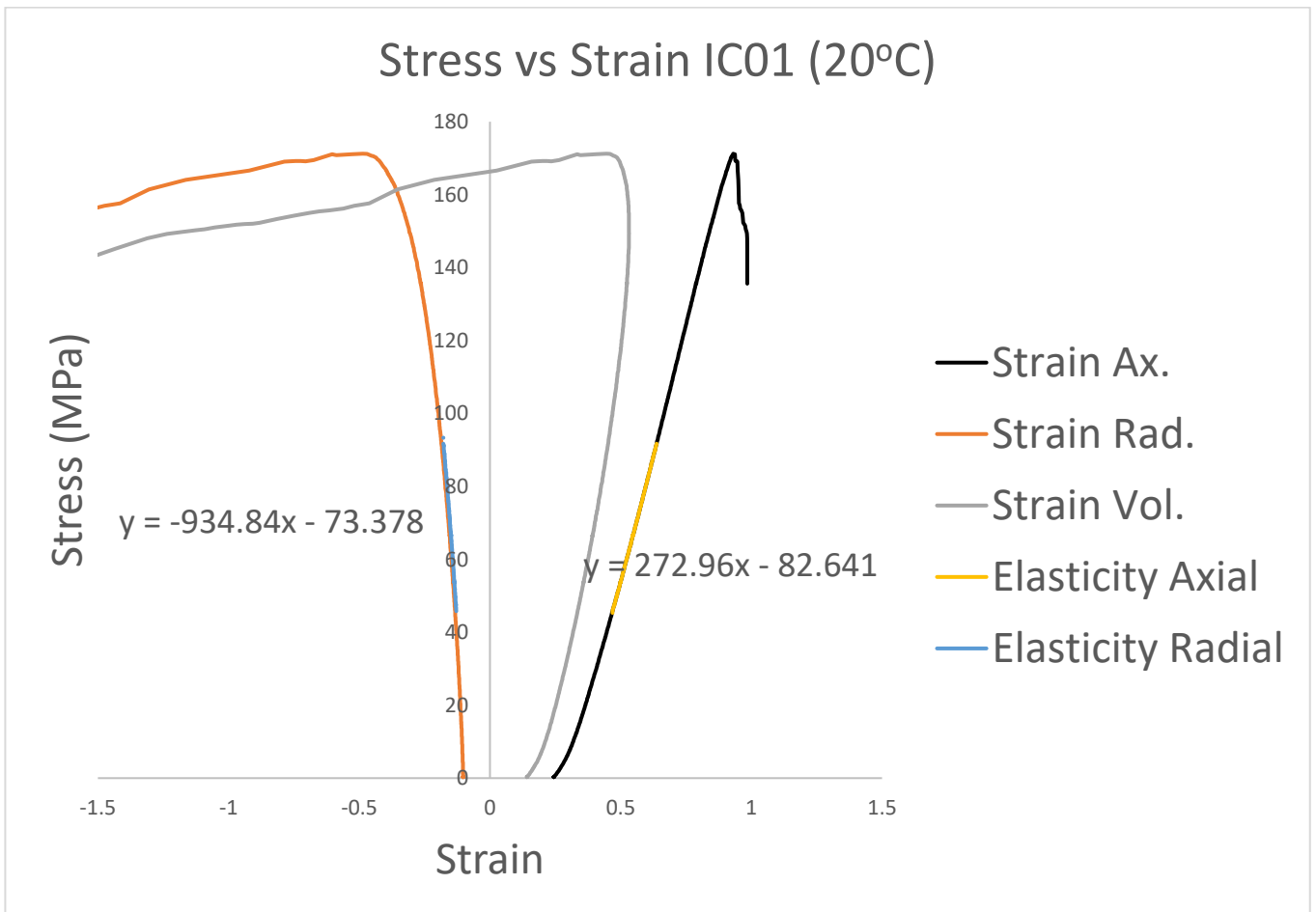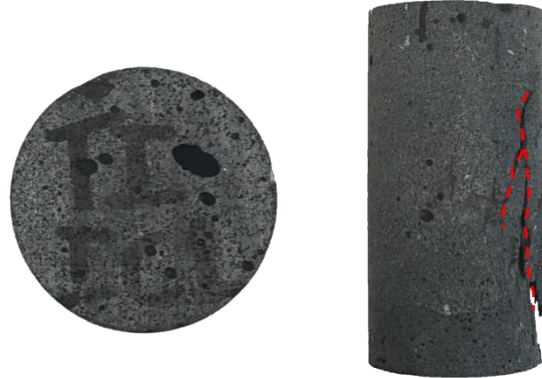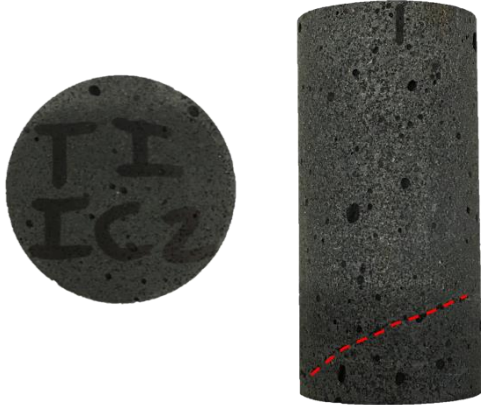Diameter: 29.82 mm
Matrix Density: 2.85 gram/cc

5. TPD05

BEFORE UCS TEST

AFTER UCS TEST

Stress vs Strain TPD05 (500°C)

y = -1225.7x + 2.7581

y = 205x - 90.254

- Strain Ax.
- Strain Rad.
- Strain Vol.
- Elasticity Axial
- Elasticity Radial

Y-axis: Stress (MPa), X-axis: Strain

Test Data
Test: Uniaxial Compressive Strength
Test Date: 18-May-2017

Test Result
Crack Initiation: 48.56 MPa
Ultimate Compressive Strength: 121.8 MPa
Young's modulus: 20.5 GPa
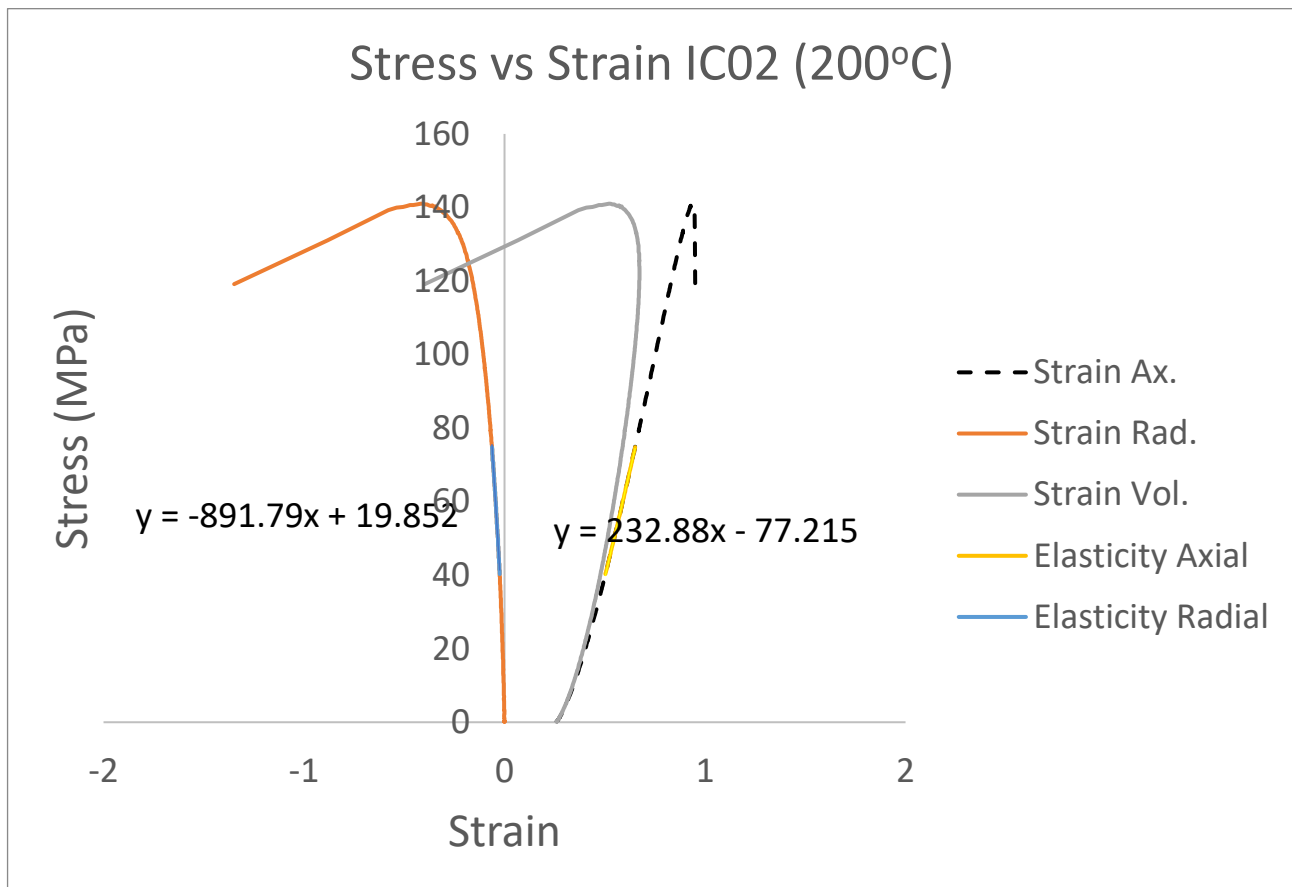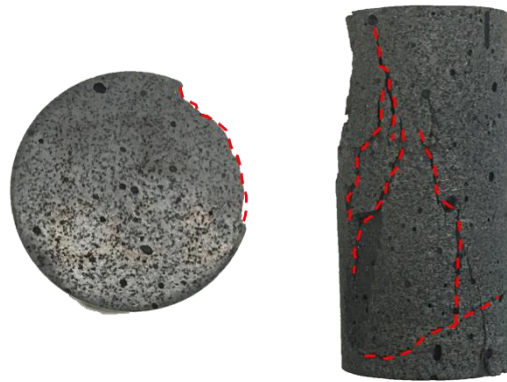Poisson's ratio: 0.17
Remark: -

Core Data
ID: TPD05
Rock Type: Andesitic Basalt
Location: Tangkuban Perahu (Indonesia)
Length: 61.15 mm
Diameter: 29.82 mm
Matrix Density: 2.84 gram/cc

REYNISFJARA (ICELAND)
1. IC01

BEFORE UCS TEST   **AFTER UCS TEST**

Stress vs Strain IC01 (20°C)

$$y = -934.84x - 73.378$$

$$y = 272.96x - 82.641$$

Legend:
- Strain Ax.
- Strain Rad.
- Strain Vol.
- Elasticity Axial
- Elasticity Radial

Stress (MPa) vs Strain

Test Data
Test: Uniaxial Compressive Strength
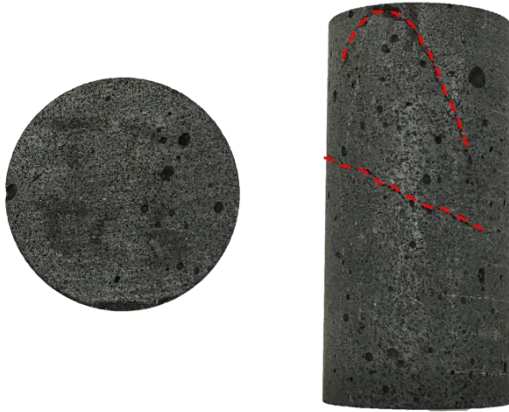Test Date: 18-May-2017

Test Result
Crack Initiation: 135.61 MPa
Ultimate Compressive Strength: 171.23 MPa
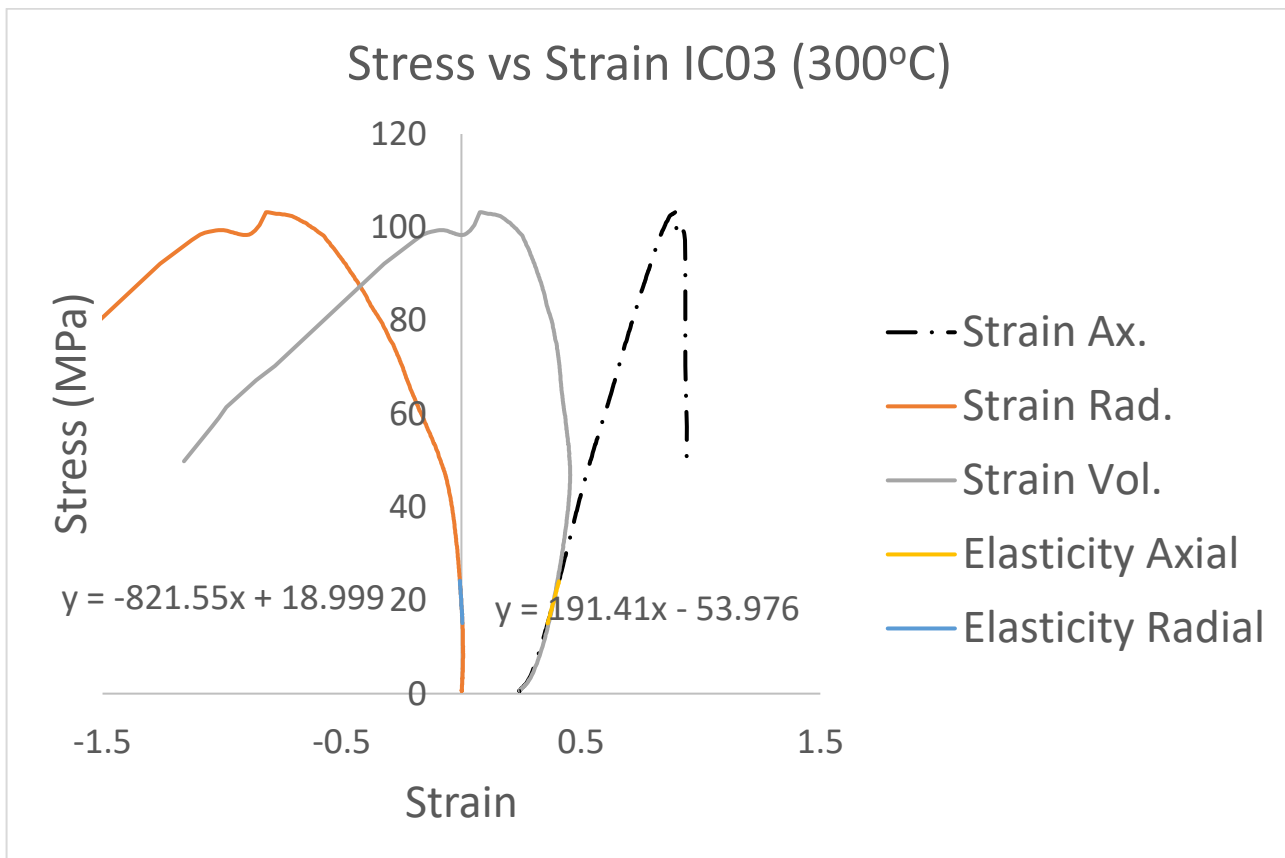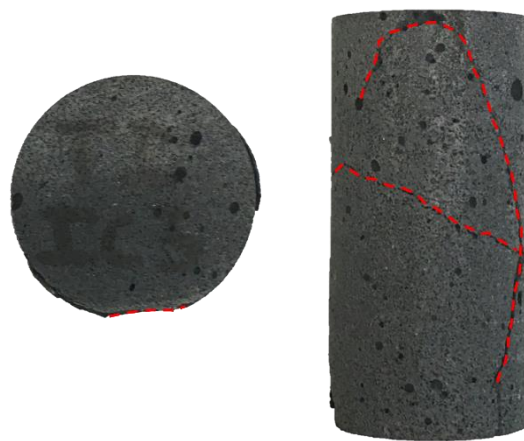Young's modulus: 27.3 GPa
Poisson's ratio: 0.29
Remark: -

Core Data
ID: IC01
Rock Type: Basalt
Location: Reynisfjara (Iceland)
Length: 59.52 mm
Diameter: 29.81 mm
Matrix Density: 3.05 gram/cc

2. IC02

BEFORE UCS TEST	AFTER UCS TEST

Stress vs Strain IC02 (200°C)

$y = -891.79x + 19.852$

$y = 232.88x - 77.215$

Legend:
- Strain Ax.
- Strain Rad.
- Strain Vol.
- Elasticity Axial
- Elasticity Radial

Test Data
Test: Uniaxial Compressive Strength
Test Date: 18-May-2017

Test Result
Crack Initiation: 74.83 MPa
Ultimate Compressive Strength: 141.03 MPa
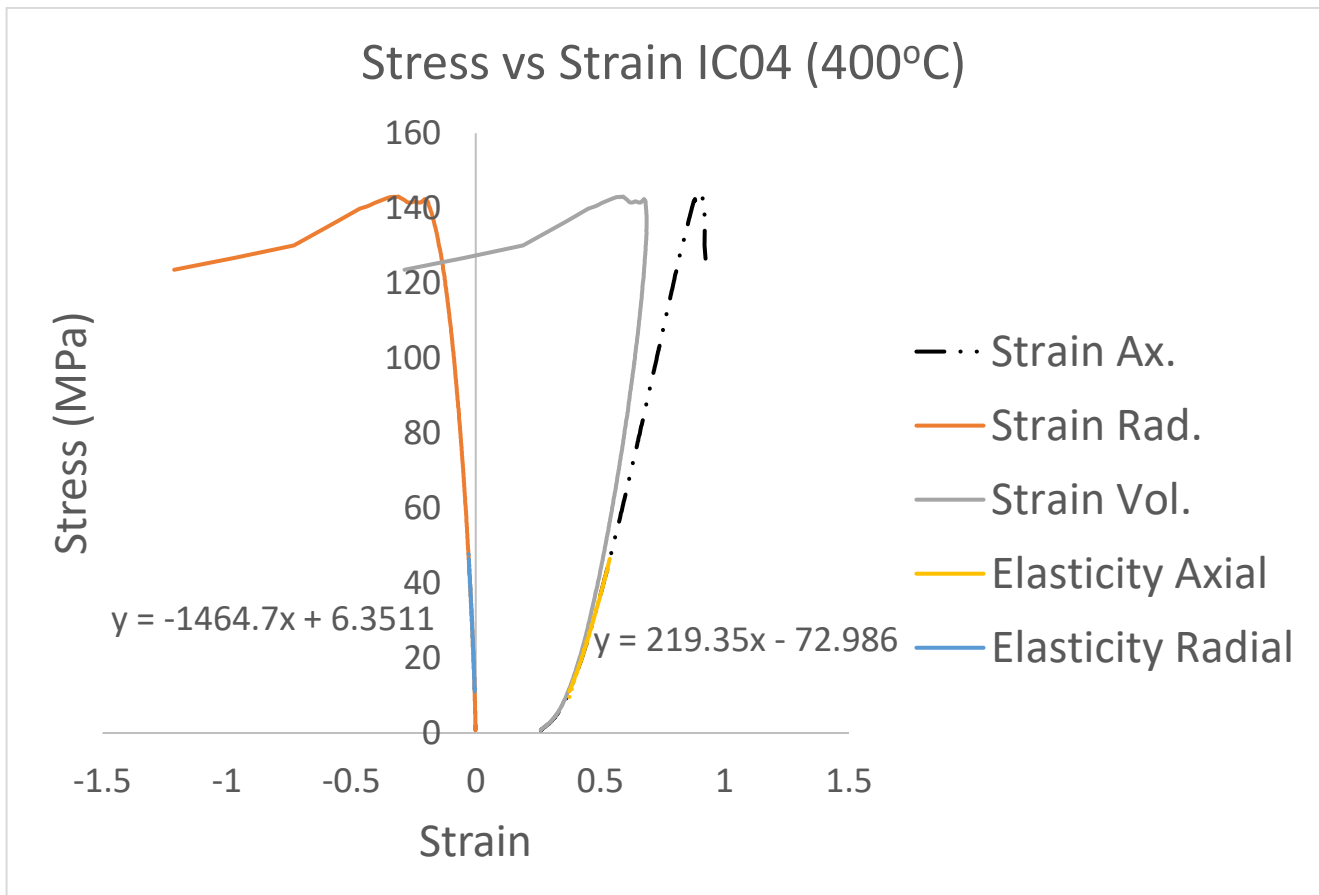Young's modulus: 23.29 GPa
Poisson's ratio: 0.26
Remark: -

Core Data
ID: IC02
Rock Type: Basalt
Location: Reynisfjara (Iceland)
Length: 61.43 mm
Diameter: 29.79 mm
Matrix Density: 3.06 gram/cc

3. IC03

BEFORE UCS TEST

AFTER UCS TEST

Stress vs Strain IC03 (300°C)

$y = -821.55x + 18.999$

$y = 191.41x - 53.976$

- — · · —Strain Ax.
- ——Strain Rad.
- ——Strain Vol.
- ——Elasticity Axial
- ——Elasticity Radial

Test Data
Test: Uniaxial Compressive Strength
Test Date: 18-May-2017

Test Result
Crack Initiation: 24.11 MPa
Ultimate Compressive Strength: 103.23 MPa
Young's modulus: 19.14 GPa
Poisson's ratio: 0.23
Remark: -

Core Data
ID: IC03
Rock Type: Basalt
Location: Reynisfjara (Iceland)
Length: 61.69 mm
Diameter: 29.8 mm
Matrix Density: 3.06 gram/cc

4. IC04

BEFORE UCS TEST

AFTER UCS TEST

Stress vs Strain IC04 (400ºC)

$y = -1464.7x + 6.3511$

$y = 219.35x - 72.986$

- Strain Ax.
- Strain Rad.
- Strain Vol.
- Elasticity Axial
- Elasticity Radial

Test Data
Test: Uniaxial Compressive Strength
Test Date: 18-May-2017

Test Result
Crack Initiation: 46.45 MPa
Ultimate Compressive Strength: 143.11MPa
Young's modulus: 21.94 GPa
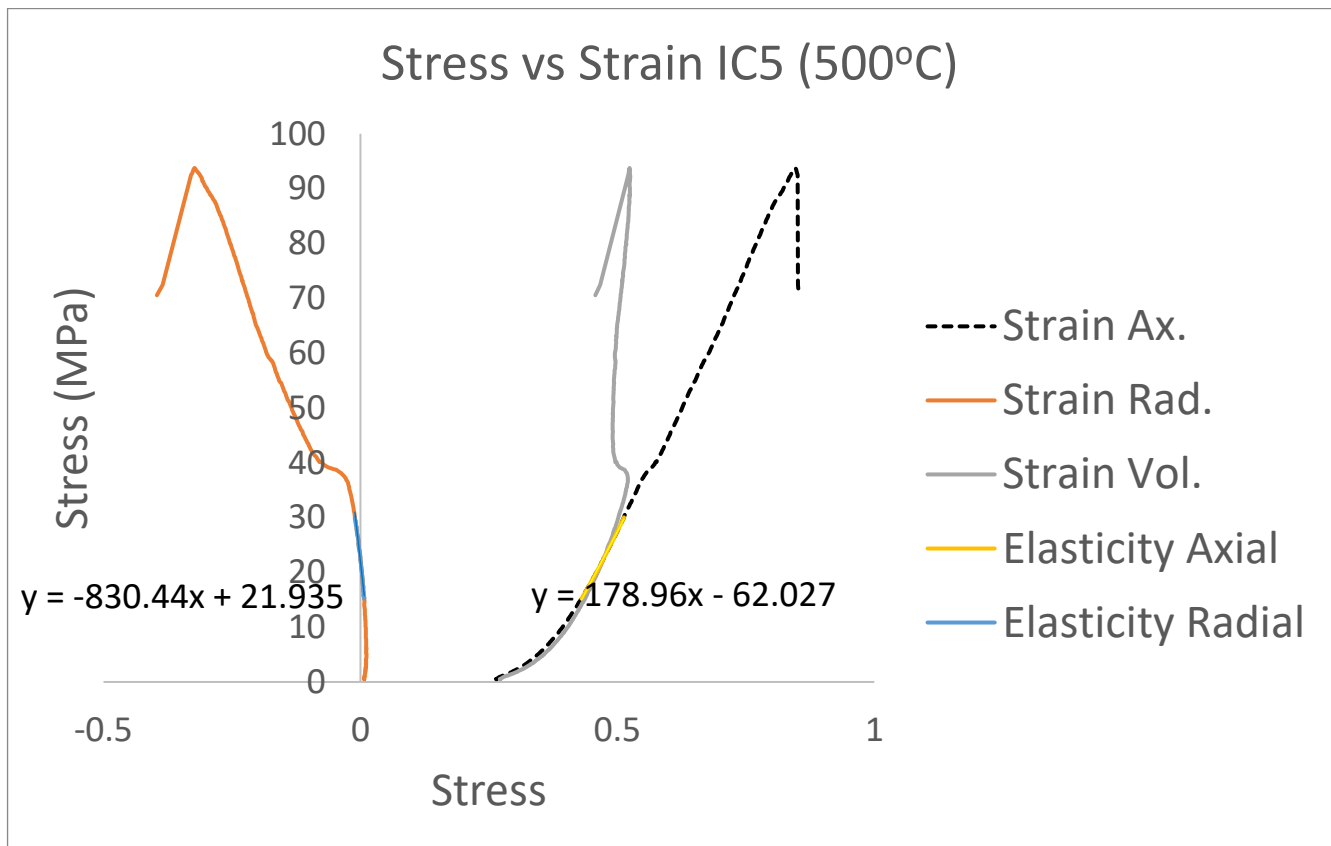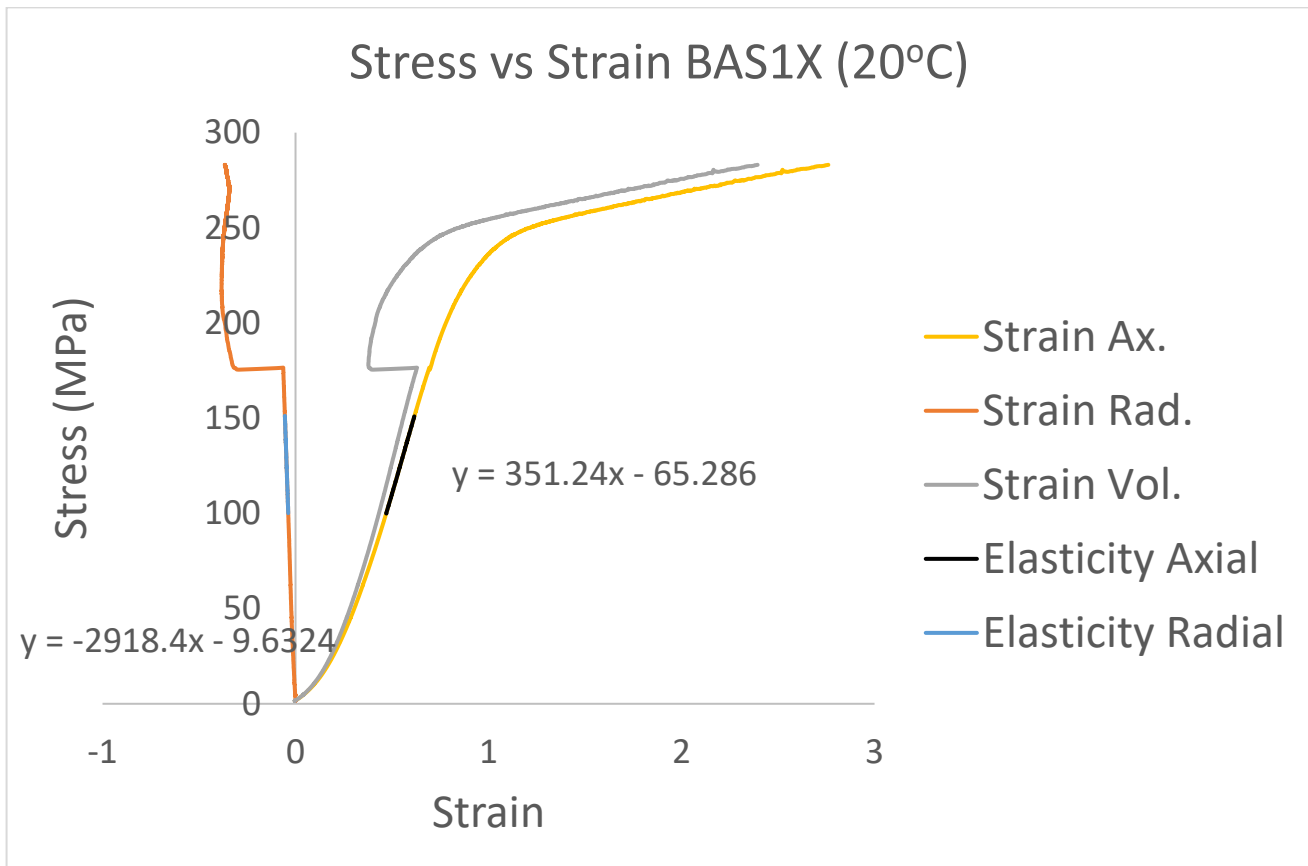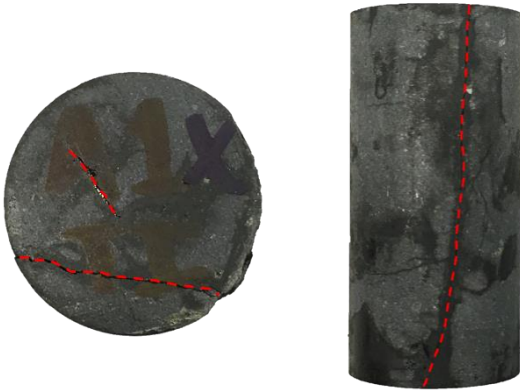Poisson's ratio: 0.15
Remark: -

Core Data
ID: IC04
Rock Type: Basalt
Location: Reynisfjara (Iceland)
Length: 61.84 mm
Diameter: 29.79 mm
Matrix Density: 3.07 gram/cc

5. IC05

BEFORE UCS TEST

AFTER UCS TEST

Stress vs Strain IC5 (500°C)

$y = -830.44x + 21.935$

$y = 178.96x - 62.027$

- - - - Strain Ax.
—— Strain Rad.
—— Strain Vol.
—— Elasticity Axial
—— Elasticity Radial

Stress (MPa) — vertical axis

Stress — horizontal axis

Test Data
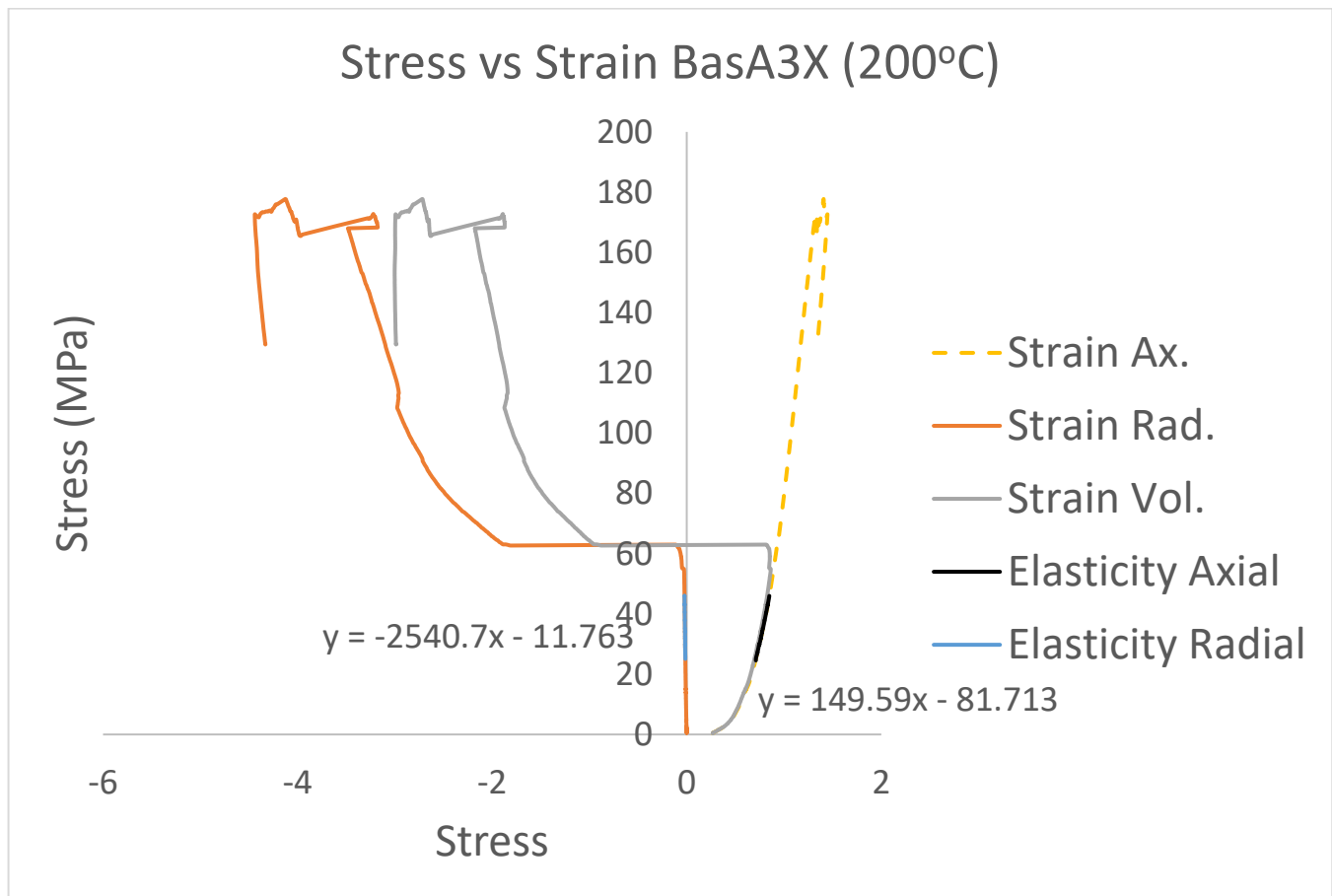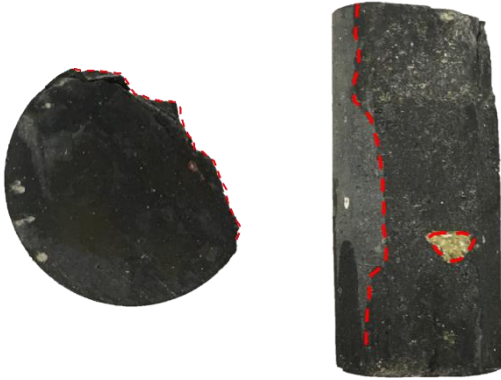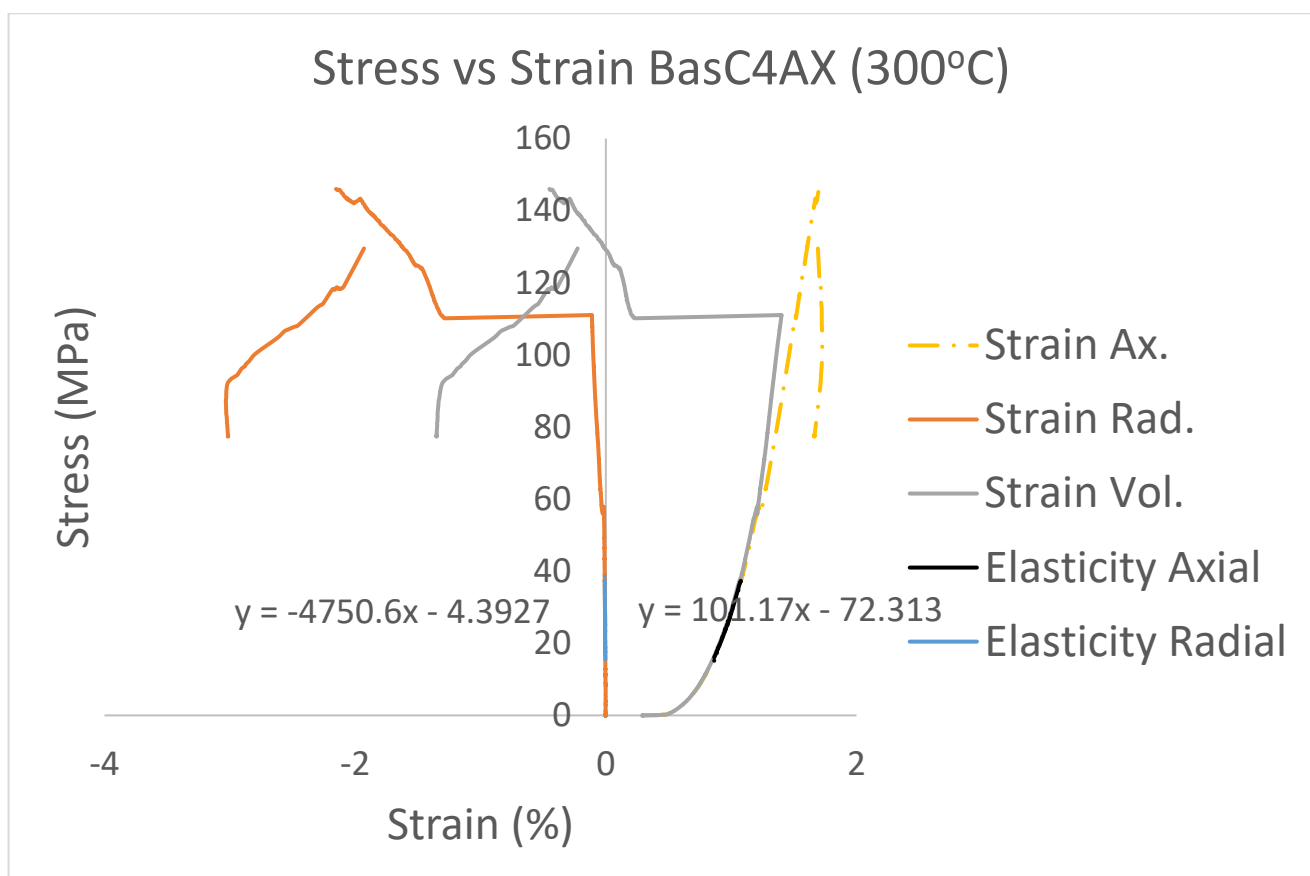Test: Uniaxial Compressive Strength
Test Date: 18-May-2017

Test Result
Crack Initiation: 40.13 MPa
Ultimate Compressive Strength: 93.77 MPa
Young's modulus: 17.90 GPa
Poisson's ratio: 0.22
Remark: -

Core Data
ID: IC05
Rock Type: Basalt
Location: Reynisfjara (Iceland)
Length: 61.41 mm
Diameter: 29.79 mm
Matrix Density: 3.07 gram/cc

EIFEL (GERMANY) – X PLANE ORIENTATION
1. BasA1X

AFTER UCS TEST

Stress vs Strain BAS1X (20°C)

$y = 351.24x - 65.286$

$y = -2918.4x - 9.6324$

Legend:
- Strain Ax.
- Strain Rad.
- Strain Vol.
- Elasticity Axial
- Elasticity Radial

Test Data
Test: Uniaxial Compressive Strength
Test Date: 23-February-2017

Test Result
Crack Initiation: 175.01 MPa
Ultimate Compressive Strength: 283 MPa
Young's modulus: 35.12 GPa
Poisson's ratio: 0.12
Remark: -

Core Data
ID: BasA1X
Rock Type: Basalt
Location: Eifel (Germany)
Length: 61.91 mm
Diameter: 29.72 mm
Matrix Density: 3.0 gram/cc

2. BasA3X

AFTER UCS TEST

Stress vs Strain BasA3X (200°C)

$y = -2540.7x - 11.763$

$y = 149.59x - 81.713$

Legend:
- Strain Ax.
- Strain Rad.
- Strain Vol.
- Elasticity Axial
- Elasticity Radial

Test Data
Test: Uniaxial Compressive Strength
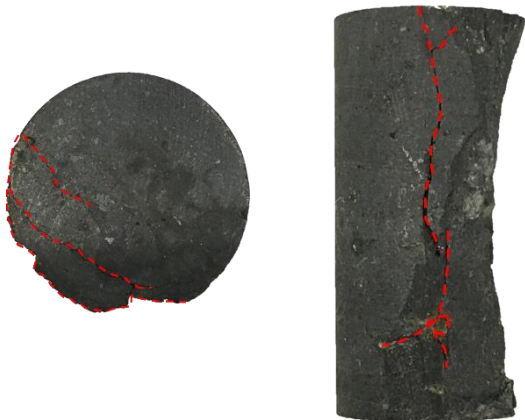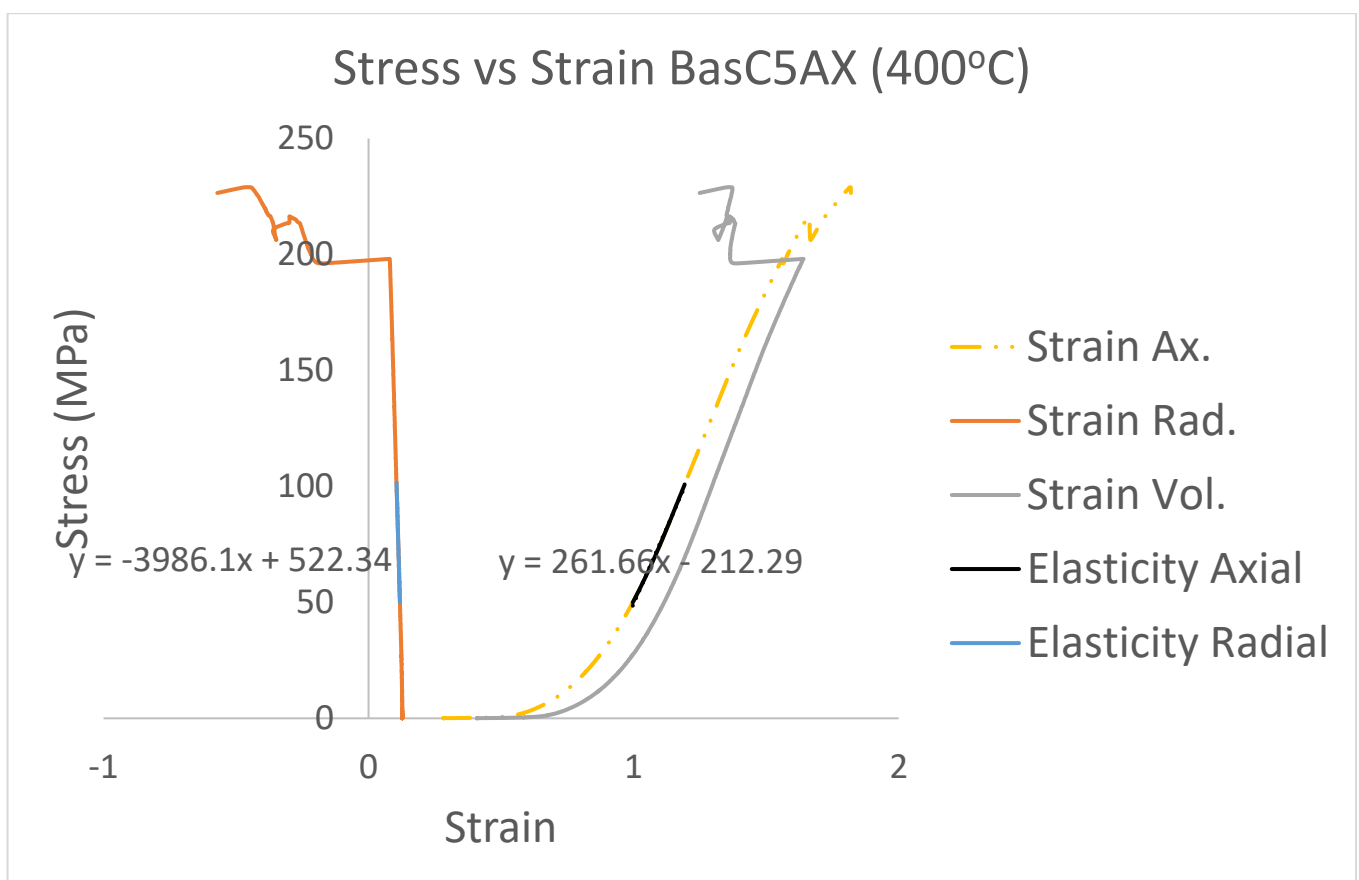Test Date: 23-February-2017

Test Result
Crack Initiation: 63.01 MPa
Ultimate Compressive Strength: 177.74 MPa
Young's modulus: 14.96 GPa
Poisson's ratio: 0.06
Remark: contains Olivine

Core Data
ID: BasA3X
Rock Type: Basalt
Location: Eifel (Germany)
Length: 62.13 mm
Diameter: 29.72 mm
Matrix Density: 3.01 gram/cc

3. BasC4AX

Stress vs Strain BasC4AX (300°C)

$y = -4750.6x - 4.3927$

$y = 101.17x - 72.313$

Legend:
- Strain Ax.
- Strain Rad.
- Strain Vol.
- Elasticity Axial
- Elasticity Radial

Test Data
Test: Uniaxial Compressive Strength
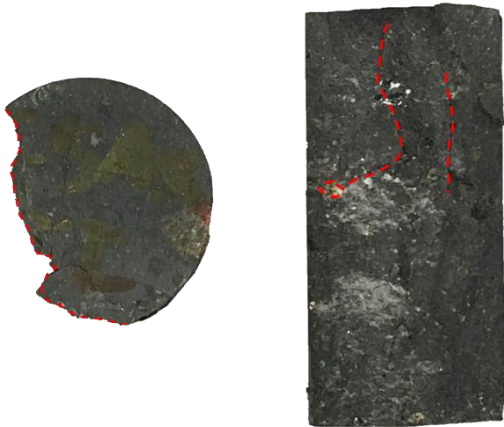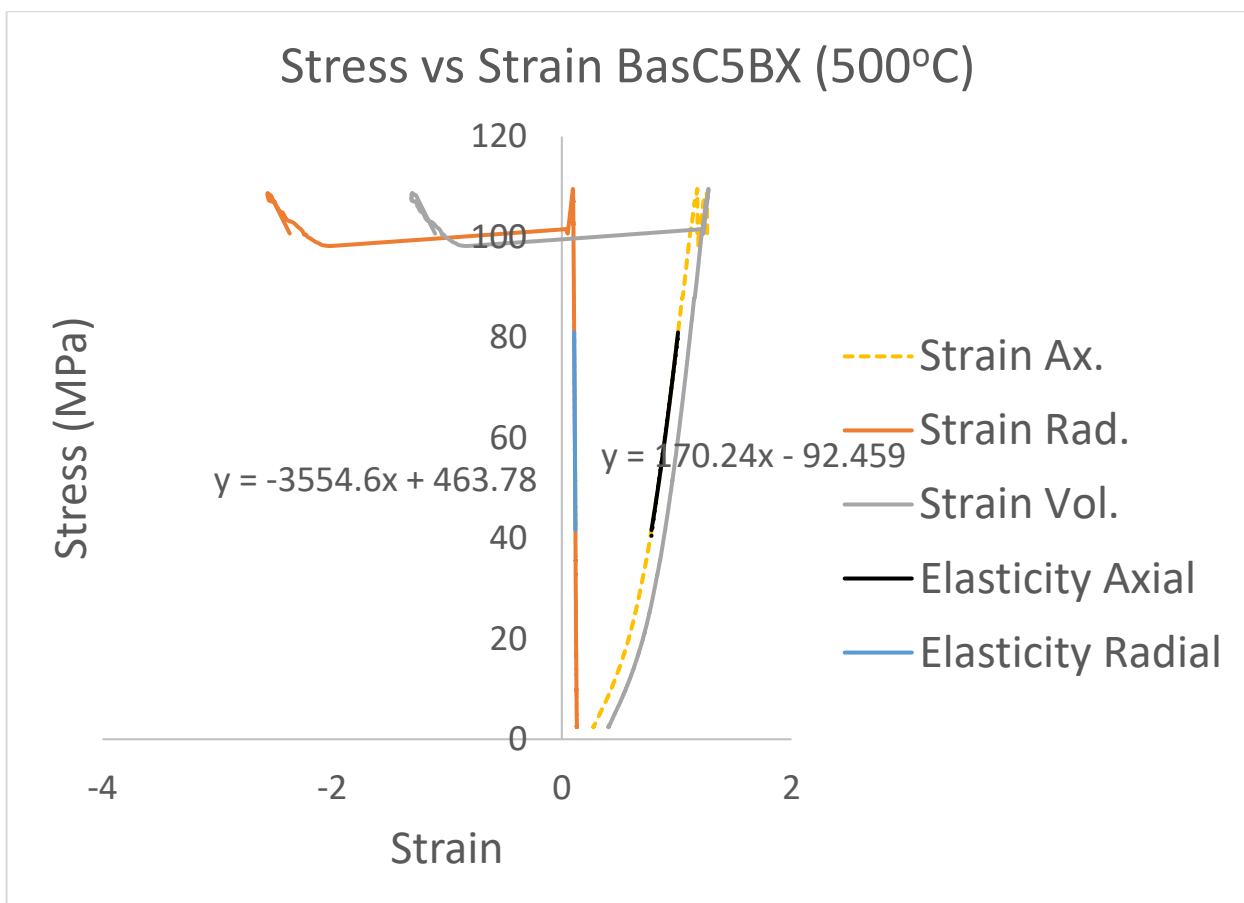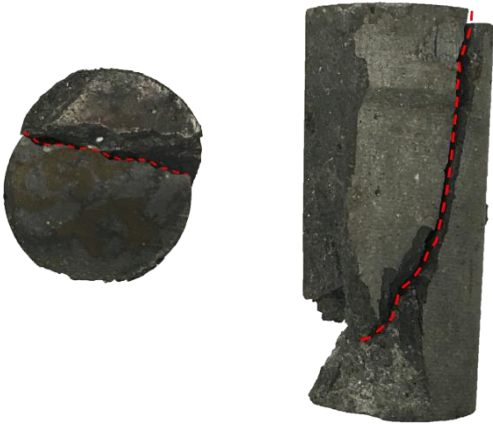Test Date: 23-February-2017

Test Result
Crack Initiation: 37.34 MPa
Ultimate Compressive Strength: 146.01 MPa
Young's modulus: 10.12 GPa
Poisson's ratio: 0.02
Remark: contains Olivine

Core Data
ID: BasC4AX
Rock Type: Basalt
Location: Eifel (Germany)
Length: 60.38 mm
Diameter: 29.73 mm
Matrix Density: 3.01 gram/cc

4. BasC5AX

AFTER UCS TEST

Stress vs Strain BasC5AX (400°C)

$y = -3986.1x + 522.34$

$y = 261.66x - 212.29$

Legend:
- Strain Ax.
- Strain Rad.
- Strain Vol.
- Elasticity Axial
- Elasticity Radial

Test Data
Test: Uniaxial Compressive Strength
Test Date: 23-February-2017

Test Result
Crack Initiation: 197.13 MPa
Ultimate Compressive Strength: 229 MPa
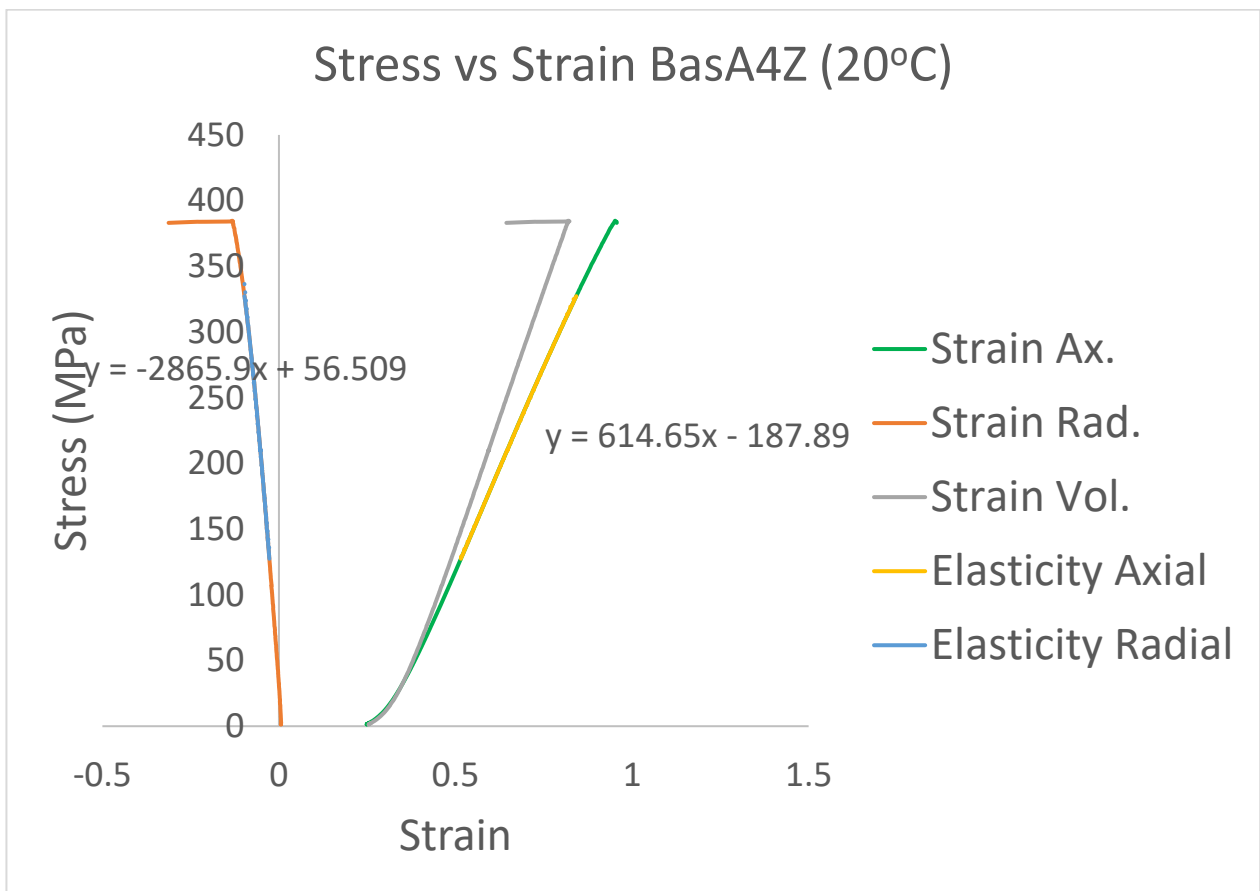Young's modulus: 26.17 GPa
Poisson's ratio: 0.07
Remark: contains Olivine

Core Data
ID: BasC5AX
Rock Type: Basalt
Location: Eifel (Germany)
Length: 62.43 mm
Diameter: 29.73 mm
Matrix Density: 3.01 gram/cc

5. BasC5BX

AFTER UCS TEST

Stress vs Strain BasC5BX (500°C)

$y = -3554.6x + 463.78$

$y = 170.24x - 92.459$

- - - - Strain Ax.
──── Strain Rad.
──── Strain Vol.
──── Elasticity Axial
──── Elasticity Radial

Stress (MPa) — y-axis: 0, 20, 40, 60, 80, 100, 120

Strain — x-axis: -4, -2, 0, 2

Test Data
Test: Uniaxial Compressive Strength
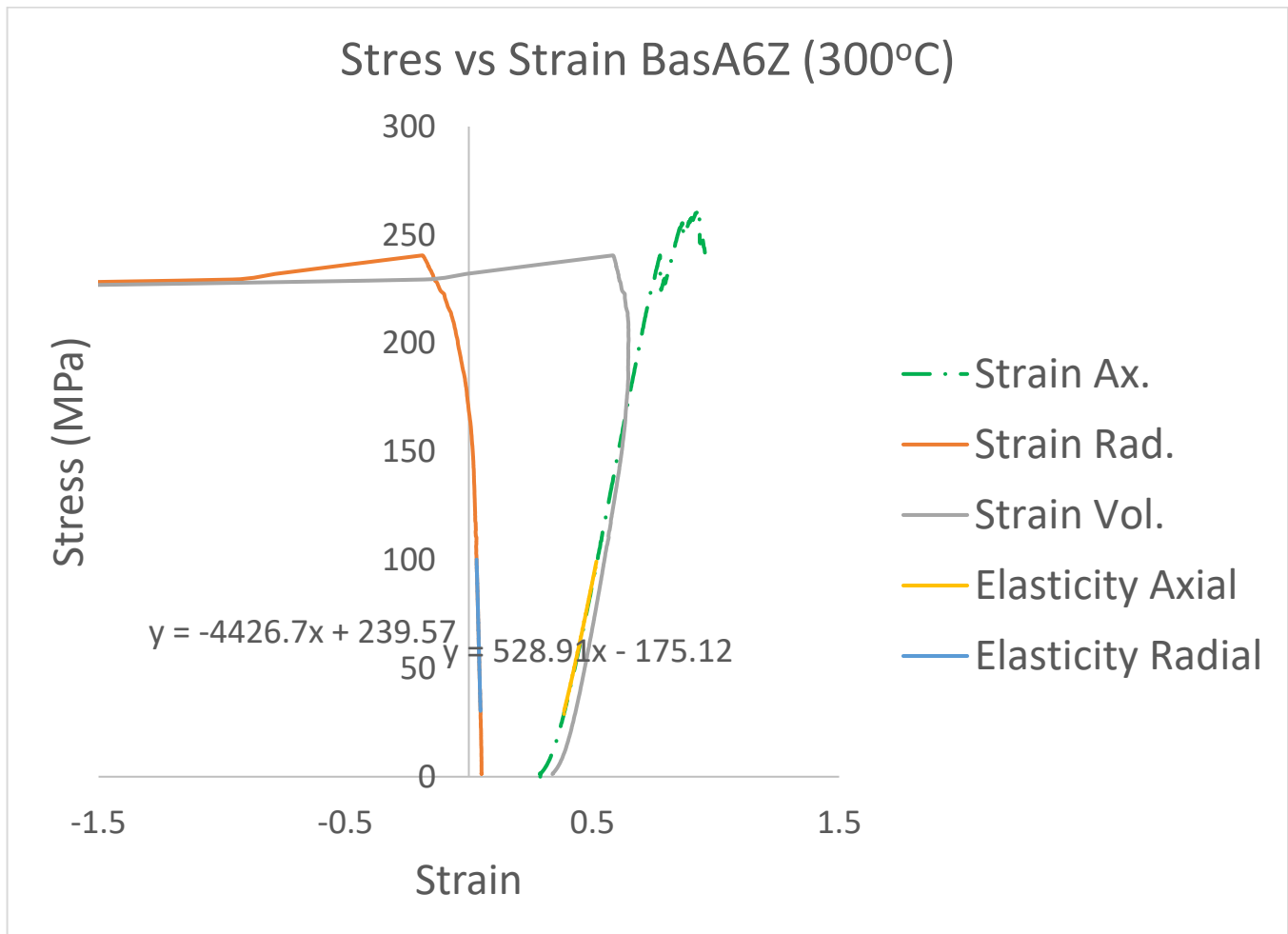Test Date: 23-February-2017

Test Result
Crack Initiation: 109.58 MPa
Ultimate Compressive Strength: 109.58 MPa
Young's modulus: 17.02 GPa
Poisson's ratio: 0.05
Remark: -

Core Data
ID: BasC5BX
Rock Type: Basalt
Location: Eifel (Germany)
Length: 61.87 mm
Diameter: 29.73 mm
Matrix Density: 3.01 gram/cc

6. BasA4Z

AFTER UCS TEST

Stress vs Strain BasA4Z (20°C)

$y = -2865.9x + 56.509$

$y = 614.65x - 187.89$

- —— Strain Ax.
- —— Strain Rad.
- —— Strain Vol.
- —— Elasticity Axial
- —— Elasticity Radial

Test Data

Test: Uniaxial Compressive Strength
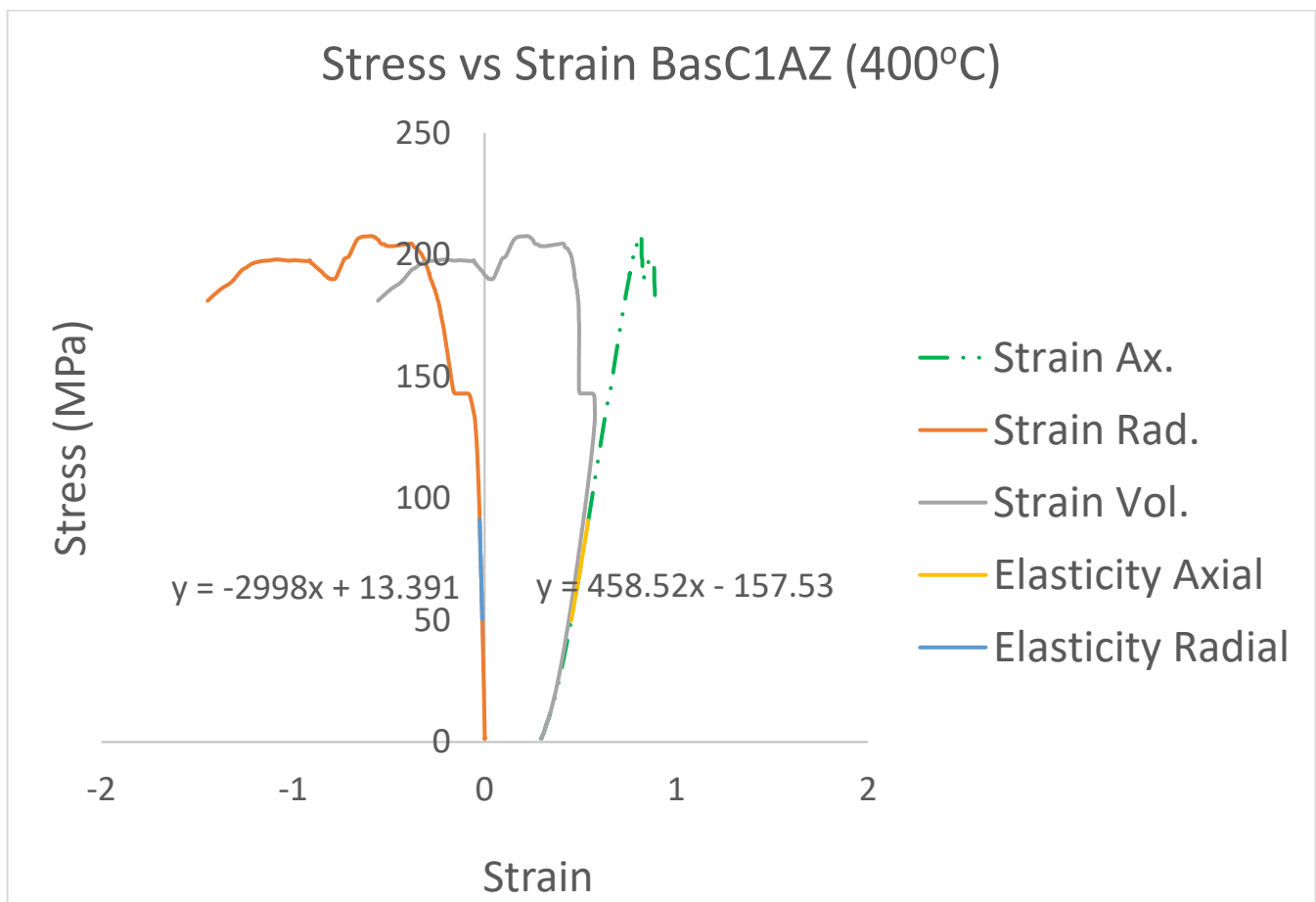Test Date: 10-March-2017

Test Result

Crack Initiation: 384.73 MPa
Ultimate Compressive Strength: 384.73 MPa
Young's modulus: 61.47 GPa
Poisson's ratio: 0.21
Remark: -

Core Data

ID: BasA4Z
Rock Type: Basalt
Location: Eifel (Germany)
Length: 61.42 mm
Diameter: 29.73 mm
Matrix Density: 3.00 gram/cc

7. BasA5Z

AFTER UCS TEST
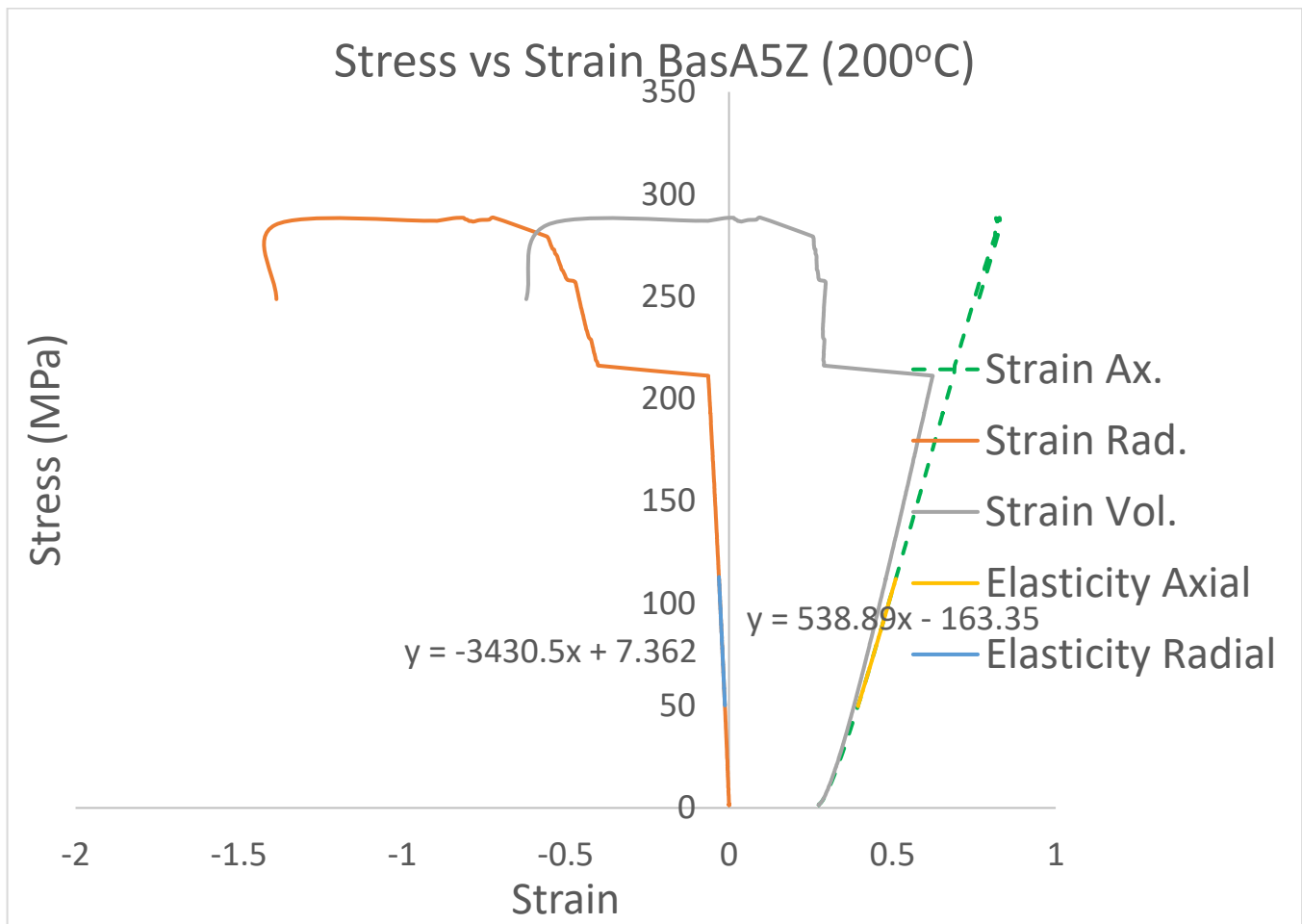
Stress vs Strain BasA5Z (200°C)

y = -3430.5x + 7.362

y = 538.89x - 163.35

- Strain Ax.
- Strain Rad.
- Strain Vol.
- Elasticity Axial
- Elasticity Radial

Stress (MPa)

Strain

Test Data
Test: Uniaxial Compressive Strength
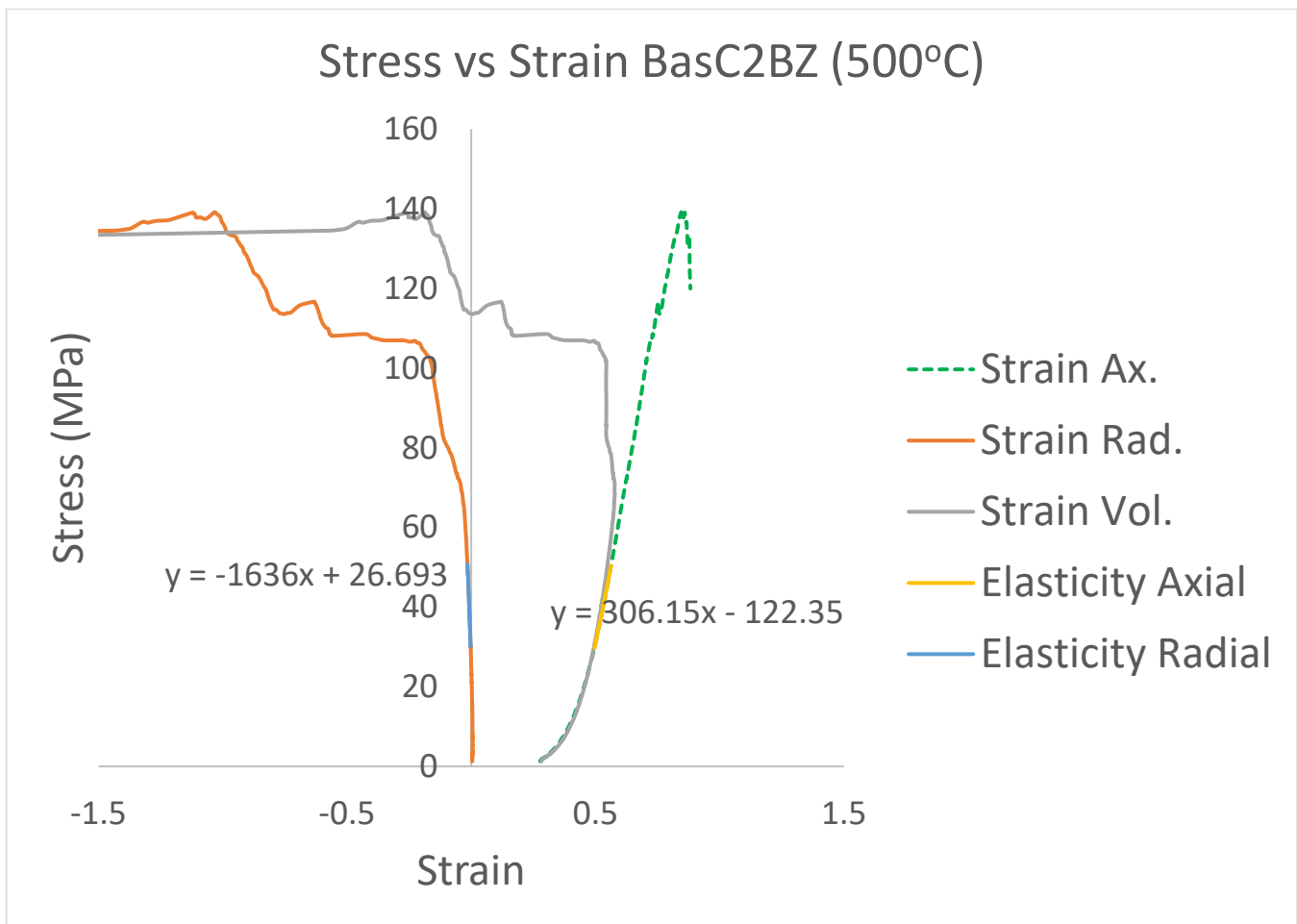Test Date: 10-March-2017

Test Result
Crack Initiation: 211.39 MPa
Ultimate Compressive Strength: 288.59 MPa
Young's modulus: 53.89 GPa
Poisson's ratio: 0.16
Remark: -

Core Data
ID: BasA5Z
Rock Type: Basalt
Location: Eifel (Germany)
Length: 61.97 mm
Diameter: 29.71 mm
Matrix Density: 3.00 gram/cc

8. BasA6Z

AFTER UCS TEST

Stres vs Strain BasA6Z (300°C)

$y = -4426.7x + 239.57$

$y = 528.91x - 175.12$

Legend:
- Strain Ax.
- Strain Rad.
- Strain Vol.
- Elasticity Axial
- Elasticity Radial

Test Data
Test: Uniaxial Compressive Strength
Test Date: 10-March-2017

Test Result
Crack Initiation: 150.37 MPa
Ultimate Compressive Strength: 261.22 MPa
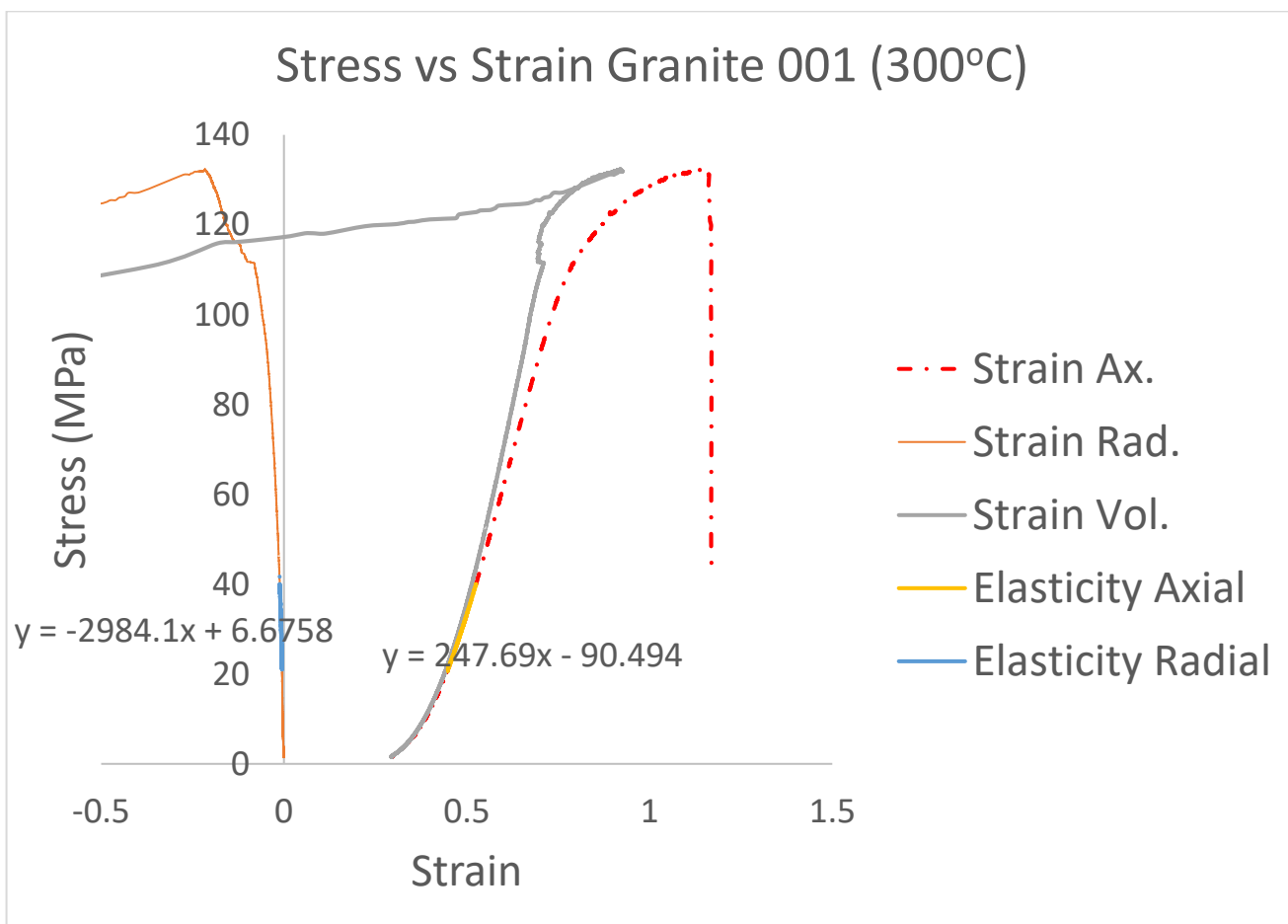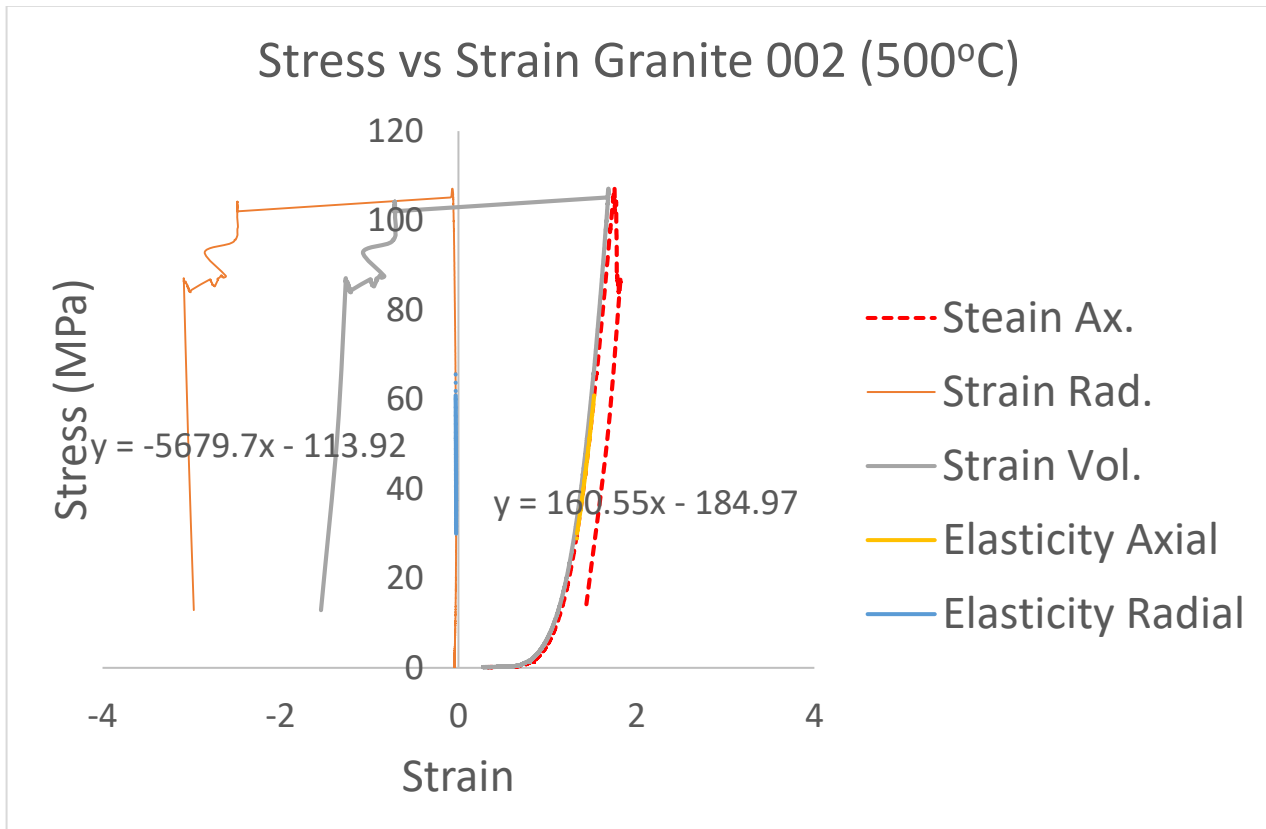Young's modulus: 52.89 GPa
Poisson's ratio: 0.12
Remark: -

Core Data
ID: BasA6Z
Rock Type: Basalt
Location: Eifel (Germany)
Length: 58.59 mm
Diameter: 29.73 mm
Matrix Density: 3.00 gram/cc

9. BasC1AZ

AFTER UCS TEST

Stress vs Strain BasC1AZ (400°C)

$y = -2998x + 13.391$

$y = 458.52x - 157.53$

Legend:
- Strain Ax.
- Strain Rad.
- Strain Vol.
- Elasticity Axial
- Elasticity Radial

Test Data
Test: Uniaxial Compressive Strength
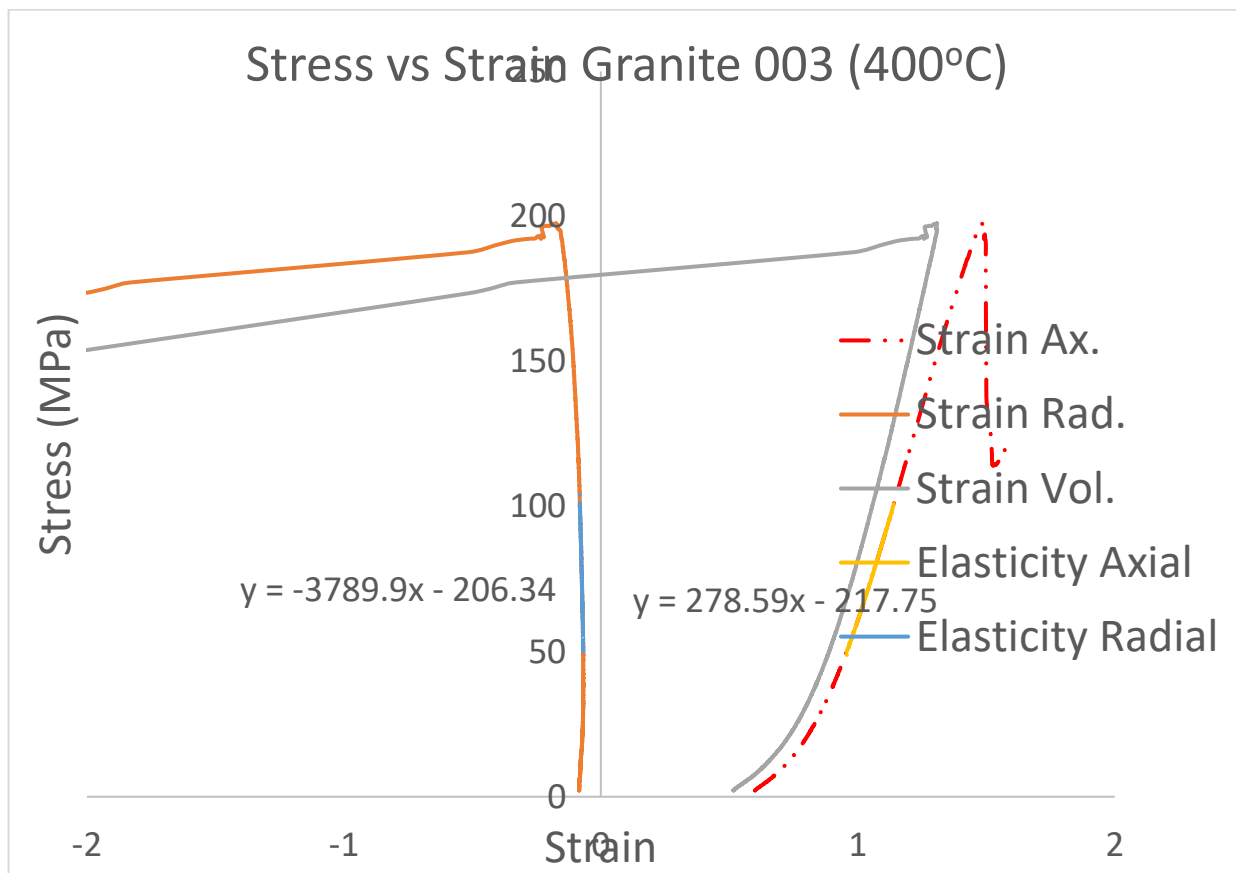Test Date: 10-March-2017

Test Result
Crack Initiation: 140.37 MPa
Ultimate Compressive Strength: 207.66 MPa
Young's modulus: 45.85 GPa
Poisson's ratio: 0.15
Remark: -

Core Data
ID: BasC1AZ
Rock Type: Basalt
Location: Eifel (Germany)
Length: 60.09 mm
Diameter: 29.72 mm
Matrix Density: 3.02 gram/cc

10. BasC2BZ

AFTER UCS TEST

Stress vs Strain BasC2BZ (500°C)

$y = -1636x + 26.693$

$y = 306.15x - 122.35$

- - - - Strain Ax.
—— Strain Rad.
—— Strain Vol.
—— Elasticity Axial
—— Elasticity Radial

Stress (MPa)

Strain

Test Data
Test: Uniaxial Compressive Strength
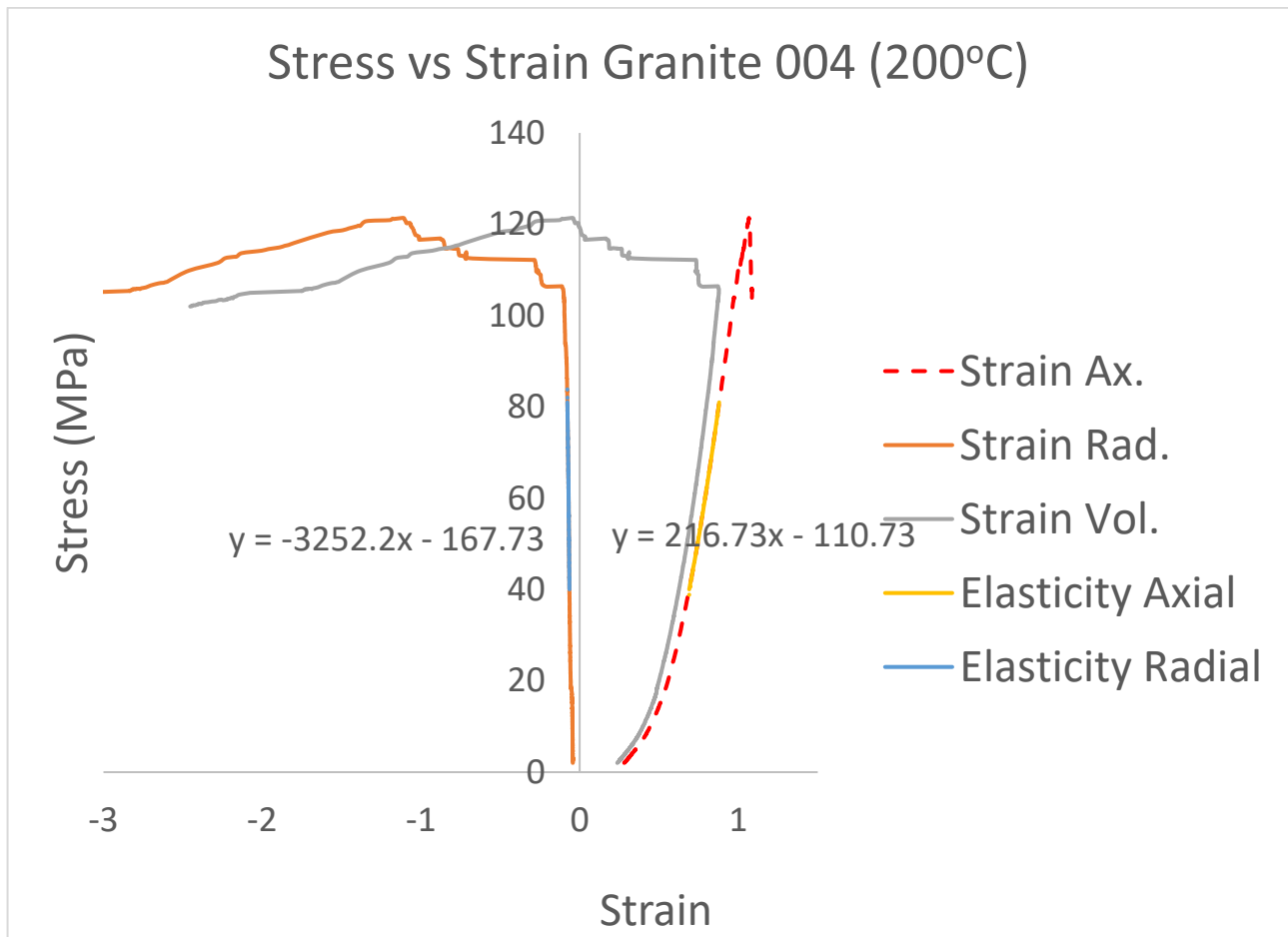Test Date: 10-March-2017

Test Result
Crack Initiation: 67.63 MPa
Ultimate Compressive Strength: 139.14 MPa
Young's modulus: 30.62 GPa
Poisson's ratio: 0.19
Remark: -

Core Data
ID: BasC2BZ
Rock Type: Basalt
Location: Eifel (Germany)
Length: 59.13 mm
Diameter: 29.74 mm
Matrix Density: 3.00 gram/cc

BENIN (WEST AFRICA)
1. TI001

AFTER UCS TEST

Stress vs Strain Granite 001 (300°C)

y = -2984.1x + 6.6758

y = 247.69x - 90.494

Legend:
- –·– Strain Ax.
- — Strain Rad.
- — Strain Vol.
- — Elasticity Axial
- — Elasticity Radial

Test Data
Test: Uniaxial Compressive Strength
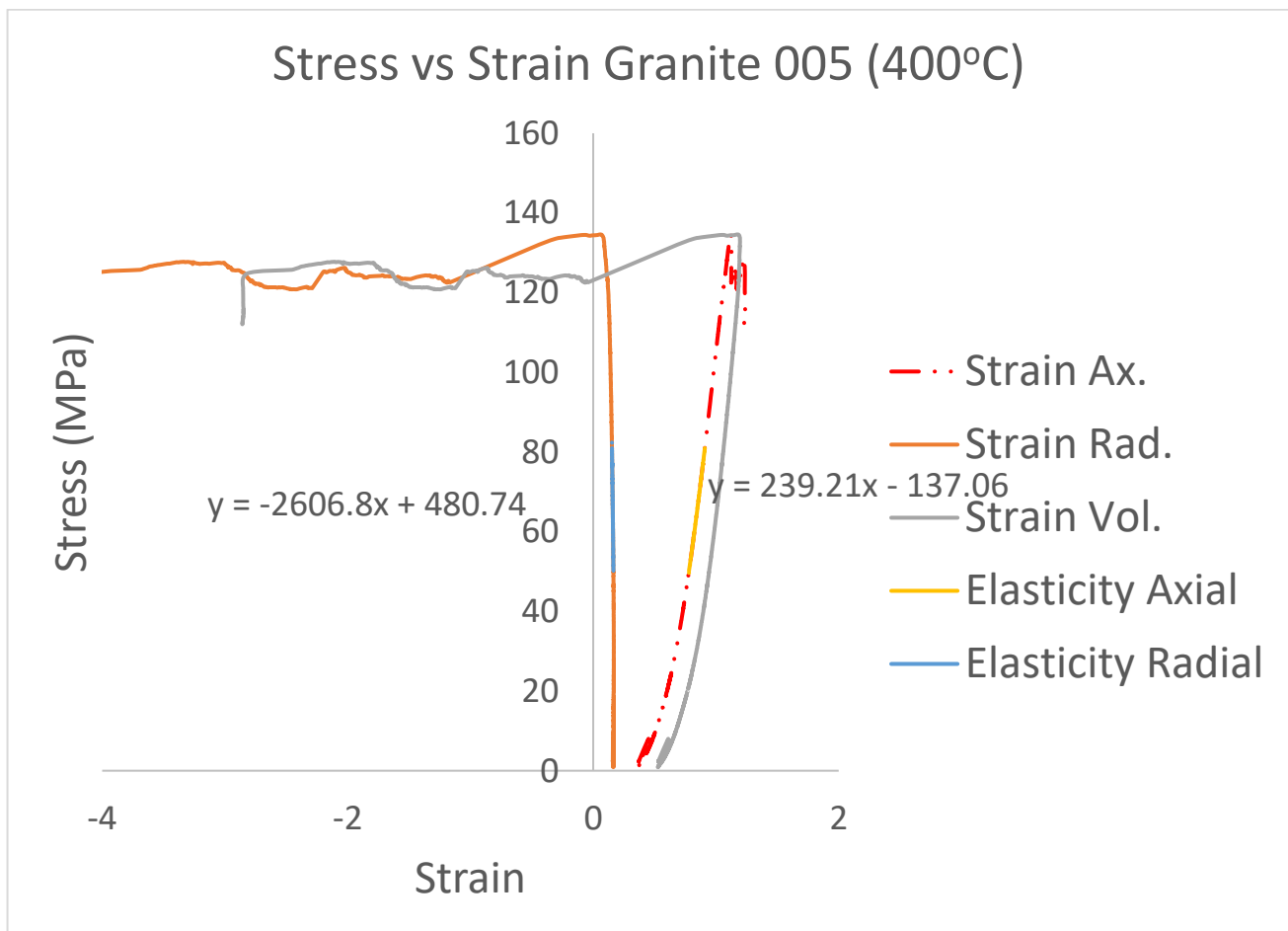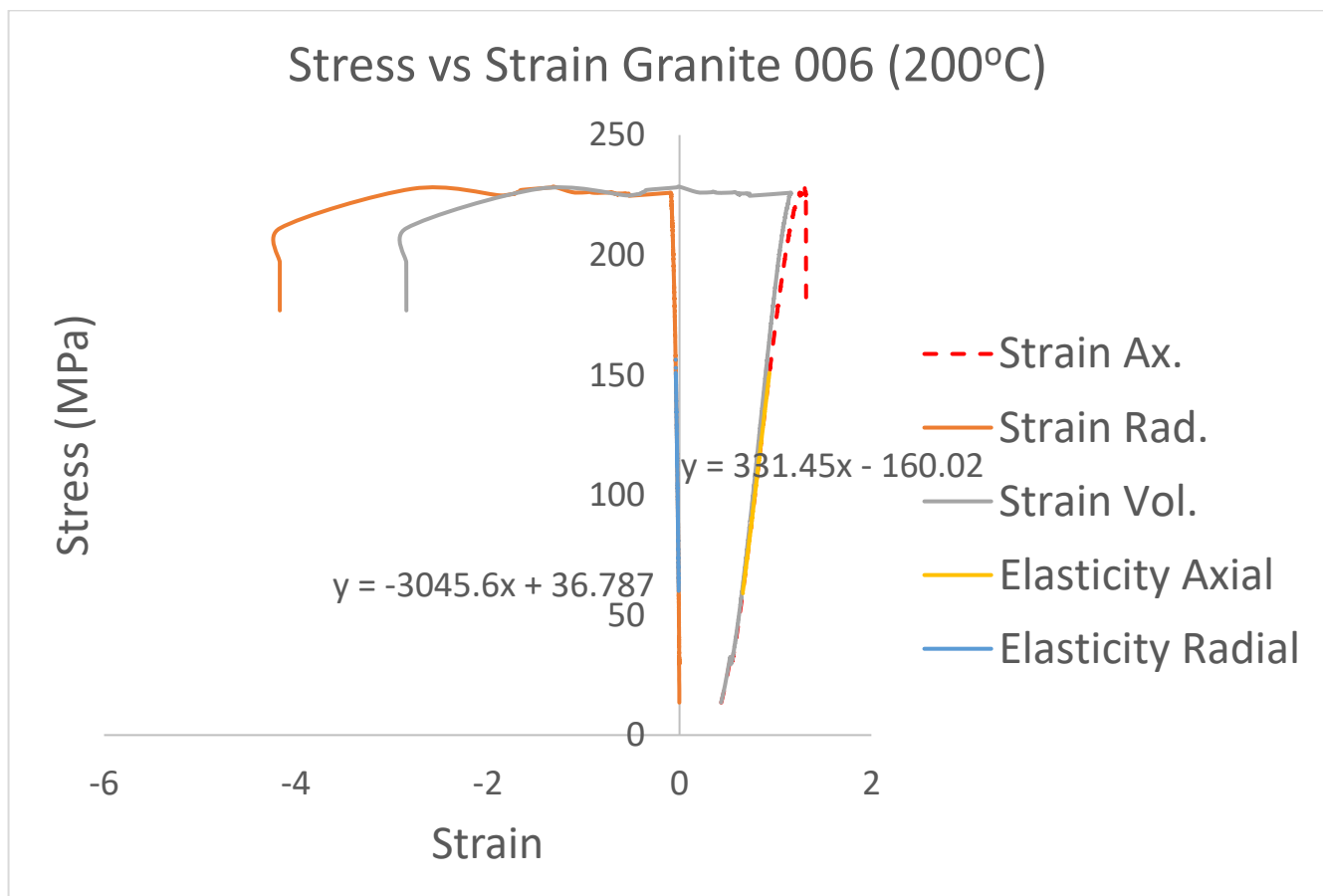Test Date: 18-January-2017

Test Result
Crack Initiation: 41.19 MPa
Ultimate Compressive Strength: 132.34 MPa
Young's modulus: 24.77 GPa
Poisson's ratio: 0.08
Remark: -

Core Data
ID: TI001
Rock Type: Granite
Location: Benin (West Africa)
Length: 59.29 mm
Diameter: 29.82 mm
Matrix Density: 2.62 gram/cc

2. TI002

AFTER UCS TEST

Stress vs Strain Granite 002 (500°C)

- - - - Steain Ax.
——— Strain Rad.
——— Strain Vol.
——— Elasticity Axial
——— Elasticity Radial

$y = -5679.7x - 113.92$

$y = 160.55x - 184.97$

Test Data
Test: Uniaxial Compressive Strength
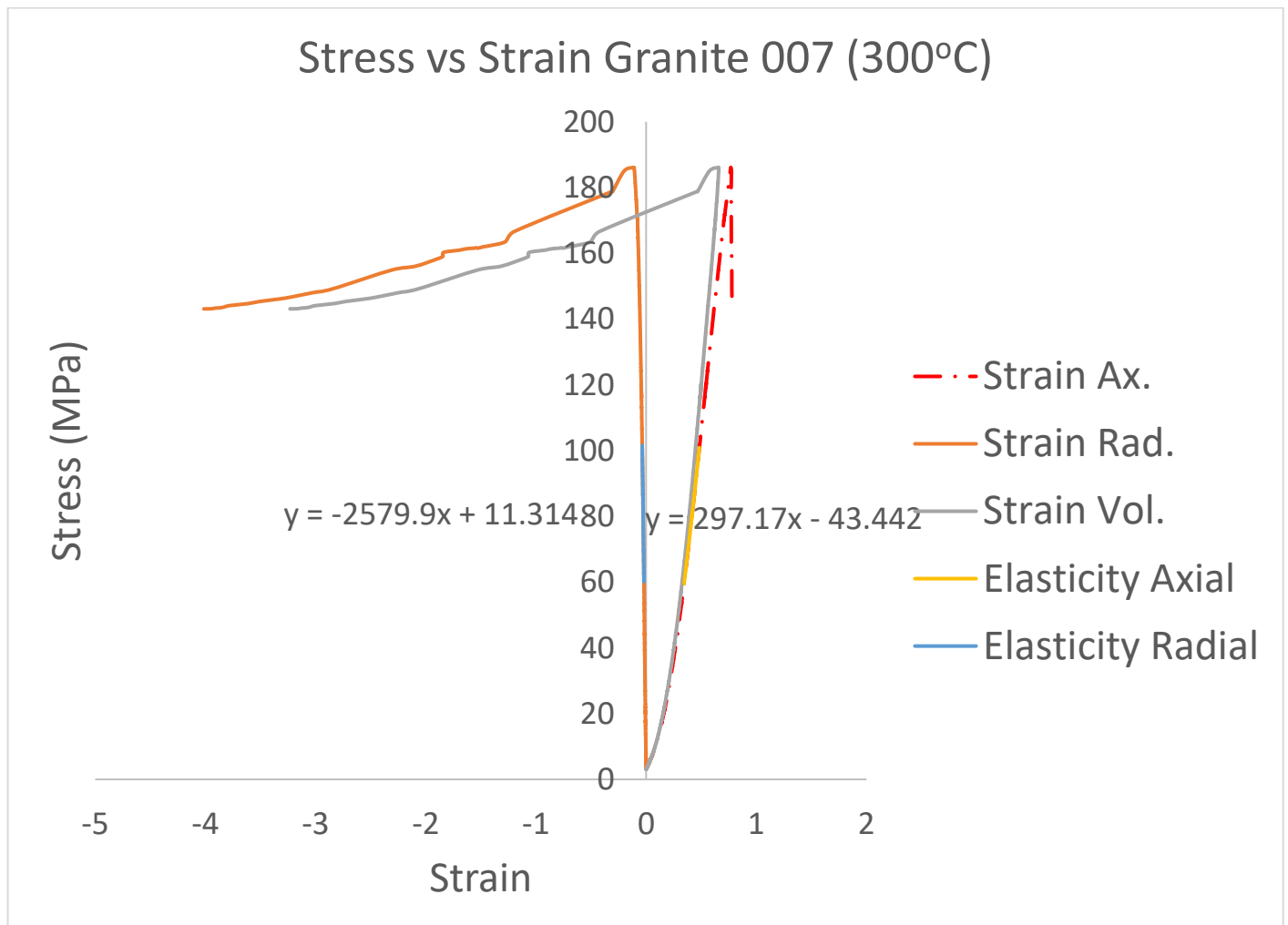Test Date: 19-January-2017

Test Result
Crack Initiation: 107.13 MPa
Ultimate Compressive Strength: 107.13 MPa
Young's modulus: 16.05 GPa
Poisson's ratio: 0.03
Remark: -

Core Data
ID: TI002
Rock Type: Granite
Location: Benin (West Africa)
Length: 60.73 mm
Diameter: 29.88 mm
Matrix Density: 2.6 gram/cc

3. TI003

AFTER UCS TEST

Stress vs Strain Granite 003 (400°C)

Stress (MPa) vs *Strain*

$y = -3789.9x - 206.34$

$y = 278.59x - 217.75$

Legend:
- Strain Ax.
- Strain Rad.
- Strain Vol.
- Elasticity Axial
- Elasticity Radial

Test Data
Test: Uniaxial Compressive Strength
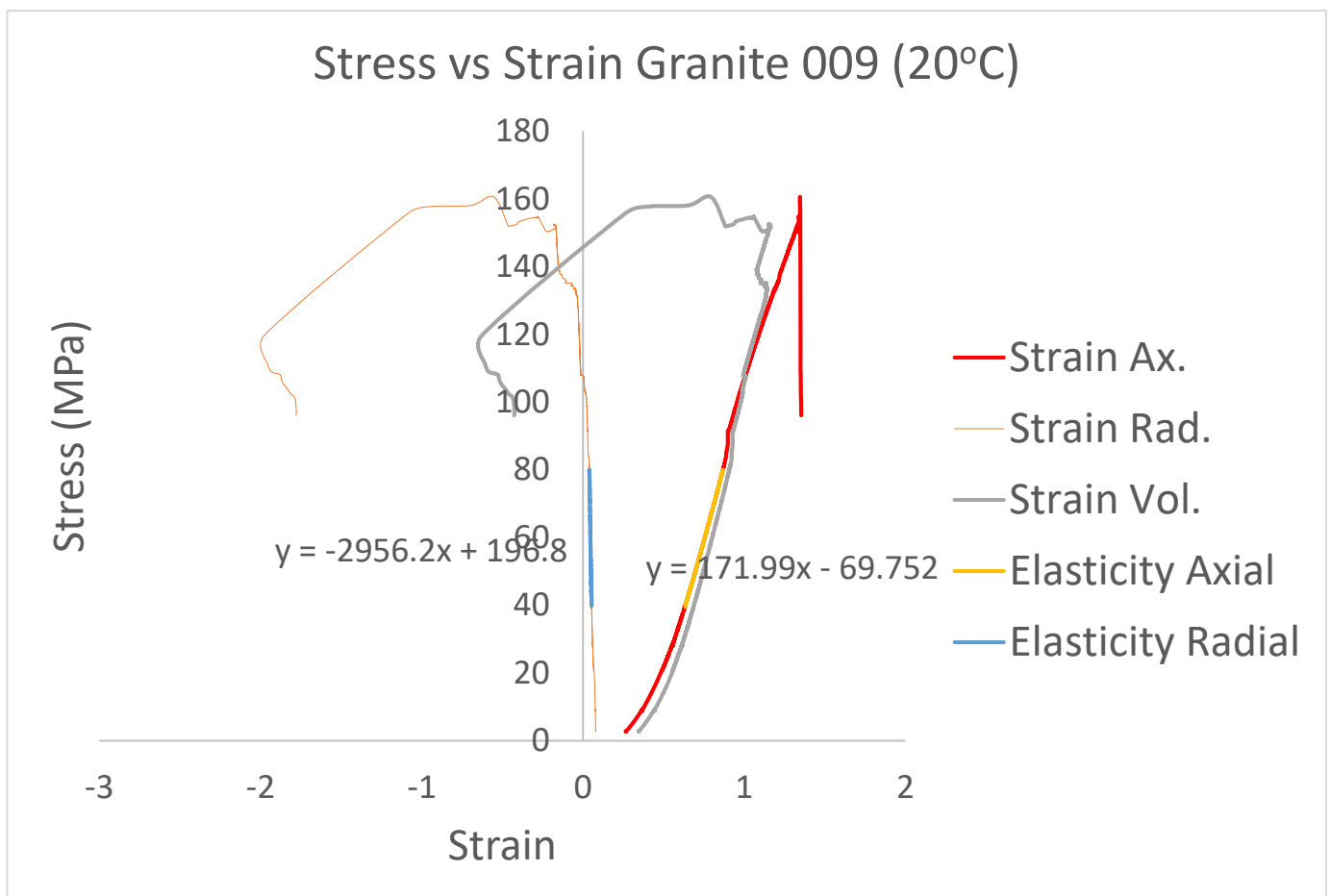Test Date: 18-January-2017

Test Result
Crack Initiation: 197.61 MPa
Ultimate Compressive Strength: 197.61 MPa
Young's modulus: 27.86 GPa
Poisson's ratio: 0.07
Remark: -

Core Data
ID: TI003
Rock Type: Granite
Location: Benin (West Africa)
Length: 59.93 mm
Diameter: 29.84 mm
Matrix Density: 2.61 gram/cc

4. TI004

AFTER UCS TEST

Stress vs Strain Granite 004 (200°C)

$y = -3252.2x - 167.73$

$y = 216.73x - 110.73$

Legend:
- Strain Ax.
- Strain Rad.
- Strain Vol.
- Elasticity Axial
- Elasticity Radial

Test Data
Test: Uniaxial Compressive Strength
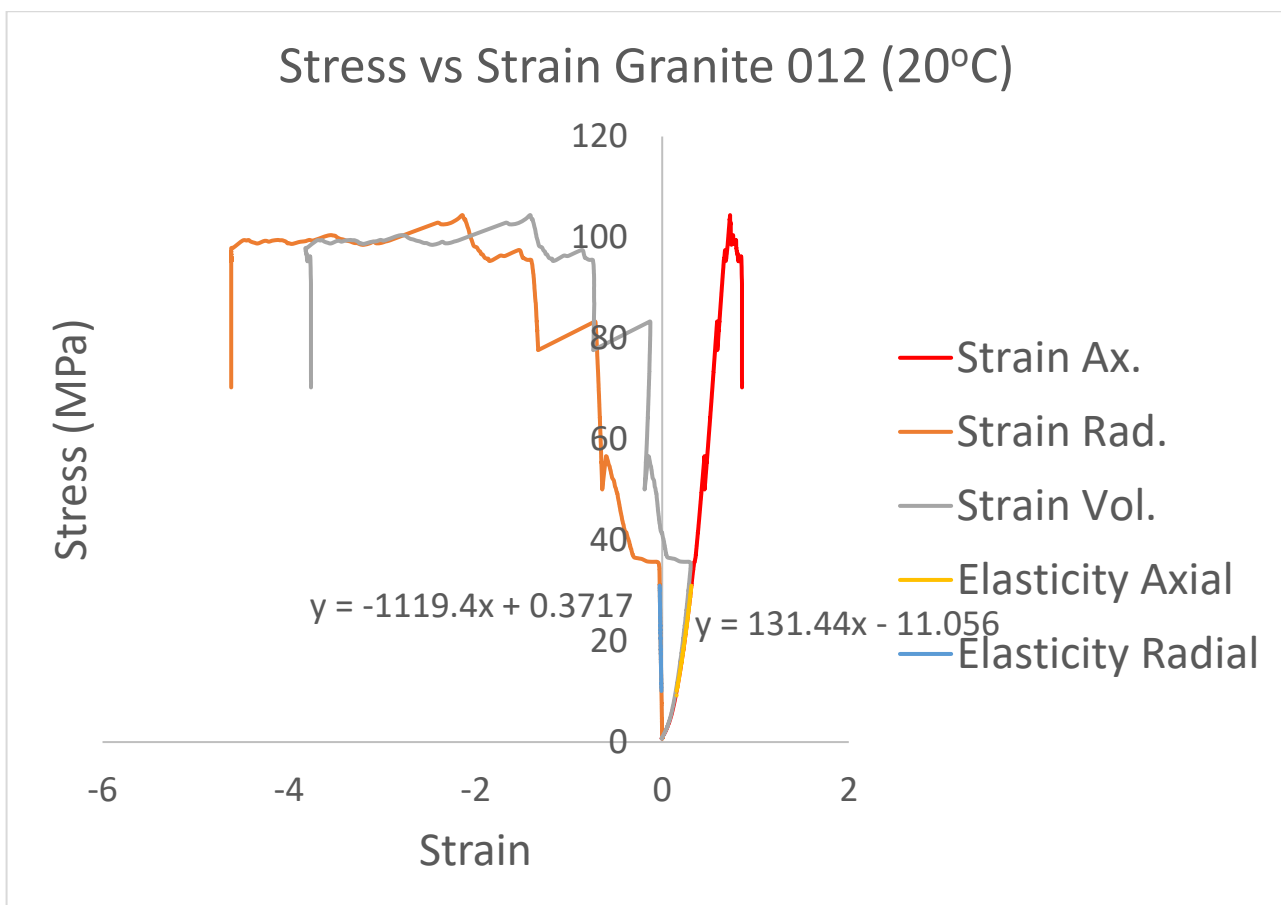Test Date: 30-January-2017

Test Result
Crack Initiation: 106.34 MPa
Ultimate Compressive Strength: 121.39 MPa
Young's modulus: 21.67 GPa
Poisson's ratio: 0.07
Remark: -

Core Data
ID: TI004
Rock Type: Granite
Location: Benin (West Africa)
Length: 59.05 mm
Diameter: 29.0 mm
Matrix Density: 2.62 gram/cc

5. TI005

AFTER UCS TEST

Stress vs Strain Granite 005 (400°C)

$y = -2606.8x + 480.74$

$y = 239.21x - 137.06$

Legend:
- Strain Ax.
- Strain Rad.
- Strain Vol.
- Elasticity Axial
- Elasticity Radial

Y-axis: Stress (MPa)
X-axis: Strain

Test Data
Test: Uniaxial Compressive Strength
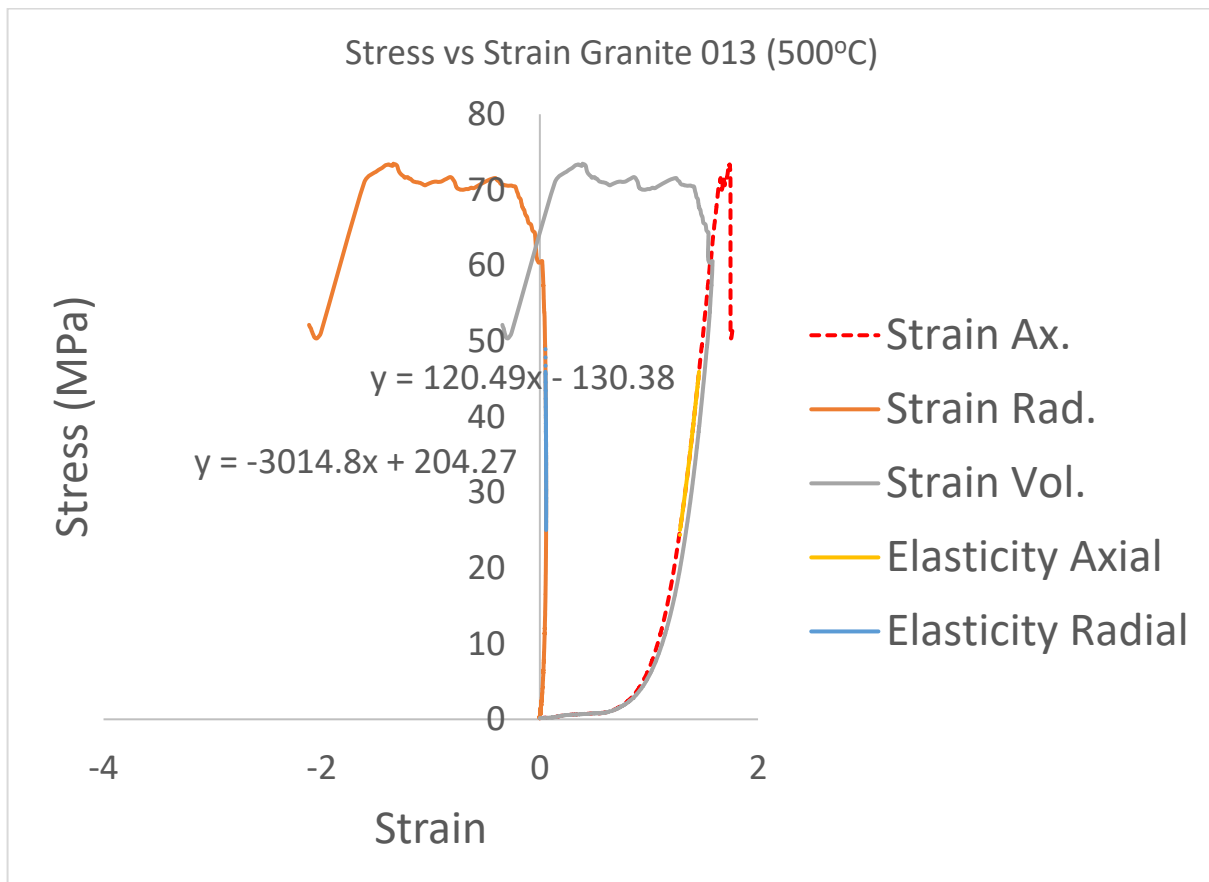Test Date: 30-January-2017

Test Result
Crack Initiation: 134.6 MPa
Ultimate Compressive Strength: 134.6 MPa
Young's modulus: 23.92 GPa
Poisson's ratio: 0.09
Remark: -

Core Data
ID: TI005
Rock Type: Granite
Location: Benin (West Africa)
Length: 60.01 mm
Diameter: 29.86 mm
Matrix Density: 2.62 gram/cc

6. TI006

AFTER UCS TEST


Stress vs Strain Granite 006 (200°C)

$y = 331.45x - 160.02$

$y = -3045.6x + 36.787$

Legend:
- Strain Ax.
- Strain Rad.
- Strain Vol.
- Elasticity Axial
- Elasticity Radial

Test Data
Test: Uniaxial Compressive Strength
Test Date: 30-January-2017

Test Result
Crack Initiation: 228.51 MPa
Ultimate Compressive Strength: 228.51 MPa
Young's modulus: 33.15 GPa
Poisson's ratio: 0.11
Remark: -

Core Data
ID: TI006
Rock Type: Granite
Location: Benin (West Africa)
Length: 59.02 mm
Diameter: 29.8 mm
Matrix Density: 2.63 gram/cc

7. TI007

AFTER UCS TEST

Stress vs Strain Granite 007 (300°C)

$y = -2579.9x + 11.314$ $y = 297.17x - 43.442$

Legend:
- – · – Strain Ax.
- —— Strain Rad.
- —— Strain Vol.
- —— Elasticity Axial
- —— Elasticity Radial

Test Data

Test: Uniaxial Compressive Strength
Test Date: 30-January-2017

Test Result

Crack Initiation: 186.16 MPa
Ultimate Compressive Strength: 186.16 MPa
Young's modulus: 29.72 GPa
Poisson's ratio: 0.12
Remark: -

Core Data

ID: TI007
Rock Type: Granite
Location: Benin (West Africa)
Length: 60.47 mm
Diameter: 29.82 mm
Matrix Density: 2.63 gram/cc

8. TI009

AFTER UCS TEST

Stress vs Strain Granite 009 (20°C)

$y = -2956.2x + 196.8$

$y = 171.99x - 69.752$

Legend:
- Strain Ax.
- Strain Rad.
- Strain Vol.
- Elasticity Axial
- Elasticity Radial

Test Data
Test: Uniaxial Compressive Strength
Test Date: 23-January-2017

Test Result
Crack Initiation: 91.69 MPa
Ultimate Compressive Strength: 160.55 MPa
Young's modulus: 17.2 GPa
Poisson's ratio: 0.06
Remark: -

Core Data
ID: TI009
Rock Type: Granite
Location: Benin (West Africa)
Length: 59.81 mm
Diameter: 29.77 mm
Matrix Density: 2.64 gram/cc

9. TI012

AFTER UCS TEST

Stress vs Strain Granite 012 (20°C)

$y = -1119.4x + 0.3717$

$y = 131.44x - 11.056$

Legend:
- Strain Ax.
- Strain Rad.
- Strain Vol.
- Elasticity Axial
- Elasticity Radial

Test Data
Test: Uniaxial Compressive Strength
Test Date: 2-March-2017

Test Result
Crack Initiation: 33.15 MPa
Ultimate Compressive Strength: 104.43 MPa
Young's modulus: 13.14 GPa
Poisson's ratio: 0.12
Remark: -

Core Data
ID: TI012
Rock Type: Granite
Location: Benin (West Africa)
Length: 63.37 mm
Diameter: 29.75 mm
Matrix Density: 2.63 gram/cc

10. TI013

AFTER UCS TEST

Stress vs Strain Granite 013 (500°C)

y = 120.49x - 130.38

y = -3014.8x + 204.27

Legend:
- Strain Ax.
- Strain Rad.
- Strain Vol.
- Elasticity Axial
- Elasticity Radial

Test Data
Test: Uniaxial Compressive Strength
Test Date: 2-March-2017

Test Result
Crack Initiation: 69.88 MPa
Ultimate Compressive Strength: 73.46 MPa
Young's modulus: 12.05 GPa
Poisson's ratio: 0.04
Remark: -

Core Data
ID: TI013
Rock Type: Granite
Location: Benin (West Africa)
Length: 62.45 mm
Diameter: 29.85 mm
Matrix Density: 2.60 gram/cc

Basaltic andesite-C-D Basalt and Pumice Tangkuban Perahu (Indonesia) Point Selection

Basaltic Andesite – Tangkuban Perahu
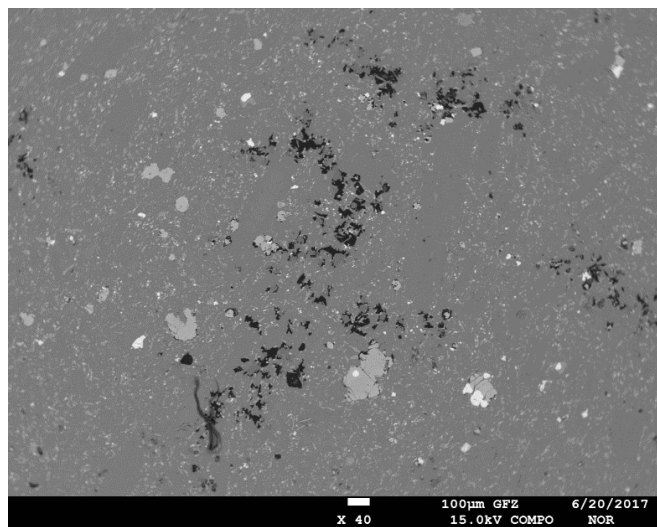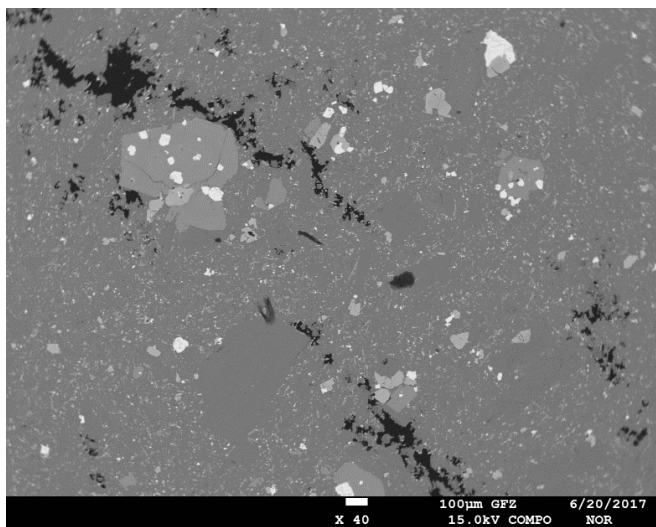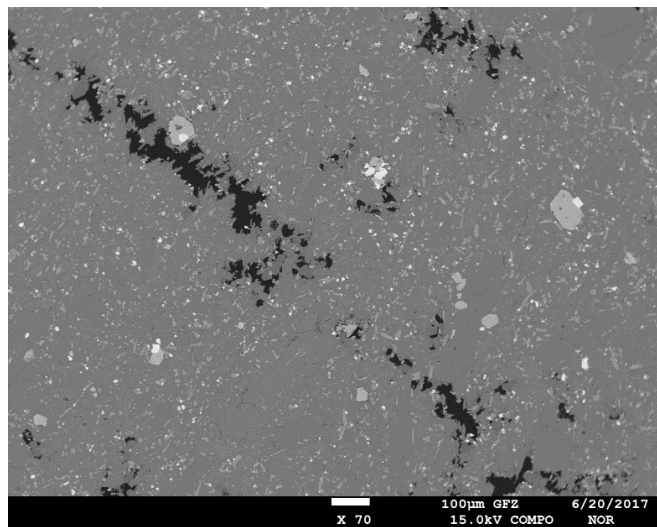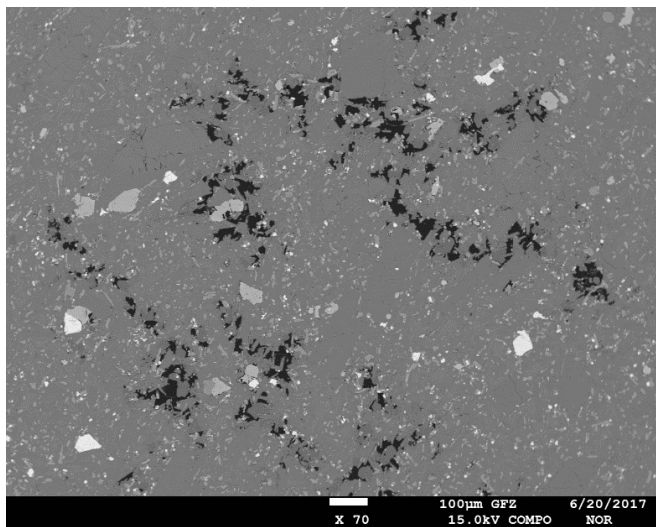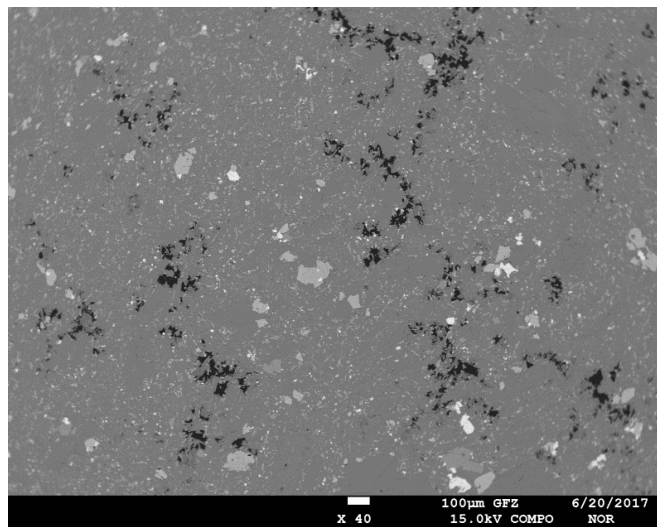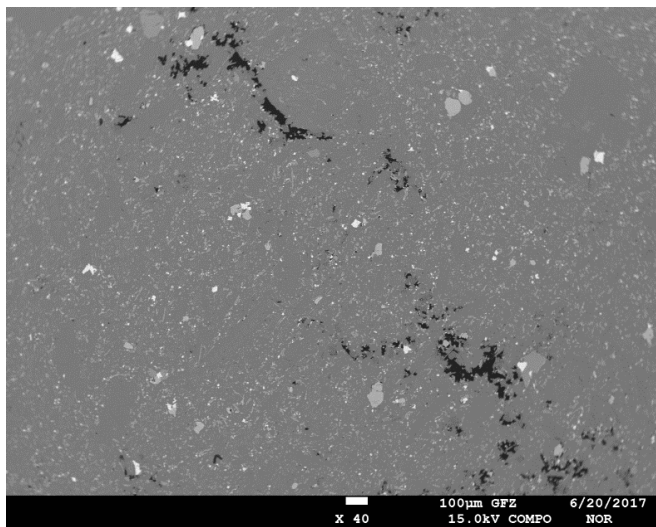
Left to right: point 1, 3, 4, 5, 8, 9
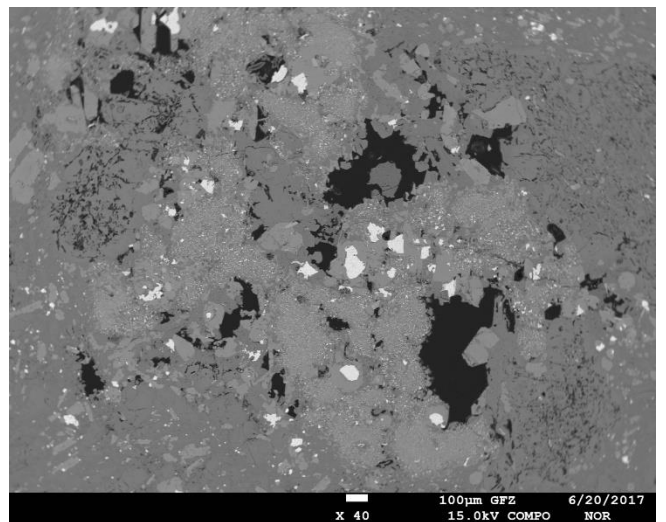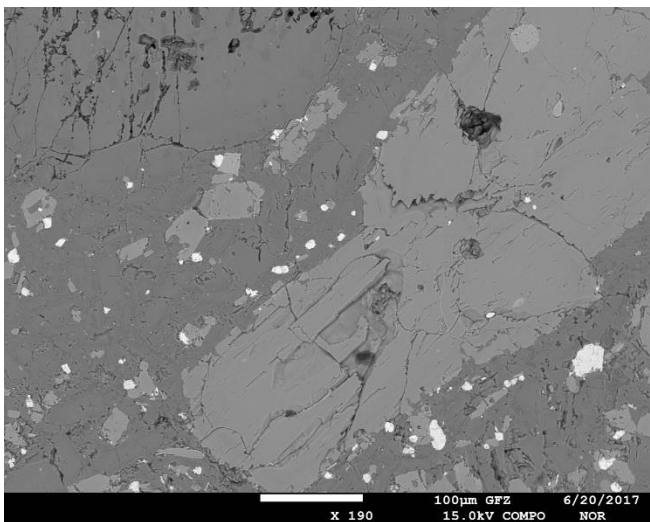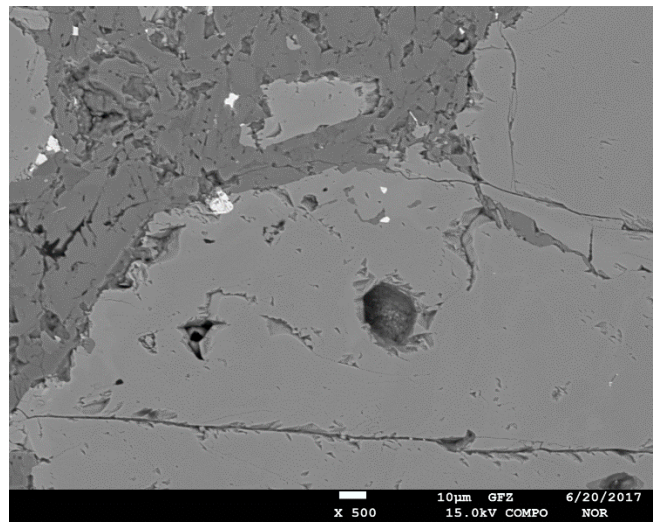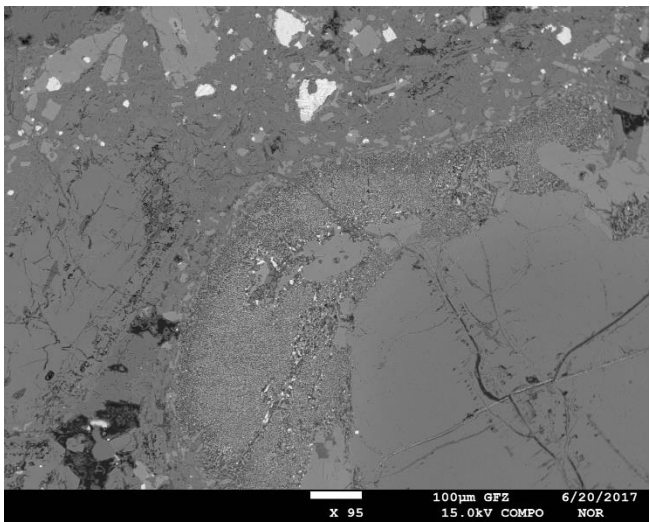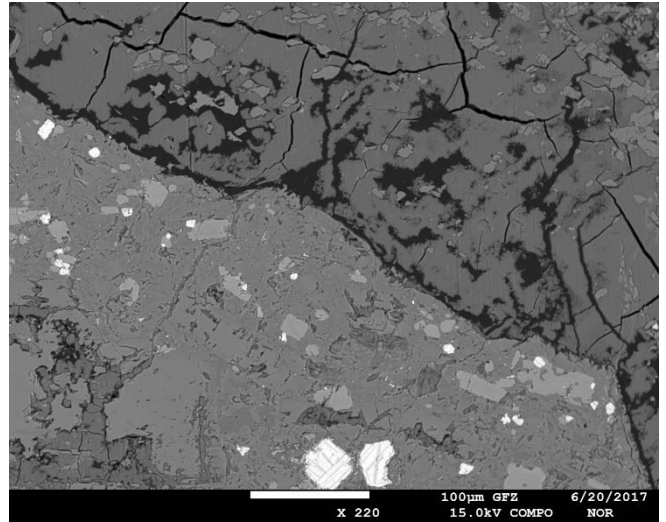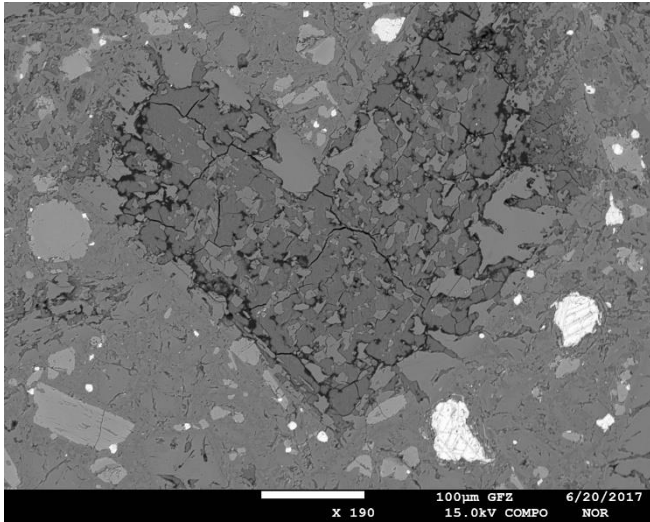
Left to right: point 8, 11, 15, 18, 19, 21
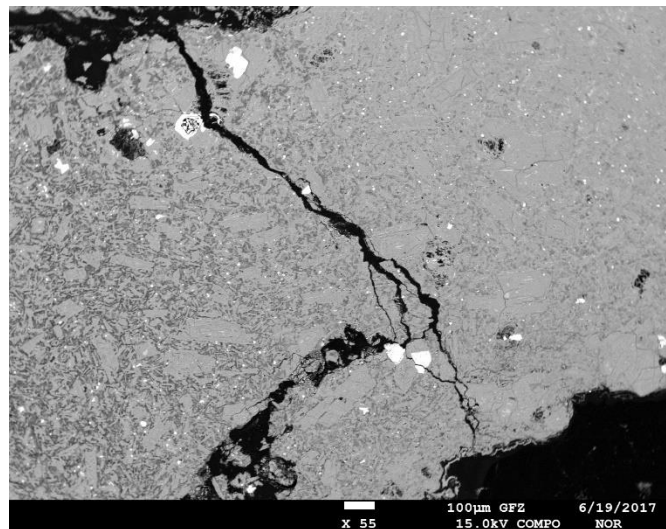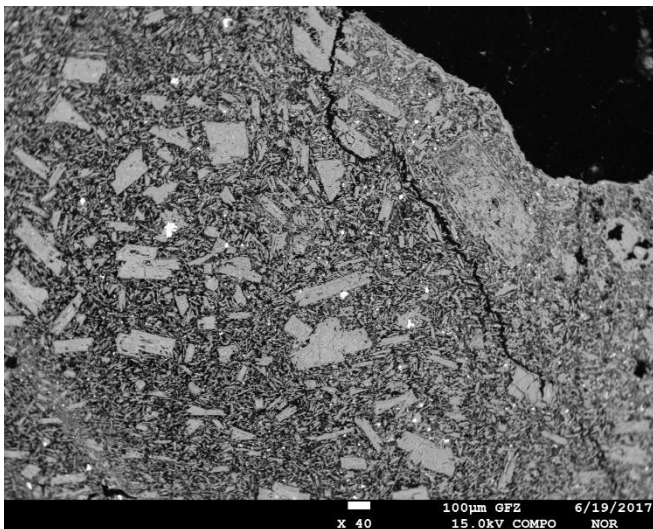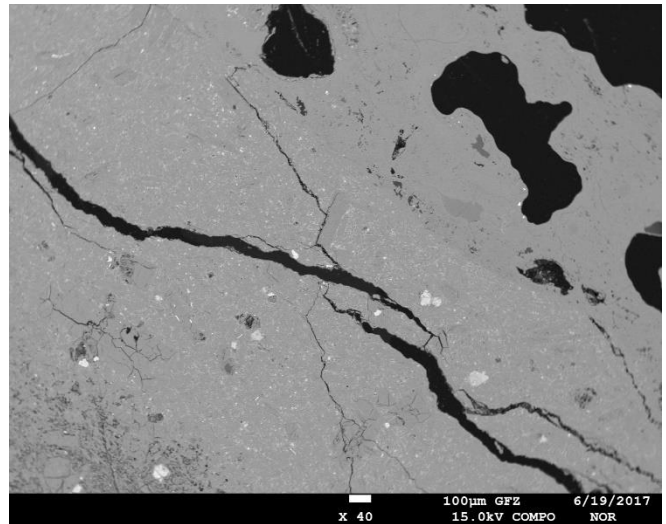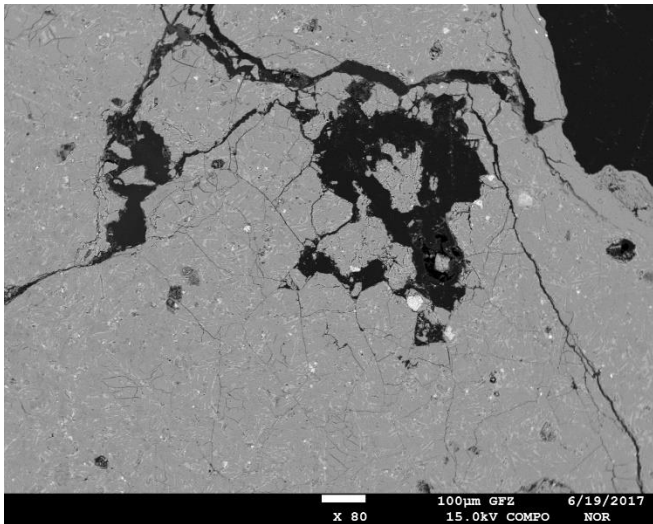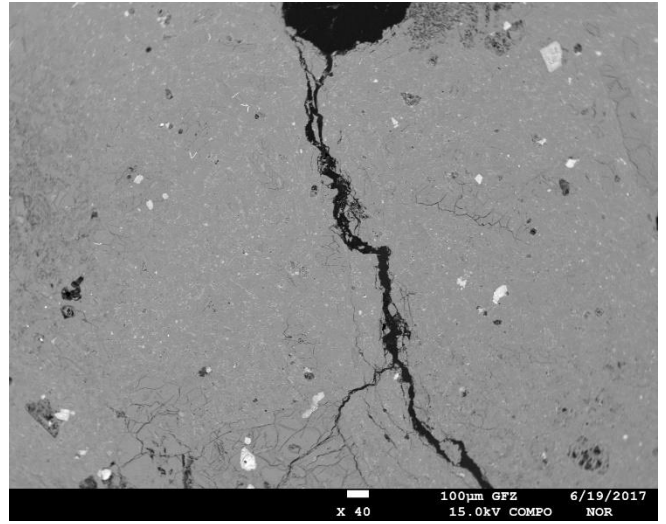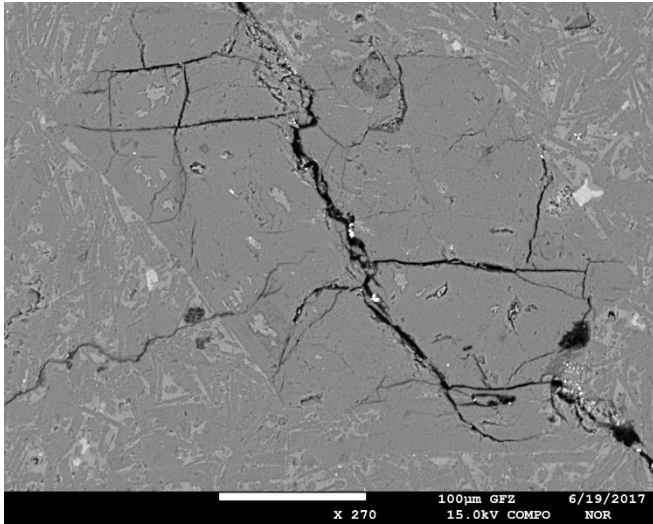
Left to right: point 4, 9, 14, 16, 19, 22

7. References

Ahmad Ghassemi, S. T. (2015). Analysis of Fracture Propagation under Thermal Stress in Geothermal Reservoirs. *World Geothermal Congress.* Melbourne.

Amir Fauzi, S. B. (2000). Geothermal Development in Indonesia: An Overview of Industry Status and Future Growth. *World Geothermal Congress 2000.* Kyushu, Japan.

Badan Geologi Kementerian Energi dan Sumber Daya Mineral. (2014, May 30). Retrieved from Badan Geologi Kementerian Energi dan Sumber Daya Mineral: http://www.vsi.esdm.go.id/index.php/gunungapi/data-dasar-gunungapi/516-g-tangkuban-parahu

Bas, M. J., Maitre, R. W., Streckeisen, A., & Zanettin, B. (1985). A Chemical Classification of Volcanic Rocks Based on the Total Alkali-Silica Diagram.

Berrizbeitia, L. D. (2014). Environmental Impacts of Geothermal Energy Generation and Utilization.

C. Baujarda, A. G. (2016). Hydrothermal characterization of wells GRT-1 and GRT-2 inRittershoffen, France: Implications on the understanding of naturalflow systems in the rhine graben. Strasbourg: Elsevier.

Cho, M. P. (2014). Brittleness revisited. *Geoconvention*.

Clément Baujard, R. H. (2017). Rate of penetration of geothermal wells: a key challenge in hard rocks. *42nd Workshop on Geothermal Reservoir Engineering.* Stanford.

Coates, D., & Parsons, R. (1966). Experimental Criteria for Classification of Rock Substances. Ottawa.

Directorate General of New Renewable Energy and Energy Conservation Indonesia. (2015).

Enayatpour, S., & Patzek, T. (2013). *Thermal Shock in Reservoir Rock Enhances the Hydraulic.* Denver, Colorado, USA: Unconventional Resources Technology Conference (URTeC).

Eslinger, E., & Pevear, D. R. (1988). *Clay minerals for petroleum geologists and engineers* . Tulsa: Society of Economic Paleontologists and Mineralogis ts .

Fiorenza Deon, H.-J. F. (2015). Geochemical/hydrochemical evaluation of the geothermal potential of the Lamongan volcanic field (Eastern Java, Indonesia). *Geothermal Energy a SpringerOpen Journal*.

GFZ Potsdam. (2017). *Electron Microprobe Laboratories*. Retrieved from GFZ Helmholtz Centre Potsdam: http://www.gfz-potsdam.de/en/section/inorganic-and-isotope-geochemistry/infrastructure/microprobe-lab/

Hals, K. M., & Berre, a. I. (2013). Thermal Fracturing of Geothermal Well and the Effects of Borehole Orientation. *Thirty-Eighth Workshop on Geothermal Reservoir Engineering.* Stanford: Stanford University.

Heap, M., & Faulkner, D. (2007). Quantifying the evolution of static elastic properties as crystalline rock approaches failure. *International Journal of Rock Mechanics & Mining Sciences*.

Hetenyi, M. (1966). Handbook of Experimental Stress Analysis. New York: John Wiley.

Holt, R. M., Fjær, E., Nes, O.-M., & Alassi, H. (2011). A shaly look at brittleness. *45th US Rock Mechanics / Geomechanics Symposium.* San Fransisco: American Rock Mechanics Association.

Hucka, V., & Das, B. (1974). Brittleness Determination of Rocks by Different Methods. *International Journal Rock Mechanics Science and Geomechanics*.

IEA. (2014). Retrieved from International Energy Agency: http://www.iea.org/

J. Fortin, S. S. (2010). Influence of thermal and mechanical cracks on permeability and elastic wave velocities in a basalt from Mt. Etna volcano subjected to elevated pressure. *Elsevier*.

Joanne T. Fredrich, T.-f. W. (1986). Micromechanics of Thermally Induced Cracking in Three Crustal Rocks. *Journal of Geophysical Research Vol.91*, 12743-12764.

Jorg V. Herwanger, A. D. (2015). Uses and Abuses of the Brittleness Index With Applications to. San Antonio: Unconventional Resources Technology Conference (URTeC).

Klinkenberg, L. J. (1941). The Permeability of Porous Media to Liquids and Gases.

Kodikara, B. F. (1999). Changes in Clay Structure and Behaviour Due to Wetting and Drying. Barton: Australian Geomechanics Society.

Kranz, R. L. (1983). Microcracks in Rocks: A Review. In *Continental Tectonics: Structure, Kinematics and Dynamics* (pp. 449-480). Texas: Elsevier Science Publishers.

Lutgens, r. K., Tarbuck, E. J., & G., D. (2014). In *Essentials of Geology, 12th Ed.* Retrieved from http://www.columbia.edu/~vjd1/igneous.htm

Manger, G. E. (1966). Method-Dependent Values of Bulk, Grain, and Pore Volumes as Related to Observed Porosity. Washington: United States Government Priting Office.

Micromeritics Instrument Corporation. (2001). *AccuPyc 1330 Pycnometer.* Micromeritics Instrument Corporation.

Ministry of Energy and Mineral Resources of Indonesia. (2016). *Statistics Book of New, Renewable Energy and Energy Conservation (NREEC)* . Jakarta.

MTS Manual Book. (n.d.). Circumferential Strain Measurement Package. In M. S. Information, *Model 815 Rock and Concrete Mechanics Testing Systems.*

N. Brantut, M. J. (2014). Rate- and strain-dependent brittle deformation of rocks. *Journal of Geophysical Research: Solid Earth*.

Oliveira, P. (2012). *The Elements - Periodic Table References.* Pedia Press.

Omdal, K. (2015). *Development of Procedure and Analysis of Hard Rock Drilling* . Stavanger: University of Stavanger.

P.G. Ranjith, D. Z. (2016). The brittleness indices used in rock mechanics and their application in shale hydraulic fracturing. Melbourne: Elsevier.

P.Y., B. P. (1994). Modelling the Evolution of Columnar Joints. (pp. 219-239). Journal of Volcanology and Geothermal Research .

Phoenix X-Ray Computed Tomography poster. (n.d.).

Primarini, M. I. (2015). *Fracture Mode Analysis, Geomechanics, Petrophysics and Fracture Characterization.* Delft: TU Delft.

Read, M. D., Ayling, M. R., Meredith, P. G., & Murrell, S. A. (1994). Microcracking during triaxial deformation of porous rocks monitored by changes in rock physical properties, II. Pore volumometry and acoustic emission measurements on water-saturated rocks. London: Elsevier.

Rick Rickman, M. M. (2008). A Practical Use of Shale Petrophysics for Stimulation Design Optimization: All Shale Plays Are Not Clones of Barnett Shale.

Roylance, D. (2001). Stress-Strain Curve. Cambridge, Massachusetts: Department of Materials Science and Engineering.

S. Vinciguerraa, C. T. (2005). Relating seismic velocities, thermal cracking and permeability in Mt. Etna and Iceland basalts. Naples.

Saefulhak, Y. (2017, April 28). The target of 7,200 MW from Geothermal Energy in 2025. (M. o. Indonesia, Interviewer)

Schultz, R. A. (1995). Limits on Strength and Deformation Properties of Jointed Basaltic Rock Masses. (pp. Rock Mech. Rock Engng. (1995) 28 (1), 1-15). Austria: Springer-Verlag.

Sigurdur H. Markússon, A. S. (2011). Geothermal surface alteration of basalts, Krýsuvík Iceland— Alteration mineralogy, water chemistry and the effects of acid supply on the alteration process. *Journal of Volcanology and Geothermal Research*.

Tomac, I. (2014). *Micro-Mechanical Aspects of Hydraulic Fracture Propagation and Proppant Flow and Transport for Stimulation of Enhanced Geothermal Systems.* Colorado: Colorado School of Mines.

Ulusay, R. (2015). *The ISRM Suggested Methods for Rock Characterization, Testing and Monitoring: 2007– 2014.* Springer International Publishing Switzerland.

United Nations. (2015). *Chapter XXVII Environment 7.d Paris Agreement 12 December 2015.* Paris.

US Department of Energy. (2017). *Enhanced Geothermal Systems Technologies*. Retrieved from https://energy.gov/

Vahid Hajiabdolmajid, P. K. (2002). Brittleness of rock and stability assessment in hard rock tunneling. Sudbury: Pergamon.

Wang Fei, B. H. (2016). Correlation of Dynamic and Static Elastic Parameters of Rock. *EJGE*, Vol.21.

Wang, D., Ge, H., Wang, X., Wang, J., Meng, F., Suo, Y., & Han, P. (2015). A novel experimental approach for fracability evaluation in tight-gas reservoirs. *Journal of Natural Gas Science and Engineering*.

Welink, C. (2017). *Geothermal Energy Master Project: Rock classification based on the whole bulk chemistry of the rock.* Enschede.

World Bank Group. (2017, June). *Indonesia Economic Quarterly*. Retrieved from
http://www.worldbank.org/en/country/indonesia/publication/indonesia-economic-quarterly-june-
2017

Yang, Y., Sone, H., Hows, A., & Zoback, M. (2013). Comparison of Brittleness Indices in Organic-rich
Shale. *US Rock Mechanics / Geomechanics Symposium.* San Francisco: American Rock Mechanics
Association.

Acknowledgment